FINE PARTICULATE MATTER AND HEAVY METALS POLLUTION STATUS IN AMBIENT AIR OF INDUSTRIAL AREAS: A CASE STUDY OF SAGAMU, OGUN STATE, NIGERIA

BY

OSHIN, TAIWO TOYIN
B.Sc (Lagos), M.Sc (Lagos)
PG/PSC1818844

DEPARTMENT OF CHEMISTRY
FACULTY OF PHYSICAL SCIENCES
UNIVERSITY OF BENIN
BENIN CITY

NOVEMBER, 2024

FINE PARTICULATE MATTER AND HEAVY METALS POLLUTION STATUS IN AMBIENT AIR OF INDUSTRIAL AREAS: A CASE STUDY OF SAGAMU, OGUN STATE, NIGERIA

BY

OSHIN, TAIWO TOYIN

B.Sc (Lagos), M.Sc (Lagos)

PG/PSC1818844

A THESIS WRITTEN IN THE DEPARTMENT OF CHEMISTRY AND SUBMITTED TO THE COLLEGE OF POSTGRADUATE STUDIES IN PARTIAL FULFILMENT OF THE REQUIREMENT FOR THE AWARD OF THE DEGREE OF DOCTOR OF PHILOSOPHY (PhD) IN ENVIRONMENTAL CHEMISTRY, UNIVERSITY OF BENIN, BENIN CITY, EDO STATE.

NOVEMBER, 2024

CERTIFICATION

We the undersigned, certify that the research work submitted in this thesis was carried out by **OSHIN TAIWO TOYIN** in the Department of Chemistry, University of Benin, Benin City, Edo State, Nigeria.

Oshin, Taiwo Toyin	**DATE**
Prof. J.M. Okuo **SUPERVISOR**	**DATE**
Prof. F.E. Okieimen **CO- SUPERVISOR**	**DATE**
Prof. Emmanuel E.I. Irabor **HEAD OF DEPARTMENT**	**DATE**

DEDICATION

This project is dedicated to God Almighty and to my Late Father of blessed memory

ACKNOWLEDGEMENT

I wish to offer my sincere appreciation and gratefulness to all who have in one way or the other contributed to making me what I am today or assisted to make my life a happier one.

I am immensely grateful to my supervisors Prof. J. M. Okuo and emeritus Prof F.E Okieimen for their intellectual mentoring, invaluable academic discussions, suggestions, encouragement, moral supports and for painstakingly going through the PhD work. They have indeed impacted my life through their rare academic genius and prowess. I cannot but say thank you and pray for sound health and longevity of life for both accomplished professors. I consider myself fortunate to have done my PhD under your tutelage. Words cannot adequately express my gratitude to you.

I also salute the Head of the Department of Chemistry, Professor Emmanuel. E. I Irabor, Departmental Postgraduate c\oordinator Dr O.K Ogbeide, Professors, Lecturers as well as Postgraduate students of the Department of Chemistry, University of Benin, for providing conducive research and learning environment with constructive criticisms especially during the course of my pre and post data presentation. Worthy of my sincere appreciation goes to my twin brother and other siblings, my-in-laws and research students at Lagos State University of Science and Technology, Ikorodu, Lagos.

I wish to express my deep gratitude to my lovely wife, Modupe Oshin and adorable sons, Tomiwa, Feranmi, Gbotemi and Boluwatife for their love, care and encouragement in making this PhD research work a success story. It was a great pleasure to have walked this journey with you all. We all made it together.

TABLE OF CONTENTS

LIST OF TABLES

LIST OF FIGURES

LIST OF PLATES

LIST OF ACRONYMS AND ABBREVIATIONS

ACRONYM	MEANING
BDL	Below Detection Limit
OMRF	Ogijo Metal Recycling Factory
CA	Cluster Analysi
CF	Contamination Factor
OLFS	Ode- Lemo Farm Settlement
SIIE	Sagamu Interchange industrial Estate
SPSS	Statistical Package for the Social Sciences
SA	Source Apportionment
$PM_{2.5}$	Particulate Matter of aerodynamic size below 2.5micrograms (μm)
TSP	Total Suspended Particulate Matter
PMF	Positive Matrix Factorisation
PLI	Pollution Load Index
GRM	Gamma Regression Model
LRM	Linear Regression Model
CMB	Chemical Mass Balance
EFs	Enrichment Factors
PCA	Principal Component Analysis
IARC	International Agency for Research on Cancer
ICP-OES	Inductively Coupled Plasma Optical Emission Spectroscopy
NAAQS	National Ambient Air Quality Standards
NESREA	Nigerian Environmental Standards and Regulations Enforcement Agency
ATSDR	Agency for Toxic Substances and Disease Registry
WHO	World Health Organization
NESREA	Nigerian Environmental Standards and Regulations Enforcement Agency
USEPA	United States, Environmental Protection Agency
$\mu g/m^3$	Microgram Per Cubic Meter

ABSTRACT

Industrial activities contribute deeply to high emission rates of particulate matter (PM) and other pollutants into the ambient air. The siting of industrial plants in proximity to a populated area can have adverse effects on human health and the environment at large. The industrialization and urbanization of Sagamu city in Ogun state, has led to increased pressure on the city especially on air quality. The chemical complexity of airborne particles makes it necessary to consider their composition and sources of emission. This study was aimed at quantifying Fine particulate ($PM_{2.5}$) and its heavy metals content in ambient air of industrial areas in Sagamu, Ogun state. The study locations of this research work were Ikorodu- Sagamu industrial area (majorly metal recycling industries) and Sagamu- Abeokuta interchange industrial area (majorly a mixed of Food, Agro-allied and Brewery industries). The control site is located at Ode-lemo farm settlement in Sagamu, Ogun state. A total of 108 air samples of fine air particulate ($PM_{2.5}$) were collected. Triplicate samples were collected each month with the aid of Conical Inhalable Sampling (CIS) head at a flowrate of $3.5Lmin^{-1}$ for 8hrs per day and for a period of one year. Meteorological data were collected simultaneously with $PM_{2.5}$ via a specialised weather monitoring equipment (Automated Meteorological station). The $PM_{2.5}$ filter papers collected were carefully sealed in a polythene bag and preserved prior to the laboratory for analysis. The $PM_{2.5}$ mass concentration was computed gravimetrically. The loaded filters were subjected to acid digestion prior to analysis. Sixteen (16) metals were identified and quantified using Inductively Coupled Plasma- Optical Emission Spectrometer ICP-OES). Pollution indices such as Contamination factor (CF), Degree of contamination (DC) and Pollution index load (PLI) were assessed on the two industrial areas. Source identification and profiling of $PM_{2.5}$- bound metals were determined using multivariate analysis which included Enrichment factor, inter-metallic correlation matrix, Principal component

analysis (PCA) and Cluster analysis (CA). The two predictive models, Linear Regression Model (LRM) and Gamma Regression Model (GLM) were acquired and tested using the data produced from this work and a software tool R version 2024 which is user friendly.

Results obtained from the temporal variations of mass concentration of fine particulate in the studied sites revealed that the annual mean of $PM_{2.5}$ mass concentration were 6-20 times and 5-17 times higher than the annual WHO and USEPA guidelines of 10 and 12μg/m^3 in all the sampling locations. The seasonal $PM_{2.5}$ levels ranged from 64.67 to 389.7 μg/ m^3 and 18.33 to 164.70 μg/m^3 during the dry and wet seasons in industrial sites and control area respectively . Therefore, the seasonal variation trend showed that dry > wet. The pollution indices were computed from the heavy metal concentrations (Cr, Mn, As and Pb) in $PM_{2.5}$ from the two industrial areas. The results showed that CF, DC and PLI values for site OMRF were; CF>6 (Cr,Mn, and Pb) and >3 (As), >32 and >1 while for site SIIE ; CF>6 (Mn) <6 (Cr, As and Pb), < 32 and >1. The results of enrichment factor analysis (EF) and principal component analysis (PCA) for source identification showed very high enrichment for the elements; Pb, Cd, Cr, Cu, Ni, Na, K, Mg, and Ca in the fine fraction ($PM_{2.5}$) while the Principal Component Analysis explained five common contributing sources of fine particulates ($PM_{2.5}$) such as fossils fuel combustion, vehicular emission, industrial emission, biomass burning and dust. To further elucidate the relationship among pollutants in the sampling sites, correlations analysis and cluster analysis were carried out.

The results of the correlations analysis and cluster analysis confirmed the results of the EF and PCA. The predictive model revealed that GRM is a choice model for the prediction of Cr and Pb in both OMRF and SIIE industrial sites while LRM is a better model for the prediction of As and Cd in both OMRF and SIIE sites.

CHAPTER ONE

1.0 INTRODUCTION AND LITERATURE REVIEW

1.1 INTRODUCTION

The unprecedented population growth and accelerated urbanization, coupled with economic advancement and fast industrialization in Nigeria, have significantly exposed the country to severe air pollution for more than two decades (Abiye *et al*., 2013, 2014; Owoade *et al.,* 2013; Sulaymon *et al*., 2020, Joseph e*t al.,* 2023). For instance, in 2021, the World Health Organization (WHO) Nigeria was ranked among the most air polluted nations in the world (WHO, 2021), which calls for great concern among Nigerian and air quality experts. The substances that constitute air pollution include particulate matter (PM), toxic metals, and volatile organic compounds (VOCs), amongst others. The identified substances are released into the ambient through human or natural sources (Omolaoye *et al.,* 2024).

The phenomenon whereby the substances are released into the ambient air, which is generally referred to as air pollution. In humble terms, air pollution is the incessant introduction of chemical substances, particulate matter, or organic materials that results in the ejection of harmful substances that result in human discomfort or other living organisms, which may result in environmental damage to the built environment or the atmosphere (Isa, 2021). These foreign bodies that cause air pollution are referred to as air pollutants.

In 2021, the World Health Organisation (WHO) ranked Nigeria among the most air polluted nations in the world (WHO, 2021), making it a great concern for the Nigerian air quality experts.

Air quality degradation leads to very serious human health impacts such as pneumonia, acute respiratory disorders, breathing problems, and chronic asthma (Croft *et al.,* 2019; Hopke *et al.,* 2019; Shen et al., 2020; Yan et al., 2018; Rizwan *et al.,* 2013), reduction in life expectancy and an increase in the health care public expenditure (James *et al*., 2018b) . Also, severe air pollution is strongly correlated with visibility reductions (Jiang *et al*., 2021; 2019; Wang *et al*., 2018). Furthermore, deterioration of air quality has a sharp negative consequences on a variety of processes on the ecosystem services which include; haze, ozone depletion, acid rain, eutrophication, climate change amongst others (Jiang *et al*., 2021 , acid rain (Owoade *et al*., 2021). Particulate matter (PM) refers to any tiny solid, semi-solid and liquid particles or a mixture that can be suspended in the air and remain for an extended period. PM has no fixed composition, the particles may consist either of only one chemical (e.g. sulphate, sulphuric acid, or lead oxide) or a number of pollutants (Organic chemicals, metals, dust). PM is described by US EPA as among the most harmful of all air pollutants.

Particles in the air are classified by aerodynamic diameter size and chemical composition, and are often referred to as particulate matter or aerosols. PM is generally measured in terms of the mass concentration of particles within certain size classes: total suspended particulates (TSP), PM_{10} or coarse particles (with an aerodynamic diameter of less than 10 micron), $PM_{2.5}$ or fine particles (with an aerodynamic diameter of less than 2.5 micron) and ultra fine particles (those with a diameter of less than 0.1 micron). The distinction between the coarse and fine particles is important because they have different sources, formation mechanisms, composition, atmospheric lifespan, spatial distribution, indoor-outdoor ratios, temporal variability, and health impacts. Some PM occurs naturally, originating from dust storms, forest and grassland fires, living vegetation, sea

spray, and volcanoes, and some PM originates as a result of human activities, such as fossil fuel combustion, industrial emissions, and land use.

Industrial activities such as fossil fuel combustion, metal processing and chemical manufacturing release large quantities of fine particulate matter into the atmosphere. These particles can travel long distances, cross national borders and affect air quality, human health and the environment. Exposure to industrially emitted fine particulate matter has been linked to various health problems including respiratory and cardiovascular disease , lung cancer, and neurological damage. The tiny size of these particles allows them to penetrate deep into the lungs, causing inflammation and oxidative stress.

Industrially emitted heavy metals in PM can include elements such as lead, mercury, arsenic, cadmium, chromium and nickel. Their toxicity depends on several factors including the dose, route of exposure, and chemical species, as well as age, gender, and nutritional status of exposed individuals. Because of their high degree of toxicity, arsenic, cadmium, chromium, lead and mercury rank among the priority metals that are of public health significance. These metallic elements are considered systemic toxicants that are known to induce multiple organ damage, even at lower levels of exposure. They are probably or knowingly classified as human carcinogens according to the U.S Environmental Protection agency, and International Agency for Research on Cancer.

However, in measuring heavy metals in industrially emitted fine particulate in the atmosphere, information is needed about its sources and level of its contribution to pollution. Source Apportionment (SA) has been useful in the estimation of the contribution of the sources at ambient levels. Source markers or profiles are one of the tools used in SA. Several methods of source apportionments have been reported in literature to identify the sources of the pollutants and

estimate their contributions. These include; Reception Modeling using statistical models, Chemical Mass Balance (CMB), Positive Matrix Factorization (PMF) and Source Apportionment Models which involves combination of reception modeling and emission inventory data. Understanding of pollutant sources, source apportionment offers several benefits such as improved air quality management, reduced pollution, enhanced ecosystem protection, improved understanding of pollutant sources and enhanced model development.

In order to improve air quality management and reduce health risk, It is imperative to forecast the concentrations of heavy metals in fine particulate matter using predictive modeling that is based on measured input parameters such as meteorological data. Several predictive models have been reported in literature such as Linear Regression Models (LRM), Artificial Neural Network (ANN), Decision Tree Models, Random Forest Models and others. LRM is a statistical model that assumes a linear relationship between the outcome variable (heavy metal concentrations) and predictor variable (meteorological data). This is considered in this study. The goal of predictive modeling is to identify the most significant factors contributing to heavy metal emission and to develop models that can accurately predict future emissions which could be useful for policy makers and relevant regulatory agencies.

Given the significant environmental and health risks associated with industrially emitted fine particulate and heavy metals, it is essential to develop effective strategies for reducing emission, improving air quality and mitigating the impacts of these pollutants

1.1.1 Background of the study

The investigation into outdoor air pollution and pollutants recently gained global attention from many researchers, which is connected to the unprecedented air quality deterioration in remote and urban areas (Soltani *et al*., 2019). Pollution-free air is a basic necessity to man and the environment (Belis *et al*., 2014). However, key anthropogenic contributors, which include overpopulation, industrialization, and transportation, often than not release toxic substances such as particulates, toxic metals, and toxic atmospheric gases with high concentrations above their normal ambient level and consequently result in deterioration of air quality (Kumar *et al.,* 2020). Fine particulate matter, which is otherwise known as $PM_{2.5}$, is a significant indicator of air quality (Rockström *et al*., 2023). $PM_{2.5}$ emissions originate from various sources, both natural (windborne dust, sea spray, volcanic activities, biomass burning, among others) and other human-mediated sources (fuel combustion, industrial processes, non-industrial fugitive sources, and transportation) (Loomis *et al*., 2014; US EPA, 2012a).

Fine particulate matters are described by their physicochemical properties. The physical attributes encompass particles such as the mass concentration, which is measured in units of mass per unit volume, and size distribution measured in aerodynamic diameter, which influence their transport and deposition (Liu *et al*., 2014). Aerodynamic is the equivalent diameter of a spherical particle that possesses velocity as that of the collected particles (Liu *et al.,* 2014).

According to Basha *et al.* (2014), the chemical makeup of $PM_{2.5}$, which includes organic molecules, elemental carbon (black soot), trace elements, and inorganic compounds, can have a major influence on agriculture, climate change, human health, visibility, and atmospheric

chemistry. Some hazardous metals, including arsenic (As), cadmium (Cd), chromium (Cr), nickel (Ni), vanadium (V), manganese (Mn), lead (Pb), iron (Fe), cobalt (Co), copper (Cu), zinc (Zn), titanium (Ti), aluminium (Al), antimony (Sb), etc., are found among the inorganic compounds. Due to their widespread presence in residential and occupational areas and the fact that inhalation is one of their exposure routes, they pose a major threat to human health (Basha *et al.,* 2014).

Important climatic variables and pollution sources might have an impact on the quantity of pollutants in a certain area (Basha *et al*., 2014). Because of its longer residence time in the atmosphere and capacity to act as a carrier of harmful trace metals into human lungs, fine particulate matter ($PM_{2.5}$) has drawn attention as a metric more closely associated with adverse health effects (Sillman *et al.,* 2021).

1.1.2 Statement of the Problem

The industrial revolution has been associated with large quantities of gaseous and particulate emissions linked to industrial production and burning of fossil fuels for energy and transportation activities. Industrial air pollution is a significant environmental and health concern due to the emission of harmful pollutants into the air, posing risks to human health, environmental quality, and sustainable development. Large volumes of air pollutants are being released from the industrial activities at concentrations above their normal ambient level and consequently result to deterioration of air quality.

Epidemiological studies reveal that PM associated with toxic metals from industrial activities have been reported to have morbidity and mortality in public health, which calls for health concern (US EPA, 2012).

However, little has been done on public awareness and engagement on the risk pose by air pollution risks associated with the industrial operations in these study areas, thereby hindering community involvement in mitigation efforts.

1.1.3 Justification of Research

Industrial development in Ogun State has been associated with the emission of large quantities of gases and particulates into the air from industrial production, burning fossil fuels for energy and transportation, which have potential health and environmental impacts on the host communities. Epidemiological studies have shown that $PM_{2.5}$ and its elemental contents have been linked to many diseases such as acute respiratory disorder, pneumonia , chronic asthma, breathing problems and Cardiovascular disorder. (Ana and Sridhar, 2009; Abiye *et al*., 2013; Ezeh *et al*., 2012; Obioh *et al*., 2013; Okuo *et al*., 2017).

However, there is little or no information on the levels of $PM_{2.5}$, its elemental composition and modeling in these study areas.

This study is therefore necessary to determine the adverse effect of $PM_{2.5}$ -bound heavy metals on human health and the environment. In addition, baseline data from this work will assist in policy formulation and regulation of industrial activities in Sagamu and Ogun State at large by the relevant regulatory bodies, researchers and environmentalists.

1.1.4 Scope of Research

This research work will be limited to tagging and geo-referencing of the designated sampling points, sampling of $PM_{2.5}$ along with meteorological data in both dry and wet seasons, followed by elemental analysis and pollution indices of $PM_{2.5}$-bound metals, identifying and apportioning pollutant sources, and developing a model for the prediction of toxic metals in the study areas.

1.1.5 Aim and Objectives of the Study

The aim of the study is to quantify $PM_{2.5}$ and its elemental contents in ambient air of industrial areas in Sagamu, Ogun State, Southwest Nigeria.

The specific objectives of the research are to;

(1) sample $PM_{2.5}$ along with meteorological data and determination of the level of $PM_{2.5}$ in dry and wet seasons for a period of one year.

(2) determine the elemental concentration of $PM_{2.5}$-bound metals using an Inductively Coupled Plasma Optical emission spectrometer (ICP-OES) instrument.

(3) determine the temporal variation of $PM_{2.5}$ and its elemental content

(4) assess the pollution risk associated with heavy metals in $PM_{2.5}$ using pollution indices

(5) identify the major pollutant sources in the study areas using multivariate statistical tools

(6) develop a predictive model to quantify and predict the concentration of heavy metals in the study areas.

1.2 LITERATURE REVIEW

The literature review begins with a brief discussion on fine particulate matter, its sources, effects, regulations in ambient air, monitoring equipments and associated heavy metals. Analytical instrumentation for chemical characterisation, source apportionment and review of $PM_{2.5}$ bound metals are also highlighted.

1.2.1 Particulate Matter (PM)

Particulate matter (PM) is defined as the suspension of minute solid, semi-solid, and liquid particles, or a combination in the atmosphere for a protracted period (Shandilya & Khare, 2014). The most common ways to classify particulate matter, or aerosols, are based on size (aerodynamic diameter) and chemical makeup, as seen in Figure 1.5. According to its aerodynamic particle size, it is divided into two categories based on inhalable sizes, as indicated in the figure: PM (0.1 to 2.5 μm) small particles and PM (>2.5 to 10 μm) coarse particles (Olawoyin *et al.,* 2018). These aerodynamic PM sizes include organic and elemental carbon, metals (nickel, zinc, lead, cadmium, copper, nickel, and vanadium), nitrates, sulphates, sodium, potassium, ammonium, and calcium, and polycyclic aromatic hydrocarbons (PAHs) (Abrams *et al.,* 2017; Kim *et al*., 2015; Qie *et al.,* 2018).

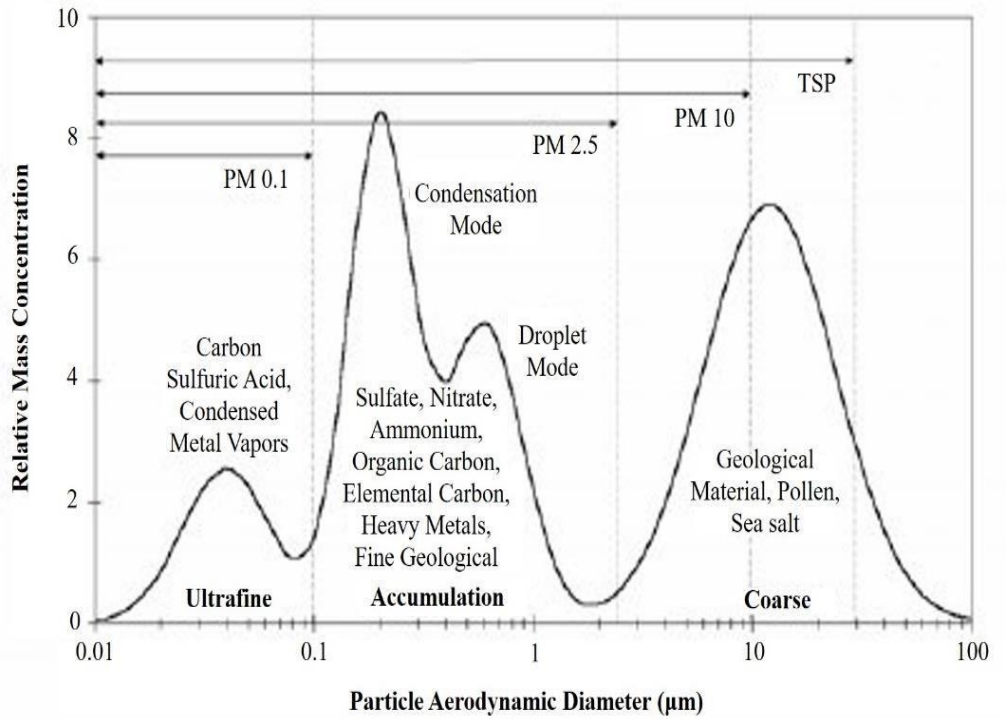

Fig. 1.1.: Particle Size Distribution (*Source*: Van Der Pol *et al.,* 2014).

1.2.2.1 Fine Particulate Matter ($PM_{2.5}$)

Particles with a diameter of not more than 2.5 micrometers (μm) are referred to as fine particulate matter, or $PM_{2.5}$. Fine particles are substantially smaller than a hair's diameter. The minuscule size of 2.5 micro meters makes it easier to breathe into the human lungs and respiratory systems, hence elevating the risk to human health. Organic carbon, sulphate, elemental carbon, nitrate, and other inorganic particles, including sea salts, crustal material, and metals, are among the fine particles that are immediately released into the atmosphere. They may travel hundreds to thousands of kilometres and have an atmospheric lifespan of days to weeks (Yu *et al.,* 2015; Eil, 2020).

Many potentially hazardous trace elements, including arsenic, cadmium, chromium, copper, iron manganese, nickel, lead, vanadium and zinc are found in various amounts in fine particles.
The amount and type of water-soluble metals on the aerosols have the ability to promote electron substitute while acting as a catalyst for the generation of free radicals. By catalysing oxidant formation, altering the pulmonary defence system, having detrimental effects on respiratory health, oxidative stress, and encouraging the release of inflammatory mediators and cytotoxicity, free radical generation can cause damage to lung tissue (Islam *et al.,* 2015; Natarajan *et al.,* 2018).

In general, highly soluble metallic components in air particulate matter are more easily bio-activated and may therefore pose a greater risk to human health. The detrimental effects of air trace metal particles on human health are influenced by several factors. These consist of particle size and shape, metallic component bonding and solubility, total human exposure, and an individual's overall health (Ovrevik *et al*., 2015). Apart from the overall concentration of distinct metals in particulate matter, the solubility of water and acid may be significant factors in determining the

utilization rate and possible harmfulness of each metal. The chemical form, particle size, and sample pH all affect how soluble a metal is in $PM_{2.5}$. Therefore, rather than focusing on the overall amount of metals present, it's crucial to ascertain the bio-available quantities in order to assess the danger caused by metal toxicity (Mukhtar and Limbeck, 2013; Fois *et al,* 2023).

1.2.2.2 Sources of $PM_{2.5}$

There are many different sources of fine particles; however, human activities, including industrial production and vehicle emissions, have been recognized as one of them (Table 1.0). The two types of emission mechanisms for atmospheric particles are primary and secondary sources. Construction sites, wildfires, wood burning, gravel pits, dusty roads from agriculture, industrial activity, traffic on the roadways, and sea spray are the main sources of airborne particles. Metals and metal oxides, ions, and carbon and organic molecules make up these main sources of particles. According to Aryal *et al.* (2013) and Belis *et al.,*(2014), gaseous primary pollutants such as ammonia, nitrogen oxides (NO_x), sulphur IV dioxide (SO_2), and volatile organic carbons undergo chemical modification to become secondary sources of $PM_{2.5}$. Both sources can further be categorized into natural and man- made sources:

(i) **Natural Sources**: These are sources that come from recurring, naturally occurring events that are not the consequence of human or man-made action. Sea spray, dust storms, volcanoes, forests, wildfires, biological sources, etc. are some of the natural sources of $PM_{2.5}$. The production of tiny particles containing crustal metals is facilitated by a variety of mechanical processes, including dust resuspension, mineral processing, mining, and grinding.

(ii) **Anthropogenic Sources**: These are sources that directly or indirectly result from human activity. As a result of human influence, or man-made causes, this is by far the biggest component contributing to air pollution today. They are mostly caused by people's dependence on fossil fuels, power plants, and heavy industry, but they may also be brought on by garbage buildup, building and demolition, burning coal and wood, contemporary agriculture, and other human-caused activities.as seen in Table 1.1

Table 1..1: Marker elements associated with various emission sources

Emission Source	Marker Elements
Soil	Al, Si, Sc, Ti, Fe, Ca
Road dust	Ca, Al, Sc, Si, Ti, Fe,
Sea salt	Na, Cl, Na^+, Cl^-, Br, I, Mg, Mg^{2+}
Oil burning	V, Ni, Mn, Fe, Cr, As, S, SO_4^{2-}
Coal burning	Al, Sc, Se, Co, As, Ti, Th, S
Iron and steel industries	Mn, Cr, Fe, Zn, W, Rb
Non-ferrous metal industries	Zn, Cu, As, Sb, Pb, Al
Glass industry	Sb, As, Pb
Cement industry	Ca
Refuse incineration	K, Zn, Pb, Sb
Biomass burning	K, C ele, C org, Br, Zn
Automobile gasoline	C_{ele}, Br, Ce, La, Pt, SO_4^{2-}, NO_3^-
Automobile diesel	Corg, Cele, S, SO42–, NO3–
Secondary aerosols	SO42–, NO3–, NH4+

Source: Chow (2005) Marker elements are arranged by priority order.

1.2.3 Effects of $PM_{2.5}$ Exposure

Exposure to $PM_{2.5}$ has significant health, climatic and environmental impacts with respect to duration of exposure.

1.2.3.1 Impacts on Human Health

Due to their tiny size, shape, density, and breathing patterns, respirable particle is easily settled down in the breathing system of humans after being inhaled. The effect of respirable particle contact in humans is mostly determined by genetic variables specific to each individual, the kind of chemicals present in the tiny particles, and the length and intensity of exposure. The ability of soluble fine particulate matter to penetrate deeply into the lungs' alveolar regions contrasts with the insoluble parts, which stick to the surface and are challenging to remove, impairing the ability of the lungs to ventilate (Ren *et al.*, 2016). According to the US EPA (2012b), this can cause illnesses including coughing, breathing problems, reduced pulmonary function, abnormal

heartbeats, heart failures, worsened asthma, severe bronchitis, skin disorders, and early mortality. Moreover, weakly bound metals including cadmium, chromium, nickel, lead, iron, zinc, manganese and other potentially hazardous elements are carried by small particles. These metals can seriously endanger human health if they are found in ambient air in high quantities (Khan *et al.*, 2016). Particulates in the blood impair haemoglobin's capacity to carry oxygen. Serious side effects from this technique include worsening respiratory conditions and cardiac failure due to obstruction. It is frequently irreversible and can cause a number of chronic upper respiratory illnesses in addition to raising the risk of lung cancer and cardiorespiratory death (Alzheimer, 2023).

According to reports based on clinical, epidemiological, and toxicological analyses, certain vulnerable populations, including children, adults (from 65 years old or above), and patients with background heart and lung diseases, are liable to short-term lung and heart stress, as well as demise from exacerbation of heart or lung disease. Children are deemed a high-risk group because of their innate tendency to breathe deeper than adults due to higher basal metabolisms, which exposes them to higher concentrations of $PM_{2.5}$ (Saadeh and Klaunig, 2014). The effects of short- and long-term exposure to $PM_{2.5}$ concentration levels on mortality and morbidity are estimated using findings from the fields of toxicology, epidemiology, and clinical studies. Numerous studies suggest a favourable correlation between $PM_{2.5}$ and respiratory and cardiovascular disorders (Ren *et al*., 2016; Chauhan *et al.,* 2024). As the 13th greatest cause of death worldwide, $PM_{2.5}$ is thought to cause around 800,000 premature deaths annually, according to WHO estimates (Swaffield and Egan, 2020).

1.2.3.2 The Impact of Climate and Environment on Particulate Matter

Elevated levels of $PM_{2.5}$ in the atmosphere have the potential to impact the radiative balance of the earth-atmospheric system by obstructing solar radiation, which in turn reduces the amount of sunlight reaching the surface (Rockstrom *et al*., 2023; Singh *et al.,* 2015). This may lead to air haze, decreased visibility, altered temperature and precipitation patterns, decreased agricultural yields, inadequate light, and negative effects on property values and transportation safety. Moreover, $PM_{2.5}$ greatly contributes to acid rain because of its strong affinity for water (USEPA, 2012a).

Previous researches indicates that seasonal variations have a significant impact on the fluctuation between pollution concentrations and certain meteorological factors (Coccia, 2020). Wu *et al.* (2012) reported that in China, summertime $PM_{2.5}$ exposure levels were lower due to high temperatures and wind speeds. Holland *et al*. (2020) investigated the fine particulate levels and local meteorological data for Carlisle, Pennsylvania. The analysis's findings indicated that summer had the highest $PM_{2.5}$ concentrations, followed by winter, with comparatively low concentrations in the spring and autumn. The main meteorological factor influencing this region's seasonality was found to be wind speed. On autumn days with high $PM_{2.5}$ concentrations, there were lower temperatures and relative humidity levels. On days with greater concentrations of fine particulate matter, the local weather was found to be ‘warmer, less windy, high or low humid, greater in pressure, and with less rainy.

Additionally, in Ile-Ife, Nigeria, Owoade, *et al.* (2021) looked at the connectivity between fine particulate concentrations and climatological factors. The study's findings indicated that, due to

atmospheric haze, there was a higher concentration of $PM_{2.5}$ mass concentration during the dry season than during the rainy season. The main conclusion of their research was that the amount of $PM_{2.5}$ that accumulated in the studied area was greatly influenced by climatic factors such as rainfall, global radiation, air temperature, and relative humidity.

1.2.4 Effects of Meteorological on PM Concentrations

The quality of the air in a given area is greatly influenced by the local and regional meteorological. Thus, meteorological factors like rainfall, relative humidity, temperature, atmospheric pressure, solar radiation, wind speed, and direction have a significant impact on the large diffusion, dilution, and accumulation of atmospheric fine particle pollution (Liu *et al*., 2014; Liang and Gong, 2020).

1.2.4.1 Wind Speed

Wind speed, also known as wind flow speed in meteorology, is a basic atmospheric quantity brought on by air shifting from high to low pressure, often as a result of temperature variations. Anemometer is now often used to measure wind speed. Because of their tiny sizes, fine particles are easily carried by wind from the emission sources to other distant areas. Transporting pollutants like nitrates, sulphates, trace metals, etc. to far-off places results in large background accumulations in the areas they end up in (Moustafa *et al*., 2015; Khalid *et al.,* 2017). Numerous reports have revealed that elevated wind speeds contribute to the dilution of air contaminants, while little wind speeds encourage the buildup of toxins. Because of variations in dispersion and transport, dry deposition, and the creation of marine particles, wind speed can therefore have a significant effect on the amounts of fine particulates (Megaritis *et al*., 2014). Compared to coarse particles, wind speed is a major factor in clearing the atmosphere of fine particles. Turbulence close to the ground is influenced by wind speed. As wind speed increases, particulate dispersion,

dilution effects, and particle transport all increase, resulting in a decrease in mass concentration (Wang and Chung, 2019).

1.2.4.2 Wind direction

The direction that the wind originates from is considered the wind direction. Typically, wind direction is expressed in degrees or cardinal directions. Pollutant dispersion has been linked to wind direction. Pollutant dispersal in a location is influenced by wind direction (Change, 2023b). The distribution of fine particle concentration to the various sources can be facilitated by wind direction and speed (Coccia, 2020). By moving particulate matter from various nearby places to the sample site, it performs influencing functions and considerably contributes to the fluctuation in particulate matter concentration (Giordano *et al.,* 2021).

1.2.4.3 Temperature

The average kinetic energy of a substance's molecules is measured and referred to as temperature. The temperature rises with increasing kinetic energy. a measurement of the air molecules' speed. Ambient chemical processes are influenced by temperature. Low temperature occurrences give rise to stagnant air masses, which in turn cause high particle levels, and vice versa (Bereiter *et al.,* 2018).

1.2.4.4 Relative Humidity

The amount of water vapor in the air relative to the greatest amount that the air could contain at that temperature and pressure is known as relative humidity. There are claims that it differs from typical humidity. The total quantity of water vapor in the air is known as normal humidity. A hygrometer is used to measure relative humidity. The effects of high and low relative humidity on $PM_{2.5}$ levels are not the same. For clouds, fog, and precipitation to occur, humidity is required. Fine particle accumulation is reduced in environments with high relative humidity and vice versa

in environments with low relative humidity. High relative humidity influences the settling down of particles to the ground. This is because particulates are bound to water molecules being a polar solvent, and over time, these particles grow in size until they are eventually removed from the atmosphere via rainfall or droplets (Hernandez *et al*., 2017). Additionally, relative humidity promotes the development of secondary pollutants (Zhang et al., 2019).

1.2.4.5 Rainfall

Rainfall, as determined by a rain gauge, is the total amount of rain that falls on a specific location in a specific length of time. The rate of precipitation has a major influence on fine particle concentrations because rainy weather leads to moist deposition of particles, which eliminates $PM_{2.5}$ from the atmosphere (Megaritis *et al*., 2014). However, moisture limits the potential for resuspended soil particles by increasing soil humectant levels, which in turn reduces the mass concentration of airborne particulate matter (Bashari *et al.,* 2018).

1.2.4.6 Pressure

It is the force that the air above a surface applies to it when gravity draws it towards Earth. A barometer is often used to measure atmospheric pressure. A mercury column within a glass tube in a barometer rises or lowers in response to variations in the atmosphere's weight. An increase in atmospheric pressure leads to a large-scale sinking of air, which traps moisture and pollutants close to the surface and increases the number of small particles. It's important to remember that under certain unusual circumstances, increased $PM_{2.5}$ levels can also be seen in low pressure when dust particles are stirred up by storm passage winds (Li, 2019).

1.2.5 Topography Effects on PM $_{2.5}$ Concentrations

The depiction of surface characteristics, including rivers, mountains, valleys and hills, is referred to as topography. Topographical characteristics of a particular area might affect fine particle dispersion and movement there. For instance, an urban location near a mountain range can exacerbate pollution issues by stabilizing the atmosphere, which leads to large concentrations of fine particles in the valleys adjacent because of cold air drainage into those valleys. Additionally, both vertical and horizontal airflow may help disperse pollutants, but a mountain range acts as a natural barrier (Li, 2019).

1.3 Regulation of Respirable Particles in Outdoor Air

The term "ambient air" describes atmospheric air in its unaltered condition, devoid of airborne contaminants found in the outdoors or in the air we breathe. Any chemical, physical, or biological substance that contaminates the natural condition of air does so in a way that affects individuals differently. In particular, breathing in large amounts of $PM_{2.5}$ can have a variety of short- and long-term health impacts. One of the main causes of the worldwide burden of disease and preventable deaths is this $PM_{2.5}$ (WHO, 2012; Cohen *et al*., 2017). Governments and organizations focused on global health concerns, such as the US EPA, WHO, and others, have set limits for the ambient concentration of particles in order to address the health impacts of particulate matter (WHO, 2006; US EPA, 2012a).

The National Ambient Air Quality Standards (NAAQS) for particulate matter that affects human health and welfare are established by the Environmental Protection Agency (EPA) in the United States. There are two categories for NAAQS: primary and secondary standards. The preservation of the public's health, particularly that of the "sensitive" groups, is the focus of primary standards.

These comprise the elderly, kids, and those suffering from respiratory conditions. In addition, the secondary requirements define a threshold level to prevent reduced visibility and to safeguard buildings, crops, animals, and plants.

As of right now, the yearly average for $PM_{2.5}$ is 12 g/m^3, with a maximum of 35 g/m^3 (Bondy *et al*., 2020). Furthermore, according to World Health Organization (WHO) air quality rules, the average daily $PM_{2.5}$ level should not be higher than 25 g/m^3 or the yearly average of 10 g/m^3. (WHO, 2006, Rockstrom *et al*., 2023). The majority of the world's largest cities frequently surpass the air pollution standards set by the World Health Organization (WHO), as seen in Figure 1.6. The Nigerian Environmental Standards and Regulations Enforcement Agency (NESREA) is the organization in charge of environmental laws, standards, policies, regulations, and enforcement in Nigeria (NESREA, 2013). NESREA states that the yearly ambient $PM_{2.5}$ concentration is 20 g/m^3 and 40 g/m^3 for a 24-hour period.

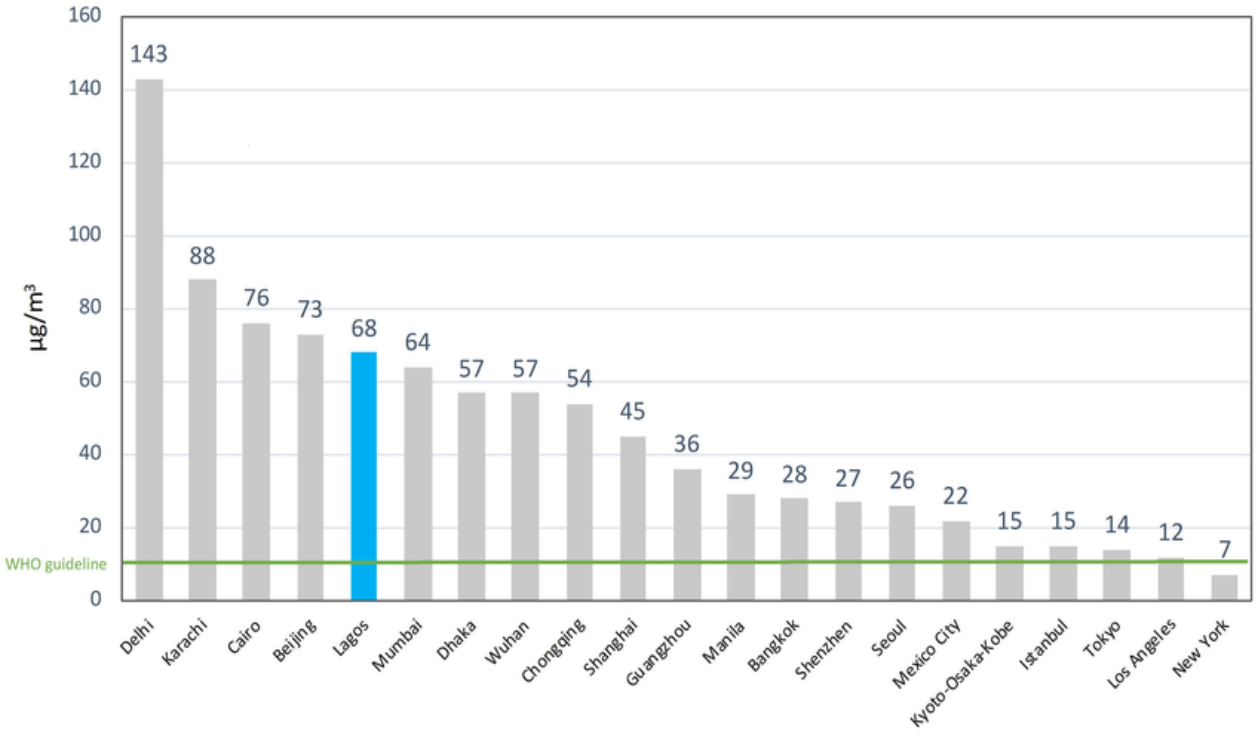

Figure 1.2: The World Health Organisation (2014) reports that ambient air pollution in cities results in concentrations of tiny particulate matter, or $PM_{2.5}$.

1.4 Heavy Metals and Particulate Matter

Any metallic chemical element with a relatively high density that is dangerous or poisonous at low concentrations is referred to as a heavy metal and metalloids that are known to naturally occur in the earth's crust and have a specific gravity five times greater than that of water (Alsafran *et al*., 2022). Naturally occurring elements with an atomic number greater than 20 are now included in the definition, which was expanded further recently (Ali and Khan, 2018; Ali *et al*., 2019).

Elements that are necessary and non-essentially make up the bulk of heavy metals. Iron, manganese, copper, zinc, cobalt, nickel, molybdenum, and selenium are among the necessary elements. The reason for their name is that they are necessary for basic metabolic processes in living things. For many different kinds of life, a large number of them operate as cofactors that are

crucial to the structural and functional properties of enzymes and the biochemical activities that they catalyse. However, organisms experience harmful physiological consequences when these "essential" metals are present in excess of a particular threshold. Many of the non-essential heavy metals are hazardous at low doses and have no known beneficial effects on biological systems. Lead, cadmium, mercury, arsenic, tin, aluminium, silver, gold, antimony, bismuth, palladium, platinum, vanadium, tellurium, strontium, titanium, uranium, and chromium especially the hexavalent form are examples of non-essential heavy metals (Liu *et al.,* 2022).

Heavy metals are a source of concern since they have the potential to damage drinking water sources or enter the food chain through bioaccumulation in plant and animal species. The latter is especially true in developing countries (like Nigeria), where a large number of rural populations rely on exposed, unprotected surface water sources for household, recreational, and drinking needs. Particularly in $PM_{2.5}$, toxic heavy metals have a longer half-life in the atmosphere. Human exposure is increased by deep lung inhalation when pollutants are transported by wind after they leave their site of emission (Sovacoo *et al*., 2021; Urman *et al.,* 2016). The major heavy metal species that were studied in this study include arsenic, cadmium, lead, chromium, lead, chromium, and nickel.

1.4.1 Arsenic

Arsenic and its compounds are metalloids that are ubiquitous as environmental pollutants and are found at low concentrations in nearly all environmental matrices (Hughes *et al.,* 2011). Although arsenic is naturally occurring in the earth's crusts, it is notable in all environmental media, including air, soil, and water due to wind-blown crustal dust, leachate from rock erosion, forest

fires, and volcanic ash (ash (Tarodi *et al.,* 2018). On the other hand, agricultural use of arsenic in pesticides, fertilizers, electronics, and semiconductors, as well as coal burning, metals mining, and metals processing, has contributed to the environmental contamination of arsenic (USEPA, 1998; WHO, 2003).

Due to high quantities of arsenic in the air, soil, and drinking water that create important routes into food chains and human exposure that poses serious health hazards, arsenic has therefore garnered attention globally in recent years (Niazi and Burton, 2016; Mandal, 2017; Shahid *et al.,* 2018). Humans can get cancer, skin lesions, cardiovascular problems, and diabetes as a result of acute and chronic toxicity from consuming inorganic arsenic through polluted drinking water and food (WHO, 2018). According to Chung *et al.* (2014), arsenic is another airborne contaminant that is linked to the surface area of particle matter emissions from fuel combustion and industrial activities. Trivalent and pentavalent arsenic are the two oxidation forms of arsenic that are present in airborne particulate matter (Islam *et al.,* 2015; Tirez *et al*., 2015).

Hotspot regions close to industrial activity have been shown to have significant concentrations of arsenic in particulate matter, despite the fact that this element is generally low in both rural and urban areas (Tirez *et al.,* 2015). People who live close to industries that smelt copper may inhale airborne arsenic due to occupational exposure. Owoade *et al*. (2013) reported that arsenic levels in $PM_{2.5}$ air samples were more than 300 times (0.20-0.47 μg/m^3) higher than the WHO's recommended threshold of 0.00066 μg/m^3 for a 1:1,000,000 carcinogenic risk from inhalation. Furthermore, trivalent arsenic is the predominant species in $PM_{2.5}$ and the most dangerous to humans, according to Tirez *et al*., (2015) study on arsenic speciation in PM_{10} and $PM_{2.5}$ air

monitoring. While inhalation exposure typically occurs at a low concentration of around 1%, human exposure to arsenic and the health concerns associated with it is more widespread in contaminated food, water, and soil (Chung *et al.,* 2014).

1.4.2 Lead

Lead is found in the environment naturally, but human activity has significantly increased the amount of lead in the ecosystem. For instance, Lead is added to metals during their manufacturing and then released during the recycling of waste metal, which might contaminate plants and soil. Lead concentrations in agricultural soils were found to be higher than the maximum of 375 µg/g (Sembhi *et al.,* 2020) in previous studies on the environmental effect of the soil surrounding a metal recycling factory in Mexico (Miguel and Hector, 2016).

Negative health impact most particularly in children result from lead exposure by consumption of tainted food and drinking water, inhalation of contaminated air or dust, and/or other means (Kumar & Singh *et al.,* 2019; Kendall *et al*., 2019). One of the main ways that lead to air pollution is through anthropogenic activities such as such as burning fossil fuels, extracting, processing, and recycling metals, as well as using lead in industrial settings (UNEP, 2010). Lead has been previously used by battery manufacturing firm for the production of lead-acid batteries even though it was previously prohibited from being used as a gasoline additive. Even with the prohibition, lead is still manufactured on a lesser scale, but when it is used as a single commodity to make lead-acid batteries, it is recycled more often (*Mineral Commodity Summaries, 2023*).

1.4.3 Cadmium

One heavy metal that is quite concerning for both the environment and the workplace is cadmium. It is present in the crust of the earth in large quantities, with an average concentration of 0.1 mg/kg. The International Agency for Research on Cancer (IARC) has classified cadmium as a carcinogenic dangerous chemical (category 1), meaning that it is known to cause cancer (Ding *et al.*, 2022). Mining, smelting, metals processing, and other human uses such as phosphate fertilizers Ni-Cd batteries, and industrial discharges are the main human-caused dispersal pathways through air emissions (Ding *et al*., 2022). Cadmium can build up in the liver and kidneys because it is soluble in water, it is harmful to human metabolism and biological processes (Rani *et al.,* 2014; Qasem *et al.,* 2021).

When Cadmium buildup is compared to other PM-bound metals like lead and manganese, the concentration of cadmium in fine particles is lower (Arshad *et al.,* 2015; Huq *et al.,* 2023). Cadmium contained in small particles nevertheless presents a serious health concern due to inhalation that can cause immediate toxic consequences, consequences, such as such as elevated blood pressure, even at low concentrations (Cakmak *et al*., 2014). People who live close to cadmium-emitting industrial companies have health concerns about human exposure to cadmium (Mittal *et al*., 2020). Lead and cadmium may enter the human body and go to the brain, where they can cause Alzheimer's disease.

1.4.4 Nickel

Nickel is a versatile element that may be used to produce alloys when mixed with other elements due to its malleability, hardness, ductility, and reasonable conduction of heat and electricity (*Mineral Commodity Summaries, 2024*). Nickel is utilized in the fabrication of nickel-metal

hydride and nickel-cd batteries. Nickel is a common and abundant heavy metal in the environment because of its uses (Kim *et al.,* 2014).

In general, nickel's distribution in the environment is comparable to that of the heavy metals that were previously covered. As a result, both human and natural processes release nickel particles into the atmosphere (Abe *et al.,* 2019). In the 1980s and early 1990s, natural emissions of nickel into the atmosphere ranged from 8 million kg/year to 30 million kg/year, according to the Agency for Toxic Substances and Diseases Registry (2005). The primary source of nickel in the ambient air is fossil fuel burning, followed by anthropogenic atmospheric emissions and nickel mining, processing, and smelting (Xu *et al.,* 2016; Abdin *et al,* 2020).

According to Kim *et al.* (2014), indoor smoke from domestic activities such as home heating, using stainless steel appliances, and cooking fuels, as well as vehicle exhaust emissions, are additional human sources of nickel in the atmosphere. Environmental and health concerns are associated with airborne and PM-bound nickel in industrial/urban hotspots for nickel production, processing, and recycling (Tsai *et al*., 2006 ; Das *et al.,* 2015). In comparison to the concentration of 1-3 ng/m^3 reported in rural regions, the air emission of nickel in metropolitan areas ranges from 5-35 ng/m^3, according to WHO (2007). The three main ways that humans come into contact with nickel are through food, drinkable water, and skin absorption. Many ecological species may become toxically exposed to environmental nickel buildup (Joseph *et al.,* 2023). The degree of concentration, speciation, and exposure route are some of the variables that affect nickel toxicity (Xu *et al.,* 2016). For instance, human urine nickel content and the prevalence of nickel sensitization have both been related to inhaling higher ambient air concentrations of nickel (Karpińska and Kotowska, 2019).

It has been discovered that long-term exposure to nickel compounds and $PM_{2.5}$-bound nickel increases the risk of kidney, lung, fibrosis, nasal cancer, cardiovascular, and pulmonary disorders as well as an increased incidence of daily death (Laden *et al*., 2000; NCI, 2019).

Airborne nickel in cities and industrialized regions has significantly decreased in recent years as a result of the enforcement and implementation of legislative and technical initiatives to reduce air pollution and related dangers to human health (Kim *et al*., 2014). However, a number of national and international organizations and agencies continue to list nickel, particularly soluble nickel compounds, as one of the most dangerous chemicals due to its toxicity and potential for human carcinogenesis (WHO, 2000; NCI, 2019, Dwivedi *et al.,* 2022). Therefore, it is still crucial to monitor PM-bound nickel in various environmental media during pollution studies in order to look for violations of legal requirements and recommendations and to spot any possible threats to the environment and public health.

1.4.5 Chromium

About 0.037 percent of the earth's crust is made up of chromium, which is ranked 21st among other metals in terms of natural abundance (Afandy *et al.,* 2022). Natural chromium exists in oxidation states ranging from -2 to +6, with the +6 natural state (hexavalent) chromium being the most relevant for the environment. The amount of (+6) hexavalent Cr (VI) in the air, water, and soil has grown as a result of anthropogenic activities, particularly industrialization and urbanization (Cheng *et al.,* 2014; Huang *et al.,* 2014; Saleem *et al* 2022).

1.4.5.1 Sources and Environmental Impacts of Hexavalent Chromium

As a byproduct of industrial activities, burning fossil fuels, coating operations, and trash incineration, hexavalent chromium Cr VI and its compounds are released into the atmosphere (Tian, 2012; Abdin *et al*., 2020). For instance, according to reports, Cr VI makes up over one-third of the US's 2700–2900metric tons metric tons of chromium emissions (ATSDR, 2008). Similarly, in 2013, coating activities in the Toronto metropolitan area discharged 17 kg/year of total hexavalent chromium into the air (Toronto Public Health, 2015). Numerous studies have reported that hexavalent chromium enrichment in $PM_{2.5}$ is a hazardous air pollutant and human carcinogen (Huang *et al.,* 2014; Yu *et al.,* 2014). A study of hexavalent chromium in the air in Windsor, Ontario, Canada, revealed that the inhalable particle fraction has the highest concentration of Cr VI in the ambient air samples of the city, ranging from 0.1 to 1.6 ng/m^3. Lung and nasal cancer, as well as pulmonary disorders, have been related to human inhalation exposure to Cr VI in ambient $PM_{2.5}$ (Ding *et al*., 2022).

The extensive industrial usage and processing of chromium (Cheng *et al*., 2014) increases the amount of Cr (VI) released into the atmosphere, which then settles in soil. The entry of ambient hexavalent chromium into the soil may be caused by wind-borne ambient particulate matter, wet and dry atmospheric deposition, sedimentation of industrial wastewater, and leachate from chromium slag (Mavroulis *et al*., 2023). The inherent risk of hexavalent chromium poisoning to humans and its buildup in the ecosystem have drawn attention from all around the world to airborne pollution. Consequently, more regulatory actions have been taken to reduce airborne Cr(VI) pollution from the atmosphere and environment as a result of environmental monitoring of chromium and its speciation.

1.5 Instrument-Based Methods for Chemical Analysis

In general, this approach yields information on the particulate matter's elemental composition. X-ray fluorescence spectroscopy (XRF), proton-induced X-ray emission spectrometry (PIXE), ion chromatography (IC), flame atomic absorption spectroscopy (FAAS), graphite furnace atomic absorption spectroscopy (GFAAS), inductively coupled plasma-mass spectrometry (ICP-MS), inductively coupled plasma-atomic emission spectrometry (ICP-AES), scanning electron microscopy coupled with energy dispersive spectrometry or X-ray (SEM-EDS/EDX), etc. are some of the conventional analytical techniques The most often used techniques are XRF and PIXE since they are reasonably priced and non-destructive. After the particles have been extracted using the proper digestion processes, FAAS, GFAAS, ICP-AES, and ICP-MS are excellent methods for quantitative evaluation; ICP is employed for soluble metals. The sensitivity, particular sample preparation requirements, and analysis costs of the aforementioned analytical procedures set them apart (Conti and Tudino,, 2016).

1.5.1 Inductively Coupled Plasma Optical Emission Spectrometry (ICP-OES)

Using plasma and a spectrometer, inductively coupled plasma-optical emission spectrometry, or ICP-OES, is a method used to identify the elements present in digested materials. This kind of emission spectroscopy creates excited atoms and ions that release electromagnetic radiation at wavelengths specific to a given element by using an inductively coupled plasma.

It has unique advantages such as analysing multiple elements simultaneously, higher sensitivity, provision of improved accuracy and precision results, broader dynamic range and faster analysis time over FAAS instrument.

1.5.1.1 Working principles of ICP -OES

The elemental composition of a sample may be ascertained using the potent analytical method known as inductively coupled plasma optical emission spectroscopy. spectroscopy. The following steps can be used to categorize the ICP-OES working principles:

1. **Sample Introduction:** The sample is typically digested or dissolved in an appropriate acid to break down its matrix. A small volume of the prepared sample is then introduced into the sample collection aided by the peristatic pump.
2. **Nebulization:** The sample solution is converted into a fine aerosol mist using a high-pressure nebulizer. This helps in generating a consistent sample stream for analysis. Analysis.
3. **Plasma Generation:** The aerosol mist is introduced into a plasma torch, typically using an argon gas flow. The plasma torch generates a high-temperature plasma flame (up to 10,000 degrees Celsius) in which the sample atoms are vaporized and ionized.
4. **Atomization and Excitation:** The vaporized sample atoms, now in the form of ions, are subjected to intense heat and energy in the plasma flame. This leads to the atomization of the ions, causing them to release energy in the form of photons.
5. **Light Emission:** The photons emitted by the atomized ions have characteristic wavelengths that correspond to specific elements or atomic species in the sample. These emitted photons are collected by a spectrometer.
6. **Spectral Analysis:** The collected photons are dispersed by a grating or prism and directed onto a detector. The detector measures the intensity of the emitted photons at various wavelengths, creating a spectral pattern for the elements present in the sample.

7. **Data Analysis:** The spectral patterns obtained from the detector are compared to a calibration curve or database of known elemental signatures. This allows for the identification and quantification of the elements present in the sample.
8. **Quantification:** The intensity of the emitted photons is used to determine the concentration of each element in the sample. The calibration curve or standards of known concentrations are used to establish a linear relationship between the intensity of the emitted photons and the concentration of the element.
9. **Reporting:** The final results are typically expressed in terms of elemental concentrations, either as weight percentages, parts per million (ppm), or parts per billion (ppb), depending on the application.

Overall, ICP-OES offers high sensitivity, wide dynamic range, multi-element capability, and low detection limits for the analysis of trace and major elements in various samples.

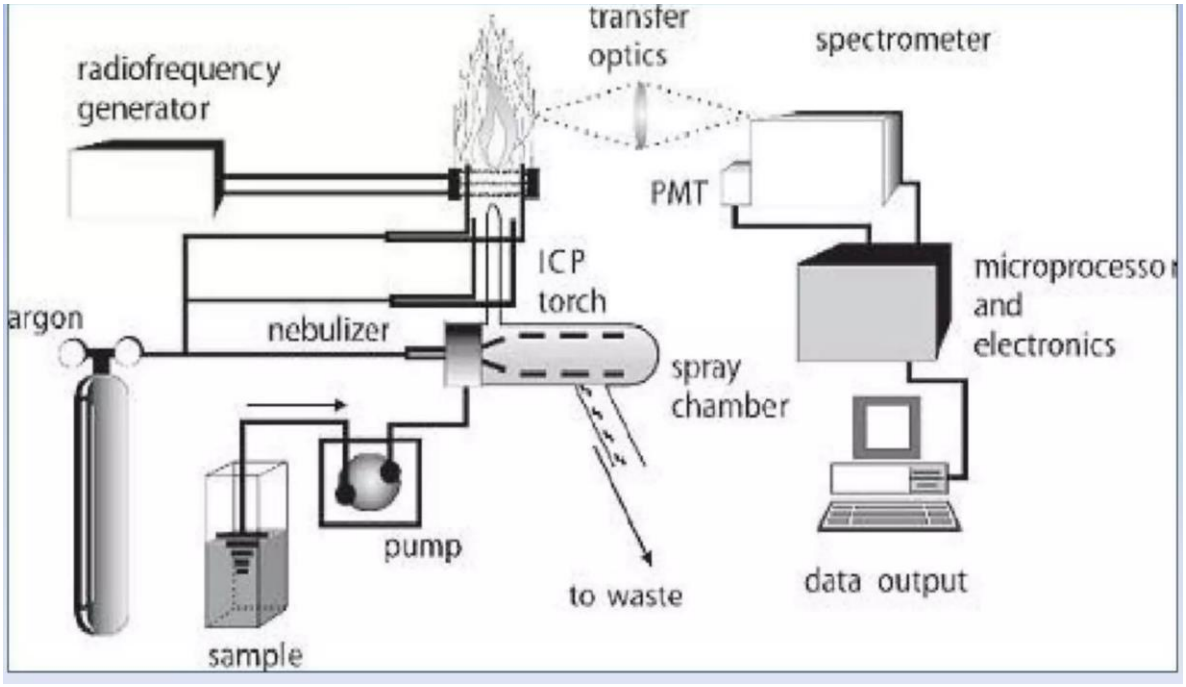

Figure1.3: Schematic diagram of ICP-OES instrumentation

1.5.1.2 ICP-OES instrumentation

ICP-OES consists of the following four essential parts**;**

a) **The sample introduction system**

The sample introduction system is responsible for converting the sample into an aerosol and introducing it into the plasma

b) **The excitation source (plasma)**

The excitation source (plasma) is where the atoms are excited and emit spectrum rays

c) **The spectrometer (for wavelength selection)**

The spectrometer is used to separate element-specific wavelengths of light and to focus the resolved light onto the detector as efficiently as possible

d) **The detector**

The detector measures the derived signals and processes them to quantify the elemental composition.

Each of these components performs specific tasks which will be explained in the next slides.

Before an ICP-OES can begin the analysis, the sample solvent must be removed, any residues vaporized, and existing molecules split into atoms.

The sample introduction system is responsible for converting the sample into an aerosol and introducing it into the plasma

1.5.1.3 ICP-OES Methodology

The samples and standards must be ready for introduction to the ICP before beginning any analysis. The aforementioned phase is contingent upon the physical and chemical properties of the specimens, ranging from a straightforward dilution to an intricate sequence of chemical reactions

and other preparatory measures (Xiandeng and Bradley, 2017). Next in the analysis is the hardware to be utilized and the procedure for introducing the sample. The basic sample introduction mechanism that comes with the instrument will be enough for the majority of ICP-OES studies. Programming the instrument to carry out the data collection and processing processes using the computer software that comes with the instrument is the next stage in developing an analytical technique. In order to do this, choices must be made about the sample analysis itself, emission measurement, equipment calibration, wavelength selection, and operating parameters. The instrument manufacturer's recommended default settings will yield good results for a large number of studies. The analysis may start as soon as the standards and samples are ready, the computer is programmed, and the hardware is configured correctly. Typically, the analyst begins by adding the first standard solution to the plasma and using the computer keypad. If all goes according to plan, the analyst proceeds to finish the instrument's calibration by adding additional standards (if applicable) and a blank solution. Samples are introduced after the calibration if no more calibrations or checks are needed. Following sample analysis, the findings can be tallied and published as needed (Rodolfo Fernández-Martínez, 2016).

1.5.1.4 ICP-OES Applications

(i) Farming and Foods

Using ICP-OES technology, a wide variety of food and agricultural items have been examined. Plant materials, soils, fertilisers, foods, feedstuffs, animal tissues, and bodily fluids are some examples of sample kinds. The elements Ca, Cu, Fe, Mg, Mn, P, K, Na, and Zn in baby formula were examined.

1.Trace metal levels in wine and beer can be found (Xiandeng and Bradley, 2017)

(ii) Medical and Biological

1. The sample is frequently contaminated with traces of the very elements being assessed in the sample when surgical instruments including scalpels, needles, scissors, and forceps are used.
2. levels of Cr, Ni, and Cu in urine measurements.
3. the measurement of Al in blood.
4. Cu content in brain tissue determination.
5. Se content measurement in the liver.
6. Ni content in breast milk determination.
7. B, P, and S values in bone are determined.
8. identification of trace elements in the tissues of tuna and oysters.

(iii) Earth Science

1. Major, minor, and trace compositions of different rocks, soils, sediments, and associated materials are determined.
2. ICP-OES is primarily utilised in this industry for prospecting reasons.
3. Application areas for this approach include marine geochemistry and the origins of rock formations.
4. calculating Uranium in material of ore grade.
5. investigation of several metals in river sediments.
6. Major, minor, and trace element analysis of carbonate drill cores.
7. finding the rare earth elements present in a given rock formation.
8. Plankton analysis for several components.

(iv) Metals

1. Identifying the primary, trace, and hazardous ingredients in coal and slags.

2. As, B, Bi, Ce, La, P, Sn, and Ta analysis of low alloy steels; high-precision Si determination in steels;
3. Finding impurities in high-purity aluminium.
4. Xiandeng Hou and Bradley (2017) conducted an analysis of superconducting materials to check for trace pollutants.
5. Metal analysis in air sample check online

1.6 $PM_{2.5}$ Surveillance Tools

Using both integrated and continuous approaches is a basic idea in the detection of mass concentrations of PM in ambient air. Particulate matter mass time-weighted averages are used into the integrated technique. In order to do this, filter-based gravimetric samplers are used, which adsorb the particulates onto a filter before weighing them in a laboratory. High volume samplers, dichotomous samplers, particle air samplers, Micro-Orifice Uniform Deposit Impactors (MOUDI), and stacked filter samplers are a few types of gravimetric samplers (Soto-Garcia *et al.,* 2011). On the other hand, the continuous technique uses direct reading devices to measure PM mass in real-time on a minute-by-minute cycle, providing the actual result of the particle concentrations as they are detected. Piezoelectric microbalance, beta attenuation monitor (BAM), dust track aerosol monitor, and Tapered-Element Oscillating Microbalance (TEOM) are a few cutting-edge technologies that can be used for automated continuous monitoring of Particulate matter (Huang *et al.,* 2022). In various contexts, time-weighted average $PM_{2.5}$ levels are estimated using gravimetric samplers. In contrast to real-time $PM_{2.5}$ samplers, they typically require lengthy averaging times to gather sufficient mass (Drventic *et al.,* 2023). Continuous automatic real-time

sampling can detect temporary elevations brought on by periods of air pollution or variations in the weather, as well as measure 10-second average concentrations.

1.6.1 Media Filtering

Air can be collected through a variety of filter media to acquire samples of atmospheric particulate matter (PM). The type of sampler, the filter's properties, and—most importantly—the analytical technique employed all influence the choice of filters for particle sampling. High particle collection efficiency, low blank values, low flow resistance, loading capacity, mechanical stability, chemical stability, artefact formation, cost, availability, and compatibility with analytical techniques are additional factors that are generally taken into account when choosing a filter media. Particle deposit measurement is not appropriate for filters with extremely high and fluctuating blank levels (Jantzi *et al*., 2016).

Teflon membranes, Teflon-coated glass fibres, glass fibres, quartz fibres, nylon membranes, cellulose fibres, etched polycarbonate membranes, and other materials can be used to capture atmospheric particulates. Since none of the previously described filters are appropriate for every kind of chemical analysis, a variety of filters may be needed depending on the intended chemical characterisation.

Nevertheless, polytetrafluoroethylene (PTFE), glass fibre, polytetrafluoroethylene-bonded glass fibre, and quartz filters are the best types of filters for gathering $PM_{2.5}$ samples. This is due to the measurement of mass concentration as well as a number of other chemical elements linked to $PM_{2.5}$, including polycyclic aromatic hydrocarbons, elemental carbon, ions that are soluble in water, organic carbon, and volatile organic carbon (Perrino *et al.,* 2013).

The majority of analytical instruments can determine elements and gravimetrically using PTFE filters. Due to their extreme insensitivity to relative humidity, they are mostly utilised in gravimetric analysis. They also have the lowest blank for metals and perform better when used for elemental analysis. In chemical analysis, filter blanks are typically examined in addition to sampling filters to account for interferences and impurities introduced into the sample by the filter media (Sause and JasiūNiene, 2021).

1.7 Pollution indices

A helpful tool for communicating risks is the pollution index (PI). The public is informed about local ambient air pollution levels and associated health risks through the use of pollution indices. According to Irudayaraj *et al* (2023), the Pollution indices (PIs) may also be used to predict an area's future pollution levels. Additionally, they alert the local regulatory authority to the need for pollution control and mitigation actions in order to enhance the quality of the air in the studied region. Usually, ranges are used to organise the PI values. A value is assigned to each range, indicating the public health advice for the population that is exposed (USEPA, 2012, Iyengar *et al.,* 2019). The Contamination Factor (CF), Degree of Contamination (DC), and Pollution Load Index (PLI) are just a few of the techniques that have been developed and used to assess the contamination status of the heavy metal concentrations and their hazardous reaction.

1.7.1 Degree of Contamination (DC) and Contamination Factor (CF)

To determine how much particulate matter has been contaminated by trace metals, utilise the Contamination Factor (CF). The CF technique made use of a single pollution index that serves as a direct reflection of environmental indicator pollution. Use of the contamination factor technique allowed for the determination of the level of heavy metal contamination in $PM_{2.5}$ released by the iron and steel smelting plant. In particular, a single heavy metal's CF is established by:

$$CF = \frac{\text{mean conc. of each heavy metals from each sample}}{\text{mean conc. of heavy metals in background sample}} \quad (2.6)$$

The CF is classified into four main groups (Du *et al.,* 2013; Nasr *et al*., 2006):

Where CF ≤ 1 = low;

CF ≤ 3 = moderate;

CF ≤ 6 = high; and

CF > 6 = very high contamination.

Degree of contamination (DOC) is an indicator that shows the extent to which the ambient air is polluted. The DOC is computed as the sum of CF for each heavy metal above the mean concentration of background sample according to the following formula:

$$\mathbf{DOC} = \sum_{i=1}^{n} CF_i \quad (2.7)$$

Where DOC ≤ 1 = low;

1 ≤ DOC ≤ 3 = medium; and

DOC > 3 = high.

Four major grades have been established for the degree of contamination: < 8 indicates low degree of contamination, 8−16 shows moderate degree of contamination, 16−32 implies considerate degree of contamination and > 32 shows a very high degree of contamination (Uslu et al., 2023)

1.7.2 Pollution Load Index (PLI)

The pollution load index (PLI) is a simple but comprehensive means of assessing air quality by providing an estimation of the metal contamination status of the ambient environment under consideration and the necessary action that should be taken by the government or environmental control agencies (Sam *et al*., 2015). In this study, the PLI was evaluated for the extent of metal

pollution as geometric mean value, which is the nth root of the product of the CF of the respective metals (Pobi *et al*.,2019). PLI calculated the geometric mean of CF value PLI is computed by the equation 2.8 (Pobi *et al.,* 2019):

$$PLI = (CF_1 \times CF_2 \times CF_3 \times \ldots \times CF_n)^{1/n} \text{ or}$$

$$PLI = \sqrt[n]{CF_1 \times CF_2 \times CF_3 \times \ldots \times CF_n} \quad (2.8)$$

where: n is the number of different heavy metals (n = 8 in this study): and, CF is the contamination factor of individual heavy metals present in the air samples.

With PLI < 1 = background, PLI > 1 = contamination.

1.8 Apportionment of Sources

The process of assigning emissions from different sources of pollution to the concentrations of air pollution at a certain place and for a specific amount of time is known as source apportionment. This strategy has the following advantages:

1. ascertains whether particular hotspots or monitoring locations surpass compliance thresholds; (ii) recognises important contaminants of concern;
2. may distinguish between the primary and secondary contributions in the particulate matter's chemical composition;
3. provides source impact calculations;
4. Determine which sources would be easiest to manage; and
5. stays clear of the uncertainties related to the necessary meteorological inputs and emission inventories.

1.8.1 Calculating Source Apportionment Methods

There are two methods for allocating sources: dispersion modelling and receptor modelling.

1.8.1.1 (i) Model of Dispersion

These are a set of formulas that explain how air pollutants behave mathematically. According to this model, the concentration of pollutants in a certain environment may be anticipated at a given distance from the source by applying physics, chemical calculations, and mathematics.

1.8.1.2 (ii) Receptor Model

Using data from pollutant concentrations, the receptor model determines and measures the origins of air particles as well as their respective contributions (US EPA, 2015b, Klimont *et al*., 2017). A crucial part of managing air quality is modelling, which necessitates keeping an eye on atmospheric concentrations. In order to identify common sources of contaminants, these concentrations are considered as natural tracers and statistically assessed (Van Sebille *et al.,* 2020). When compared to the dispersion model, it is the source apportionment technique that is most frequently utilised. For the purpose of allocating the sources of pollutants at receptor locations, a number of receptor models, including enrichment factors (EFs), factor analysis, chemical mass balance (CMB), principal component analysis (PCA), cluster analysis, and fourier transform time series, have been employed (Belis *et al.,* 2014, Pipalatkar *et al*., 2014). In source apportionment studies including aerosol pollutants, principal components analysis (PCA), positive matrix factorisation (PMF), and chemical mass balance (CMB) are the three techniques most frequently utilised in Nigeria. Principal component analysis (PCA), cluster analysis, and enrichment factor are some of the receptor models that will be covered and used in this study.

1.8.1.3 Factor of Enrichment (EF)

In atmospheric research, source apportionment studies typically employ the enrichment factor (EF) correlation approach. The EF is computed for both sea and crustal salt sources in atmospheric investigations. A crust is utilised as a reference material to determine the crustal enrichment factor (ERc); on the other hand, sea salt is employed to calculate the marine enrichment factor (ERm). The most often employed elements that serve as reference elements for ERc are Al, Fe, and Li. Moreover, Na serves as the ERm's reference element. Equation is used to calculate the enrichment factor.

Equation 2-1 shows that the concentration of an atmospheric element is represented by Cx, while reference materials are represented by Cr, which is mentioned above. The element's source can be determined by comparing the aerosol's Cx/CR ratio to the reference medium. It can be determined that the element has a crustal or marine source if the ratio is nearly equal to unity. On the other hand, as EF typically have a geologic or natural origin, we may deduce that the element has an anthropogenic origin if the value is significantly higher than 1 (Hamzehpour *et al.,* 2022).

1.8.1.4 Principal Component Analysis (PCA)

Because PCA converts a group of linked variables into a set of uncorrelated variables, it is an exploratory statistical technique used to identify the main sources of air pollution (Bharati *et al*., 2022). The main applications of principal component analysis are information extraction and data reduction. This is one of the most popular multivariate statistical methods used to extract the linear relationship between a set of variables and provide information on the pertinent parameters with the least amount of original data loss. The number of independent variables is equal to the number

of transformed variables, also known as Principal Components, or PCs. According to Awad, and Khanna (2015), the first PC has the greatest percentage of data variability, whereas the second PC has the largest percentage of variability not shown in the first component. Since the PCs produced by PCA are not easily interpreted, they must be rotated using the orthogonal rotation method (varimax). The varimax rotation yields new variable groups known as Varimax Factors (VFs), which are useful in determining the various potential causes of air pollution. The Kaiser Criterion for Eigenvalues determines the statistical significance of PCs and states that those with eigenvalues larger than or equal to one are the PCs that are selected (Guo *et al.,* 2018). The fundamental factor behind PCA's success is its capacity for chemical interpretation of eigenvectors (Chen *et al,* 2013; Faaique, 2023).

1.8.1.5 Analysis of Clusters

In a broad family of data-analysis techniques, cluster analysis seeks to discover groupings, or clusters, of related objects that are typified by a multivariate feature set. The most popular cluster analysis technique is hierarchical cluster analysis (HACA). Using the original data matrix, HACA creates a suitable matrix of object similarity measures, combining the most similar pair of objects to create a new “clustered” item. The process is ongoing and is deemed finished when every object has at least one cluster. For cluster analysis, the Euclidean distance metric is a more popular similarity metric. A two-dimensional graphic called a dendrogram, or "tree diagram," which depicts similarity levels and the mergers that occur at subsequent levels, is used to illustrate how the clusters are categorised. The dendrogram's horizontal axis shows the items and clusters, while the vertical axis shows the separation or dissimilarity between clusters. Clustering techniques are

popular and frequently used because hierarchical clustering approaches may reduce complex multidimensional data in a systematic and two-dimensional manner (Khraisat *et al.,* 2019).

1.9 Trace Metals bound to $PM_{2.5}$ Review

Since $PM_{2.5}$ size is linked to a number of health problems and the degradation of the environment's air quality, there have been a lot of recent studies on the transit and transformation of $PM_{2.5}$ over TSP. Odekanle *et al*. (2016) examined the coarse and fine particulate matter fractions during the rainy and dry seasons in an industrial district of Lagos State, Nigeria. For a period of four to twenty-four hours, both fractions were collected using a low-volume Gent Stacked Filter Unit sampler. Compared to the fine particle fraction, which had a mass concentration range of 10 to 462 $\mu g/m^3$, the coarse fraction had a greater range, 86 to 8765 $\mu g/m^3$. In a portion of the sites under investigation, the concentrations of six elements (Cr, Mn, Fe, Cu, Zn, and Pb) detected in both fractions of the particles were higher, which suggests potentially harmful effects on human health. Similarly, in five urban locations in Abuja, north-central Nigeria, Abiye *et al.* (2013) measured the mass and elemental concentration of $PM_{2.5}$ and PM_{10} airborne particulate matter. Using a proton-induced X-ray emission (PIXE) spectrometer and a "Gent" stacked filter unit sampler fitted with a double stage filter in series, the 18 elements in both fractions were sampled and characterised. According to the results, PM_{10} had a larger particle mass concentration than $PM_{2.5}$. The PM_{10} percent contained the majority of the elements, and the results of their correlation matrix showed that many metals had strong, significant correlations ($r > 0.53$ to 0.90). The baseline $PM_{2.5}$ concentration, as well as the geographical and temporal change, were recorded by Aziakpono *et al.* (2013) in Isoko land, Delta State, Nigeria. The sampling of airborne particle matter was done using the Microdust Pro real-time dust meter. The particle mass concentration result that was

obtained fell between 4 and 310 μg/m^3. According to their findings, every sampling site had $PM_{2.5}$ levels over the national ambient air quality standard limit (NAAQS) for 24 hours. Additionally, compared to the wet season, the dry season recorded noticeably greater levels of particle mass loadings.

In Ife, Nigeria, Owoade *et al*. (2015) recently looked into the chemical makeup and source identification of $PM_{2.5}$ and $PM_{2.5}$-10 fractions. Using a low volume GENT sampler, samples were obtained using nucleopore polycarbonate filters. The fine PM component measured had a mass concentration ranging from 14.4 to 986.5 μg/m^3. These levels are higher than the 35 μg/m^3 allowable daily limit (NAAQS) for $PM_{2.5}$. X-ray fluorescence (XRF) was used to determine the elemental composition. Mn, Ni, As, Cd, and Pb were measured at high amounts. Additionally, the four source categories that contributed to the fine fraction were identified by positive matrix factorisation (PMF) as follows: coking coal (83%), soil (10%), metallurgical industry (6%), and electronic waste processing (1%). The particulate matter pollution in an industrial and a non-industrial area of Lagos state was evaluated by Okuo *et al*. (2019). Atomic absorption spectroscopy was used to do elemental analysis. The findings demonstrated that in the industrial region and control area, respectively, the mass concentration of the particle varied from 41.62 to 88.80 μg/m^3 and 51.28 to 190.48 μg/m^3. The principal component analysis revealed five possible sources of contamination. Pb, Cd, Cu, Ni, and Na were found to be severely enriched in almost all of the sites, whereas K and Ca were found to be moderately enriched, according to the enrichment factor analysis. A baseline study on TSP in an indoor microenvironment of a Lagos state residential area was conducted in 2018 by Okuo *et al*. Over the course of a year-long sampling program, samples were gathered using a portable high-volume sampler. The results revealed that during the sampling

period's wet and dry seasons, there was a high concentration range of 833.32-1944.45 μ g/m^3 and 1111.11-2777.78 μ g/m^3, respectively. Principal Component Analysis was used to identify three possible sources, and as a result, it was determined that the concentration of contaminants in the majority of the sites exceeded the safe levels suggested by regulatory organisations.

Okuo *et al*. (2019) also used a pre-weighed filter paper and a portable air metric sampler to collect samples for their investigation on the chemical composition and source apportionment of $PM_{2.5}$ in industrial and non-industrial sites in Lagos. Heavy metals in respirable dust and PM near industrial locations in Kano, Kaduna, and Jos were also examined by Ayua *et al*. (2020). In several of the regions under investigation, the levels of Cd, Ni, and Pb were found to be higher than the WHO-established standard limits. Strong correlations between PM and heavy metals were found in the study, indicating that industrial activities were the true source of the toxins.

Research on $PM_{2.5}$ has also been done in other countries. According to this research, especially in industrialised and urbanised areas, anthropogenic activities have greatly increased the average burden of particulate matter over time (Lee *et al.,* 2021). Using inductively coupled plasma mass spectrometry (ICP-MS) and the microwave aided acid digestion method, the levels and sources of $PM_{2.5}$ bound trace metals from Canadian locations were examined. The results showed that human activity greatly increased ambient $PM_{2.5}$ loadings. According to Li *et al* (2022), sites near industrial facilities and high traffic regions exhibited higher levels of trace metals compared to sites situated in areas with similar land use. Silwana *et al* (2017) conducted a study evaluating standard operating procedures used in Rustenburg, South Africa, metal analysis and air particle matter monitoring. Tapered element oscillating microbalance was used for sampling, and ICP-MS and scanning

electron microscopy combined with energy dispersive spectrometry (SEM-EDS) were used to analyse the particulate matter's elemental concentrations. The order of the assessed filters' efficiencies was teflon-coated glass fibre, ringed-teflon, and quartz filters. Si, Fe, Mg, K, Na, and C were the elemental compositions found on ringed-teflon filters using the SEM-EDS, whereas Fe, Al, Ca, Mg, K, Na, Cr, Ni, Pb, Cu, Zn, and Mn were found using the ICP-MS. Based on the findings, it was concluded that ICP-MS is a preferable instrument for metal analysis. In Coccia (2020) looked into seasonal fluctuations in the elements and fine particulate matter concentrations. In comparison to the summer (18.1 μg/m^3), the mean values of $PM_{2.5}$ were higher in the spring (23.2 μg/m^3). The summer time decreases in $PM_{2.5}$ levels was linked to an increase in precipitation. ICP-MS was used to analyse the following metals: Zn, Cd, Fe, Mn, Cu, Cr, Pb and Ni. The results for metals likewise revealed higher levels in the spring than in the summer. These seasonal fluctuations were ascribed to variations in the weather, particularly the direction of the wind. Road dust and industry were identified by the principal component analysis as the main sources of hazardous heavy metals and $PM_{2.5}$ at the sampling site for the $PM_{2.5}$-bound metals. Qiao *et al*. (2013) examined twelve-hour $PM_{2.5}$ samples that were taken in Guiyang, China, using an air particulate sampler. On each sampling occasion, twelve hours were dedicated to the process of sampling. Using a Kevex energy dispersive X-ray spectrometer, elemental analysis was performed (XRF). Ti (30±22 ng/m^3), Mn (250±400 ng/m^3), Fe (340±280 ng/m^3), Zn (290±330 ng/m^3), and Pb (130±130 ng/m^3) were all found to be at significant levels in the results. The observed data led to the conclusion that the temporal variability of heavy metals was caused by local anthropogenic sources. Chen *et al.* (2015) looked at Beijing, China's ambient air quality and the effects of the new ambient air quality standard from 2012. When compared to the other five pollutants (ground-level ozone, carbon monoxide, sulphur oxides, nitrogen oxides, and lead), $PM_{2.5}$ was found to be

the primary contributor to the air quality index (AQI) based on results derived from the computation of the index, which includes monitoring of $PM_{2.5}$. Furthermore, a spatial study of the air quality showed that urban and suburban stations had air quality above the national level, whereas the national standard was only reached at a backdrop station. Khan *et al*. (2016) recently carried out research on fine particulate matter, health risk assessment, and source allocation in Southeast Asia (SEA). Through the use of a high-volume air sampler operating around the clock, PM2.5 samples were taken during various seasons. The findings demonstrated that there was a 48% and 19% deviation, respectively, from the national ambient air quality standard (NAAQS) set by the US EPA and the World Health Organisation (WHO) for $PM_{2.5}$. ICP-MS was used for instrumental analysis, and As, Pb, Cd, Ni, Mn, V, and Cr were found. Using positive matrix factorisation (PMF) 5.0, five possible sources of contamination were found. As was the heavy metal that was cancerous and harmful to health. According to the results, there was a 3–4 lifetime cancer risk per million individuals at the study site related with exposure to dangerous $PM_{2.5}$-bound metals.

Asghar *et al*. (2024) used a Youngteng YT-HPC 3000a handle particulate counter to collect samples in order to evaluate the levels of PM $_{2.5}$ and PM $_{10}$ and the health risks associated with them in Hanpur, Pakistan.

CHAPTER TWO

MATERIALS AND METHODS

2.1 MATERIALS

2.1.1 Chemicals / Reagents

1. Trioxonitrate (v) acid (Loba Chemie)
2. Silical gel
3. Double distilled water
4. Hydrofluoric Acid (Loba Chemie)
5. Hyperchloric acid

2.1.2 Apparatus/ Equipments

1. Four digit scale (Mettler Toledo)
2. Apex 2Is Casella standard pump
3. Conical Inhalable Sampling (CIS) head
4. Agilent 72 ICP-OES Instrument
5. Professional weather monitoring equipment
6. Desiccators
7. Muffle Furnace (Carbolite AAF-1100)
8. 37mm Polytetrafluoroethylene (PTFE) Teflon filters
9. Polyurethane foam (PUF)
10. Crucibles and Lids
11. Beakers
12. Tweezer

13. Funnel

14. Conical flasks

2.2 Description of the Study Area

Ogun State, one of Nigeria's most industrialized states with a population of 3,751,140 as of 2006, served as the research's study area (NPC, 2016; OGS), with a geographical size of 16,762 km³, Ogun State is now the 24th largest state in Nigeria and the 16th most populous state in terms of landmass (Aderoju, 2015). Ogun State is a state in southwest Nigeria, situated between latitudes 70º 5′ N and 70º 20′ N and longitudes 3° l7′ E and 30º 27′ E in the derived Savannah region. It shares boundaries with the Republic of Benin to the west, Lagos State to the south, Oyo State and Osun State to the north, and Ondo State to the east. The majority of Ogun State is covered in rain forest, with a woody savanna in the northwest. The two common seasons in the region are the wet season, which runs from March to September, and the dry season, which runs from October to February. These seasons correspond to the weather in Nigeria, a tropical region of West Africa (Aderoju, 2015). The headquarters and largest city of Ogun State is Abeokuta; other significant cities in the state are Sagamu, the principal Kola nut-growing region in Nigeria, and Ijebu Ode, the royal capital of the Ijebu Kingdom (Oludare, 2021). The state is known as the "Gateway to Nigeria" and is a significant hub for industry in Nigeria, with a large concentration of industrial estates.

2.2.1 Description of Sampling Sites

The research location region, as depicted in Figure 2.1, is made up of two industrial areas: the Ode-Lemo Farm Settlement (OLF) as a background area and the Ogijo Metal Recycling Factory (OMRF) and Sagamu Interchange Industrial Estate (SIIE). These locations are all found in Ogun State's Sagamu Local Government. The sampling sites were found using a land-laid Garmain-GPS MAP 765-type global positioning system. Table 2.1 shows the coordinates and main activity at these places. In order to generate a representative sample that accurately reflected the sampling of the study areas, great consideration was given to the ease of access, operator safety, equipment security, and the presence of anthropogenic activities responsible for air pollution while choosing the receptor locations.

As shown in Fig.2.1, the Metal Recycling Factory (MRF) is situated in Ogijo, under the Sagamu Local Government, and its geographic coordinates are longitude 3° 30³ 55.8 and latitude 6° 41³ 57.9. The study area is primarily surrounded by metal recycling factories (MRFs), with a few other industries like food processing, cement, and polymer. These industries are located in densely populated residential areas and do not follow any particular pattern. These factories are well-connected by easily accessible roads, only a few meters apart, and share a similar source of emissions. This region may be the greatest receiver of trucks loaded with scrap metal from all across the states, as well as home to what is perhaps Nigeria's largest MRF business. As a result of these scrap metals being recycled into billets and iron rods, there are large stockpiles of scrap metal hills and slags that are disposed of as waste in the nearby area, creating harmful emissions. The land usage surrounding the sampling location includes burning of garbage, construction

activities, industrial emissions, road dust from unpaved roads, heavy metal-enriched soil pollution from metal scraps, and poisonous vapours from metal recycling facilities' chimneys. substantial truck exhaust, air pollution from dust, and a stockpile of leftover metal, etc.

The master plan of Sagamu interchange, which links Abeokuta, Ibadan, Ore, and Lagos, respectively, designates the Sagamu Interchange Industrial Estate (SIIE) sampling site as an industrial zone (Fig. 2.2). The site's primary land use practices are controlled by the manufacturing and processing sectors. Among these are industrial emissions from the food and beverage processing, brewing, and agro-allied sectors. A few further examples of anthropogenic activity are building projects, car emissions, agricultural methods, the production of concrete blocks, food vendors, exposed quarry materials, and the burning of diesel as an alternative to hydropower for energy.

As seen in Fig. 2.3, Ode-Lemo Farm Settlement (OLFS) is a town located in the Sagamu Local Government area of Ogun State, Nigeria, to the south of Sagamu. Its geographic coordinates are 3° 40° 0° East and 6° 45¹ 0° North. Southwest Nigeria. Situated a short distance between Lagos and Imota, the town is on the border of Ogun and Lagos states. The trading and cultivation of kolanuts are among the Ode-Lemo people's economic pursuits. For this investigation, OLF is regarded as a backdrop site. The main uses of the land surrounding the site are construction, agro-waste dumpsite, bush burning as a pre-planting operation, planting, harvesting, pest control, a farm house where small-scale construction and repair of farm tools are carried out, re-suspended dust from unpaved roads, ploughing, a farm store, farm machinery operation, and construction.

Tables 2.1, 2.2, and 2.3 show the site description, coordinates, and principal local emission sources of the corresponding sampling points, respectively. There are two distinct seasons in the research areas: dry (November–April) and wet (May–October). While April is noted for moderate to high wind speeds, July is dominated by high temperatures and frequent rainfall, and October features high temperatures and consistent, heavy rainfall. January is characterized by cold air, no precipitation, and greater wind speeds. In Sagamu, harmattan incidents typically occur during the dry season.

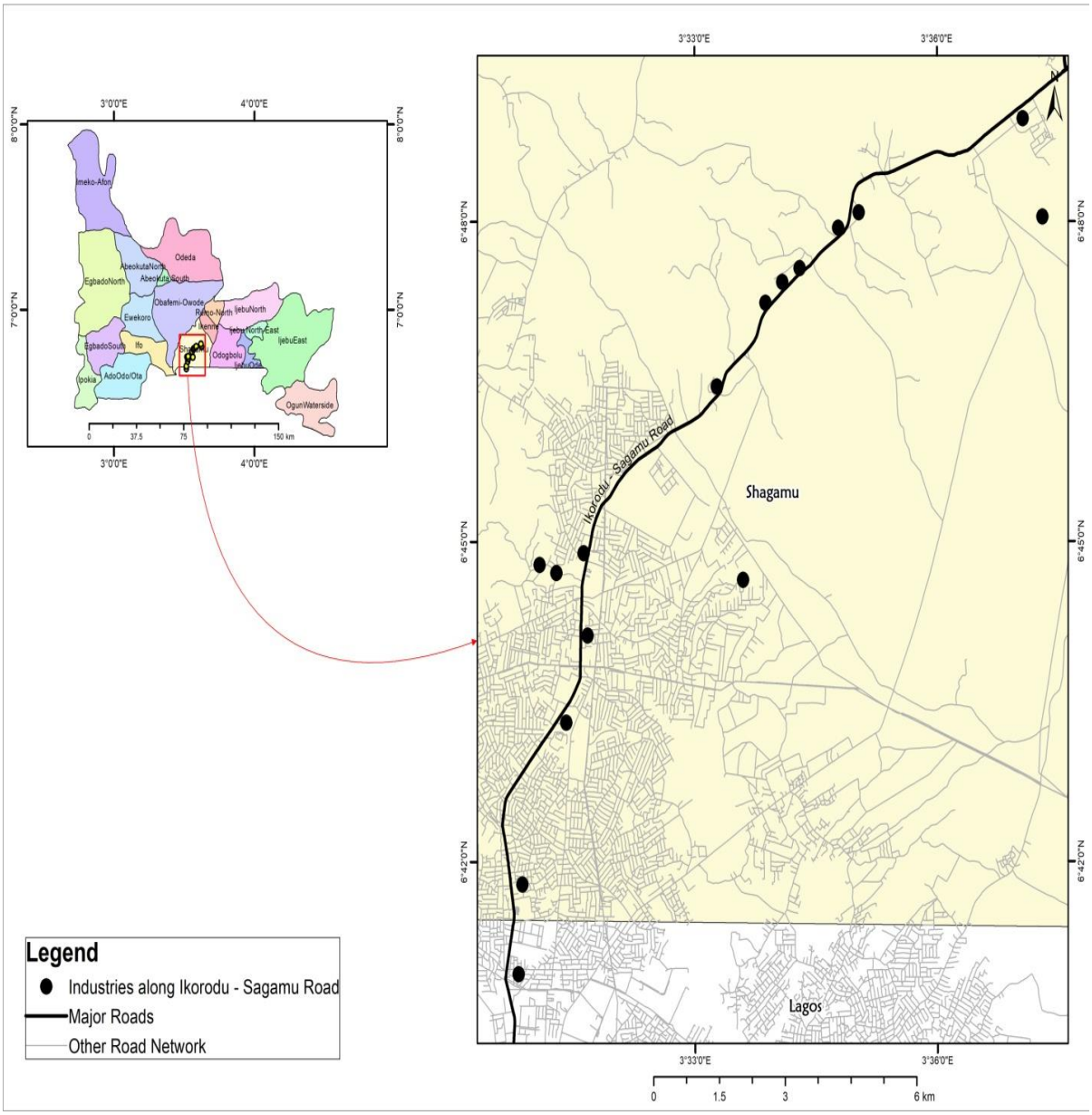

Fig. 2.1 Sampling sites of industries along Ikorodu- Sagamu (Insert; Map of Ogun state displaying the study area)

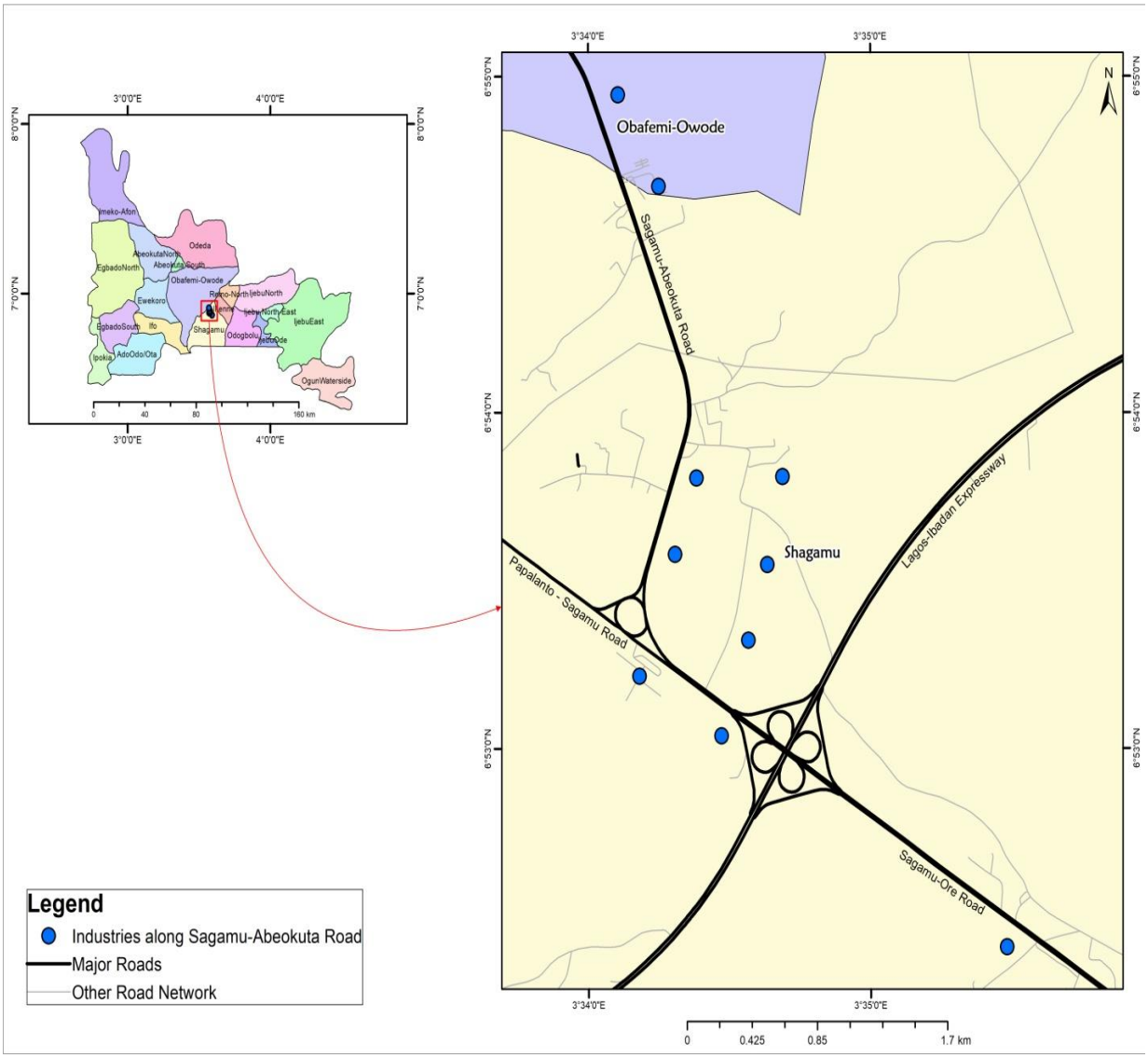

Fig. 2.2 Sampling sites of Industries along Sagamu-Abeokuta (Insert; Map of Ogun state displaying the study area)

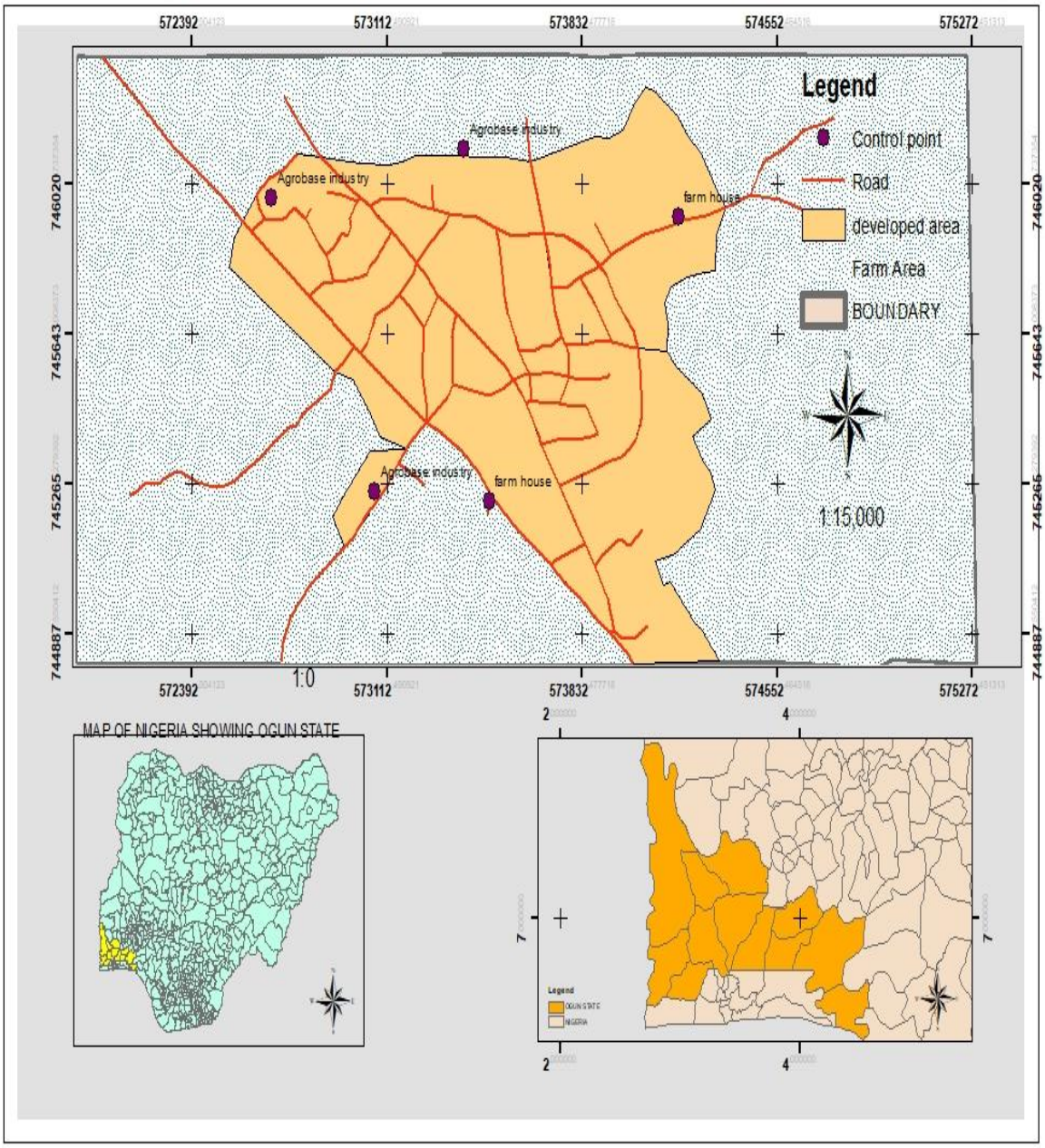

Fig. 2.3: Background Sampling site
(Insert; Maps of Nigeria and Ogun state displaying the study area)

Table 2.1 Monitoring stations and major emission sources along Ogijo – Sagamu road, in Ogun state

S/N	Site / Location	Code	Coordinates	Site Description/activities
1	Production factory opposite Military Barak.	ISA	6° 40' 31.7119" N, 3° 30' 44.6304" E	Vehicular traffic, fuel station, residential houses commercial shops
2	Polymer factory at around Ita Oluwo.	ISB	6° 41' 19.1620" N, 3° 30' 41.0644" E	Vehicular emission, solid waste, farming activities, mechanic workshops, churches, schools
3	Metal recycling factory at Odogun, Sagamu road	ISC	6° 43' 14.1191" N, 3° 31' 07.7314" E	Recycling of scraps, mechanic workshop, farming, wind blow dust. Smelting of iron
4	Metal recycling industry At PZ Estate junction	ISD	6° 43' 56.0021" N, 3° 31' 33.4116" E	Industrial emission, combustion of solid waste, vehicular emission
5	Metal recycling factory (Phoenix)	ISE	6° 44' 46.8870" N, 3° 31' 15.2896" E	Burning of fossil fuel. Smelting of iron, industrial emission, road dust
6	Iron and steel smelting factory at Gbaga	ISF	6° 44' 47.5080" N, 3° 31' 13.2055" E	Residential houses, dust storm, traffic emission, industrial emission, commercial activities
7	Metal recycling factory Ita Sanni	ISG	6° 44' 47.6785" N, 3° 31' 36.3990" E	Smelting of iron, dust, mechanic workshops, fuel station, hotel Residential, heavy trucks parks.
8	Iron and Steel Smelting Factory (Energy)	ISH	6° 46' 19.2791" N, 3° 33' 06.9632" E	Iron slag waste, residential houses, industrial emission, vehicular emission, residential houses, food vendors, road dust
9	Metal Recycling Factory Lukosi	ISI	6° 46' 19.2791" N, 3° 33' 06.9632" E	Residential houses, vehicular emission, commercial activities, industrial emission, mosque,
10	Quarry processing plant Sawmill	ISJ	6° 47' 05.3495" N, 3° 33' 42.2316" E	Farming activities, road dust. Tipper Park, residential houses church, Busy market.
11	Metal Recycling Industry At Mosimi	ISK	6° 47' 16.1469" N, 3° 33' 54.1349" E	Industrial emission, fossil fuel combustion, vehicular emission, road dust, residential house, NNPC depot.
12	Food Processing Industry (Niger)	ISL	6° 47' 24.8295" N, 3° 34' 04.4396" E	Residential houses, industrial emission, vehicular emission, School, Church, Bush burning
13	Metal Recycling Industry Abara	ISM	6° 47' 47.5889" N, 3° 34' 34.4380" E	Industrial emission, Abbattor, road School, farming activities, residential houses.

14	Quarry and granite processing plant.	ISO	6° 47' 59.6214" N, 3° 34' 48.0049" E	Unpaved road, mechanic shop, solid waste, residential houses Road construction, road dust,Bush burning
15	Iron and Steel Processing Factory (Shotubo)	ISP	6° 47' 58.0223" N, 3° 37' 02.5177" E	Farming activities, Residential, road dust, schools, Industrial emission road construction, unpaved road, Police Station.
16	Cement production factory (Lafarge)	ISQ	6° 48' 56.4690" N, 3° 36' 40.9925" E	Industrial emission, solid waste, road dust, farming

Table 2.2 Monitoring stations and major emission sources along Sagamu – Abeokuta road, in Ogun state

S/N	Site/Location	CODE	Coordinates	Site description/Activities
1	Wires & Cables Factory at Sagamu-Ore, road Junction	SAA	6° 52' 32.6568" N, 3° 35' 25.4465" E	Vehicular emission, car park, farming activities.
2	Food and Beverage Industry close to Sagamu -Abeokuta Interchange	SAB	6° 53' 10.6360" N, 3° 34' 23.8444" E	Industrial emission, vehicular emission, farming activities, residential houses
3	Flour mill Factory A at interchange close by	SAC	6° 53' 28.0524" N, 3° 34' 28.2642" E	Brewing industry, schools, vehicular emission, solid waste,
4	Flour Mill Factory B at interchange close by	SAD	6° 53' 36.3209" N, 3° 34' 30.5225" E	Industrial emission, commercial shops, residential houses, parks
5	Polymer Factory along Sagam-Abeokuta road	IAGE	6° 53' 55.0065" N, 3° 34' 35.5631" E	Brewing industry, schools, vehicular emission, solid waste,
6	Food & Beverage Industry Sagam - Abeokuta road	SAF	6° 53' 21.6947" N, 3° 34' 07.4678" E	Vehicular emission, farming activities, road dust, food, beverage industry, gas plant
7	Agro-allied Food Processing Factory	SAG	6° 53' 35.4325" N, 3° 34' 11.0033" E	Manufacturing industry, car parks, shops, industrial emission, vehicular emission
8	Agro -allied processing industry	SAH	6° 53' 52.2275" N, 3° 34' 17.7033" E	Feed waste, vehicular emission, commercial activities, food vendors
9	Brewery Industry along Abeokuta Road	SAI	6° 54' 46.2312" N, 3° 34' 06.9496" E	Industrial emission, trucks park, vehicular emission, road dust, gas plant
10	Animal feeds Processing Factory along Sagam-Abeokuta Road	SAJ	6° 55' 04.8681" N, 3° 33' 58.3039" E	Industrial emission. Shops, farming activities, fuel station, vehicular emission

Table 2.3: Description of a Background sampling sites and major local emission sources of ODE-LEMO in Sagamu, Ogun–state

S/N	Site / Location	Code	COORDINATES	SITE DESCRIPTION/ACTIVITIES
1	Palm oil processing unit.	OLA	6°44'54.254"N 3°39'27.785"E	Made shift houses. unpaved road
2	Agro-based processing industry	OLB	6°44'30.146"N 3°39'40.133"E	Farming activities, ploughing, tiling
3	Cassava flake processing industry	OLC	6°44'58.201"N 3°39'50.894"E	farm operational machine, cropping, harvesting, plowing
4	Animal Feeds milling factory	OLD	6°44'29.354"N 3°39'53.950"E	Unpaved road, dust,
5	Farm house/store	OLF	6°44'52.640"N 3°40'16.755"E	Agro waste. Biomass burning

2.3 Sampling Strategy for Particulate matter

The study involved the selection of 32 receptor sites, which were subsequently reduced to three (3) locations based on the similarity in the modes of operation and clustered nature of these industries. Triplicate samples were collected each month for a period of one year making a total of 108 air samples . Standard methods were also used to measure and record the meteorological data concurrently during collection of the samples

2.3 Sampling of $PM_{2.5}$

Sampling of $PM_{2.5}$ involved the collection of fine particulate matter along with meteorological data for subsequent elemental analysis.

2.3.1: Filter Preparation

To remove the impact of humidity and get precise $PM_{2.5}$ readings, the filters were equilibrated in a desiccator for 24 hours prior to and following sampling. Then, using a four-digit scale (Mettler Toledo Me 204), 37 mm diameter polytetrafluoroethylene (PTFE) Teflon filter sheets were weighed three times. Laboratory blank and field blank filters were gathered to lessen the gravimetric distortion.

2.3.2 Equipment Preparation and Set up

Standard techniques were employed to gather ambient air $PM_{2.5}$ samples, utilising a gravimetric sampler, an Apex 21s Casella standard pump, and conical inhalable sampling (CIS) head (plates 5 and 6). Samples were collected at a flow rate of 3.5 L/min simultaneously with weather data using a specialised weather monitoring equipment. Eight (8) hourly sampling per day was carried out. A sampling height of 2.5 meters above the ground which is within human breathing zone was maintained throughout the sampling period. Following the sampling process, a charged desiccator

was used to equilibrate the filter, cassette containing the $PM_{2.5}$ small particles and PUF before they were weighed. Before doing additional analysis, the $PM_{2.5}$ filter papers were taken out using a tweezer, placed in a petri dish, conditioned, weighed in triplicates, and refrigerated at 4 °C to avoid heat decomposition and escaping of volatile constituents.

PUF Filter Head Cap

PUF Filter Holder ($PM_{2.5}$)

Silver Grid & Quartz filter

Cassette Housing

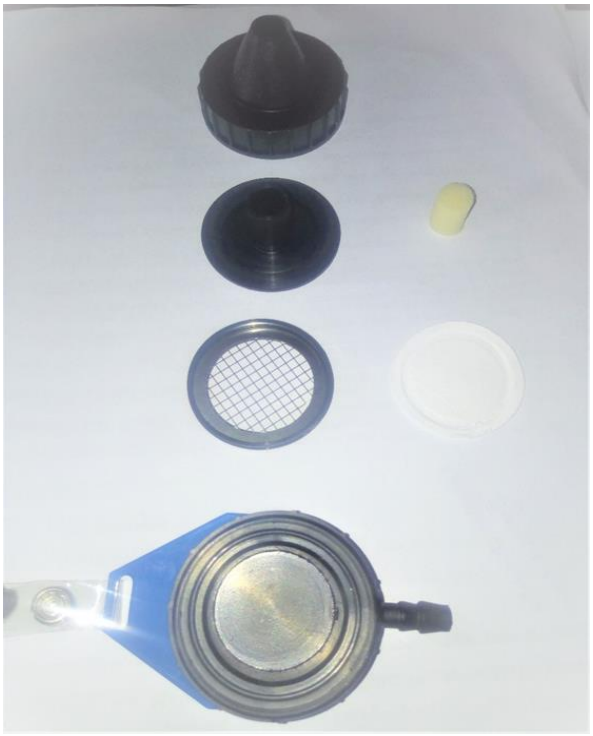

Plate 1: CIS Conical Inhalable Sampling Head

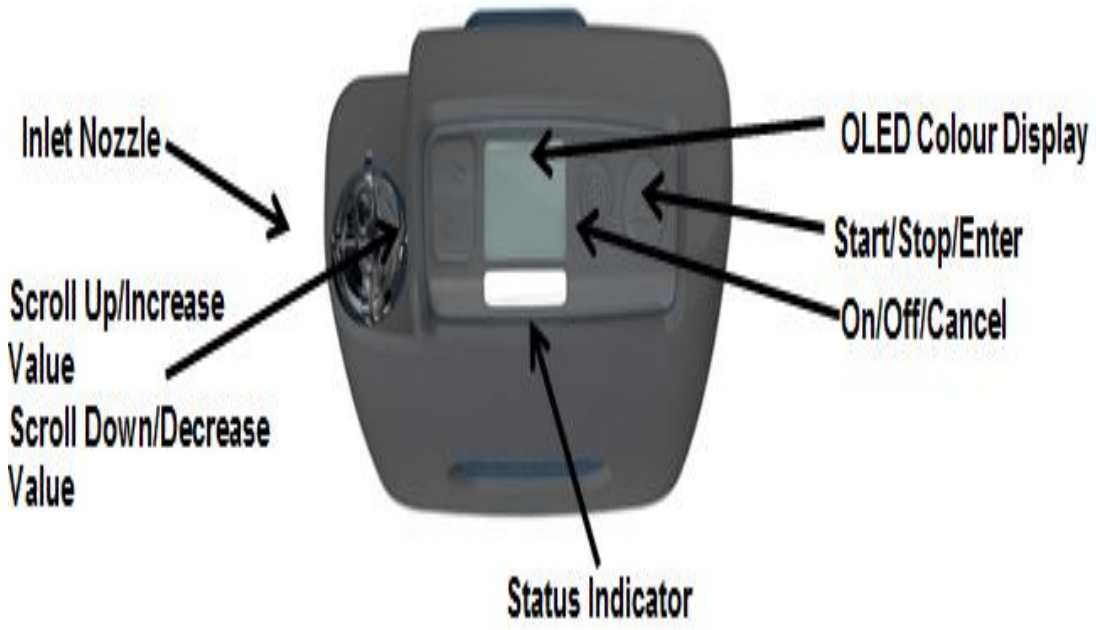

Plate 2: Apex21s Air Sampling Pump (Casella)

Plate 3: Apex2Is Standard Pump Fitted to Conical Inhalable sampler supported with Professional weather station equipment

2.4 $PM_{2.5}$ Mass Concentration Determination

The gravimetric analysis method was used to determine the particle mass concentrations. To do this, deduct the blank filter's initial average mass from the sampled filter's final average mass. An electric micro-weighing balance (Mettler Toledo Me 204) was used to weigh filters repeatedly until a consistent result was achieved. The observed flow rate and the sampling duration were used to calculate the total volume of air that the sampler gathered (CEPA, 2002; US EPA, 1999b, Dris *et al.,* 2017). The following equation was then used to calculate the mass concentration of $PM_{2.5}$ in the ambient air:

$$M_{2.5} = M_{f(2.5)} - M_{f(2.5)}\, X\, 10^6. \qquad (2.1)$$

where:

$M_{2.5}$= total mass of fine particulate matter collected during sampling period (µg)

$M_{f(2.5)}$= final mass of conditioned filter after sample collection (g)

$M_{i(2.5)}$= initial mass of conditioned filter before sample collection (g)

10^6= unit conversion factor for grammes (g) to microgram (µg)

Therefore,

$$PM_{2.5} = \frac{M_{2.5}}{V} \qquad (2.2)$$

$PM_{2.5}$= mass concentration of $PM_{2.5}$ particulate (µg/m^3)

V= total volume of air sampled (m^3)`

$$V = Q_{avg} \times t \times 10^{-3} \qquad (2.3)$$

Q_{avg}= average flow rate over the entire duration of the entire sampling period 3.5 (L/min)

t =duration of sampling period in minutes

10^{-3}= unit conversion factor for litres (L) into cubic metre (m^3)

A pre- and post-field calibration of the pump was carried out for each field sampling to meet the recommended flow rates of ± 10% for each sampling period (Ashley, 2016)

2.5 Meteorological Data Collection and Analysis

An automatic weather monitoring system (a professional weather station) mounted at 2.0 meters above ground level at each sampling location close to the $PM_{2.5}$ sampler recorded the daily mean meteorological data from the parameters such as ambient temperature, rainfall, relative humidity (RH), wind speed (WS), wind direction (WD), solar radiation, and ultraviolet radiation. It was designed to retain memory and gather data in every five minutes. Using the weather-smart application, the collected measurements were transferred to a computer (Liu *et al.,* 2016). Data on the weather were gathered for both the rainy and dry seasons.

2.6 Elemental Analysis

The elemental characterization of $PM_{2.5}$ was carried out using ICP-OES instrument

2.6.1 Digestion of Particulate filters for ICP-OES analysis

The gathered PTFE filter was divided into two equal portions, one of which the filter's half was utilised to measure the heavy metal content. After being reduced to extremely small fragments, this half filter was transferred into a Teflon container. After that, 4 hours at 170 °C were spent in an oven with 10 mL of nitric acid, 3 mL of perchlorate acid, and 1 mL of hydrofluoric acid added. The gadget was not used for thirty minutes. After that, a heater was set up behind a hood and the lids of Teflon containers holding acids and pulverised filters were carefully opened. This was done to give the acids time to dry completely (between 90 and 100 °C). Double-distilled water was used

to dilute the contents of the Teflon containers to a volume of 25 ml after they had dried. Finally, a 0.45-micron syringe filter was used to filter the resultant solution. Prior to ICP-OES analysis, the resultant solution was transferred into acid-washed polypropylene containers and refrigerated at 4 °C in accordance with US EPA procedure IO-3.5 (US EPA, 1999b).

2.6.2 Analysis of Metals using Inductively Coupled Plasma Optical Emission Spectrometry (ICP –OES)

All solution samples were analyzed for 16 metals, namely; Cr, Pb, As, Ni, Mn, Fe, Ti, Cd, Al, Ca, V, Zn, Cu, Mg, K, and Na, using Agilent 72 ICP-OES. Sample introduction was done using the Agilent SPS3 auto-sampler under the operating parameters specified in Table 2, while simultaneous measurement was achieved using the Agilent 72 ICP-OES with megapixel CCD detector. The device was operated and data was collected using Agilent Expert II software. Using the serial dilution procedure, suitable concentration ranges of working standards from the multi-element stock standard were established. The ICP-OES Expert software was used to construct a new spreadsheet, in to which the various sample codes were encoded. To assess the analytical precision, each sample was examined three times during the acid digestion and successive extraction processes. Samples were analysed concurrently with blank filters and field blanks.

Table 2.4. Operating conditions of the Agilent 720 ICP-OES Instrument

Parameter	Setting
Power	1 Kw
Plasma gas flow	15 L/min
Auxiliary gas flow	1.5 L/min
Spray chamber type	Glass cyclonic
Torch	Standard axial torch
Nebulizer type	Sea Spray
Nebulizer gas pressure	220 kPa
Pump speed	15 rpm
Sample uptake	30s
Replicate read time	30 s
Number of replicates	2
Sample delay time	20 s
Stabilization time	15 s
Rinse time	10 s
Fast pump	On

However, determination of metal concentrations was performed from prepared calibration curves, and each sample was analyzed in triplicate, and the mean concentration was calculated. The results obtained from trace metal analysis were converted from mg/L or ppm to µg/m^3 using equation 2.4 as reported by Muhammad *et al*., (2011)

$$C_s = \frac{(C_1 - C_b)V}{V_o} \tag{2.4}$$

Where

C_s = concentration of metals in µg/m^3

C_1 =metal concentration in solution of samples in mg/L

C_b = metal concentration in the solution blank of in mg/L

V= volume of the sample solution in (100 mL)

V_o = sampling air volume (m^3) at standard condition

$$V_o = \frac{V_r \times 298}{1000T} \tag{2.5}$$

V_r = sampling air volume at ambient condition (L/Min)

T= Average temperature during sampling (K)

2.7 Examining Statistics

XLSTAT PRO 2015 was used to perform basic statistical parameters, correlation analysis, and multivariate statistical procedures such as Enrichment factor, Principal Component Analysis (PCA), and Hierarchical Agglomerative Cluster Analysis (HACA) on the dataset.

2.7.1 Factor of enrichment

A thorough analysis of the chemical composition is required to identify the many sources of pollution and pinpoint the amount of human influence (Mihai, 2021). The distinction between soil and man-made sources was made by enrichment factor (EF) calculations. The enrichment factor (EF) is commonly employed in the identification of the anthropogenic source of metallic elements. It is primarily utilised to demonstrate the extent of enrichment of a particular element in relation to its relative abundance in crustal materials (Changela *et al*., 2021). To distinguish between the anthropogenic and crustal sources of atmospheric heavy and light metals, enrichment factors (EFs) were computed (Diana *et al.,* 2022). The following relationship is typically used to define the Enrichment Factor (EF): EF= [(E/R) crustal / (E/R) sample] (2.9) where R is the reference element for crustal material and E stands for considered element. The concentration ratio of E to R in the particulate matter sample is denoted by (E/R) sample, whereas the mean concentration ratio of E to R in the crust is denoted

by (E/R) crustal. According to Huang *et al*. (2010), EF levels around unity imply a crusted origin, those below 1.0 point to a potential metal mobilisation or depletion, while EF values above 1.0 point to an anthropogenic origin for the element. Five forms of contamination are identified and understood in accordance with (Birth, 2003). Fe was employed in this work as a reference element to calculate the EF in relation to crustal abundance.

2.7.2 Matrix of Pearson Correlation

To find the metals' Pearson correlation matrix, statistical analysis was performed on the trace metal concentrations in $PM_{2.5}$ samples. At the 0.05 level, correlation was deemed significant (Basha *et al*., 2014; Mustaffa *et al.,* 2014).

2.7.3 Analysis of Principal Components

A multivariate statistical technique called principal component analysis (PCA) is utilised to determine potential origins for the items that have been found. By putting up a set of new variables based on the interrelations found in the original data set, PCA breaks down the number of elements into components. The PCA did not include any elements that were detected at levels lower than the limit of detection in more than half of the samples. When an element was found in less than 50% of a given sample and its concentration was below the limit of detection, the concentration was taken to be half the limit of detection. This was carried out in order to prevent the need for additional data set reduction (Mustaffa *et al*., 2014). According to Taira *et al.* (2017), equation may be used to determine the principal components (PCs).

$$Z_{ij} = a_{1i}x_{1j} + a_{2i}x_{2j} + \ldots\ldots\ldots a_{ni}x_{nj} \quad (2.10)$$

where:

Z = component score,

a= component loading,

x = measured value of the variable,

i = component number,

j = sample number and

n = total number of variables.

In order to compute the PCs, the variables were arranged so that the first variable (PC) explained the largest percentage of the variability in the original data. The largest percentage of the variability not described by the first PC is explained by the second PC. To improve the link between the PCs and the original variables, varimax rotation was used. According to Montgomerie *et al.* (2021), varimax rotation makes sure that each variable has a near-zero correlation with the other components and a maximal correlation with just one component. Only PCs with significant values whose eigen value is greater than one (1) were taken into consideration in order to derive the new varimax factors. The scree plot indicated the number of elements that were kept in each scenario.

2.7.4 Hierarchical Agglomerative Cluster Analysis (HACA)

A statistical technique called HACA is used to group or cluster variables. Using Ward's approach and Euclidean distance measurement, HACA was used to investigate the spatial connections between the items. This required measuring the distances between them, creating a visual representation of the clustering of these items, and publishing the findings as a dendrogram (Shah *et al.,* 2012; Latif *et al.,* 2015).

2.8 Development of Mathematical Models for predictions of toxic Metals in the study areas

The Meteorological data generated in this work study from the months of February 2022 to January, 2023 were used to develop a mathematical model for the prediction of toxic metals. The data were represented in the form of equation.

$$y = f\ (x_1, x_2, x_3, x_4, x_5, x_6 x7\ ) \tag{2.11}$$

where y = concentration of metals[5]

X_1 = wind speed value

X_2 = humidity value

X_3 = temperature value

X_4 = pressure value

X_5 = rainfall value

X_6 = wind direction value

X_7 - $PM_{2.5}$

Using the provided data and an integrated solver tool in `R Software version 2024, two (2) distinct models were produced. The experimental results were predicted using the models that were produced. Because this R software is a statistical program that is relatively easy to use even for those without much statistical training, it was employed in this study.

2.8.1 Error Functions Analysis

Error evaluation functions analytical model`s, which are mathematical representations of processes and are given in Equations 2.12–2.21, were applied to the experimental and expected data in order

to verify the degree to which the predicted data coincided with the experimental data (Olafadehan, 2021).

$$(ARE) = \frac{1}{N}\sqrt{\sum_{k=1}^{N}\left(\frac{y_{expt} - y_{pred}}{y_{expt}}\right)^2} \tag{2.12}$$

where *y expt* = experimental data

Y pred = predicted data

N = number of experimental data

$$ERRSQ = \frac{1}{N}\sum_{k=1}^{N}\left(y_{expt} - y_{pred}\right)^2 \tag{2.13}$$

$$MPSD = \frac{1}{N - N_P}\sqrt{\sum_{k=1}^{N}\left(1 - \frac{y_{pred}}{y_{expt}}\right)^2} \tag{2.14}$$

Where N_p = number of parameter(s) to be determined.

$$HYBRID = \frac{1}{N - N_P}\sum_{k=1}^{N}\left[\frac{\left(y_{expt} - y_{pred}\right)^2}{y_{expt}}\right] \tag{2.16}$$

$$RMSE = \frac{1}{N-2} \tag{2.17}$$

$$EABS = \sum_{k=1}^{N}\left(y_{expt} - y_{pred}\right) \tag{2.18}$$

$$x^2 = \sum_{k=1}^{N}\left[\frac{\left(y_{expt} - y_{pred}\right)^2}{y_{pred}}\right] \tag{2.19}$$

$$SEE = \sqrt{\frac{\sum_{k=1}^{N}\left(y_{expt} - y_{pred}\right)^2}{N-2}} \tag{2.20}$$

$$MRPE = \frac{1}{N}\sum_{k=1}^{N}\left(\frac{y_{expt} - y_{pred}}{y_{expt}}\right) \tag{2.21}$$

2.8.2 Statistical Modelling Analysis

As an additional tool for choosing a suitable model that accurately reflected the experimental data to a very high degree, statistical analyses were also conducted on the anticipated and experimental data. Equations 2.22–2.26 show the statistical instruments utilised in this investigation.

$$\boldsymbol{r} = \frac{\sum_{k=1}^{N}(\boldsymbol{y_{expt}} - \boldsymbol{y_{expt}}^{-})(\boldsymbol{y_{pred}} - \boldsymbol{y_{pred}}^{-})}{\sqrt{\sum_{k=1}^{N}(\boldsymbol{y_{expt}} - \boldsymbol{y_{pred}}^{-})^{2} \sum_{k=1}^{N}(\boldsymbol{y_{pred}} - \boldsymbol{y_{pred}}^{-})}} \quad (2.22)$$

where $y_{expt}{}^{-} = mean\ value\ of\ experimental\ data$

$y_{pred}{}^{-} = mean\ value\ of\ predicted\ data$

$$R^2 = 1 - \frac{\sum_{k=1}^{N}(y_{expt} - y_{pred})^2}{\sum_{k=1}^{N}(y_{expt} - y_{expt}{}^{-})^2} \quad (2.23)$$

$$K^2 = \frac{\sum_{k=1}^{N}(y_{expt} - y_{pred})^2}{\sum_{k=1}^{N}(y_{expt} - y_{expt}{}^{-})^2} \quad (2.24)$$

$$t - test = \frac{(y_{expt} - y_{pred}{}^{-})}{\sqrt{s^2\left(\frac{1}{N_1} + \frac{1}{N_2}\right)}} \quad (2.25)$$

Where $s^2 = standard\ error$

N_1 and N_2 = number of experimental and predicted data respectively (Rebecca ,2020)

$$F - test = \frac{\frac{\sum_{k=1}^{N}(y_{expt} - y_{expt}{}^{-})^2}{N-1}}{\frac{\sum_{k=1}^{N}(y_{pred} - y_{pred}{}^{-})^2}{N-1}} \quad (2.26)$$

2.9 Quality Control of Filters, Samplers, and Glassware

Throughout the whole study project, from sampling to data analysis and report preparation, a thorough quality assurance/quality control (QA/QC) program was maintained. Following rigorous adherence to specified standard operating procedures and thorough documenting of the sample logbook, field quality control, recovery tests, reproducibility tests, and method detection limits were rigorously carried out (US EPA, 1999a and US EPA, 1999b). It was made sure to clean the

sampler on a regular basis to prevent skewed findings. To avoid any surface contamination of the filters, all of the filters used for the samples were produced on a clean surface. Before the first weighing, the filters were visually examined in a dark room located in the laboratory for problems such as discoloration, filter nonconformity, and an uneven surface. Filters with detected flaws were thrown away. Using clean, smooth, non-serrated tweezers, filters were handled gently at the edge. For both the pre-weighed and post-weighed quartz filters, the identical microbalance was utilized. When returning from the field to the laboratory, each filter was equilibrated in a desiccator. The $PM_{2.5}$ filter was constructed using field and laboratory blanks. The purpose of the lab blanks was to look for any weight variations between pre- and post-sampling weigh-ins that may be caused by environmental contamination in the lab. Before the exposed filters were collected for post-sampling weighing, they were brought to the sampling location, placed in the sampler filter case, removed, and kept in a covered petri dish container within the sampler's case. All glass wares and filter assemblies were immersed in an ultrasonic cleaner (KQ 400KED) for a whole night, followed by an acid wash and oven drying to prevent contamination during the trace metal analysis process. To verify if the sample's filter sheets were interfering, blanks were examined.

CHAPTER THREE

RESULTS AND DISCUSSION

3.1 Spatial-Temporal Distribution of Fine Particulate Matter ($PM_{2.5}$)

The characterization of spatial variability is usually done to give a representation of the background particle. spatial factors such as topography, distance from a point source and combination of other pollutants affects fine particulate and levels from one location to the other.

Temporal variation shows how fine particles and related component varies with time. Meteorological variables and traffic intensity amongst other factors are known to contribute to the dispersion of fine particles and associated components (Fang *et al.,* 2016)

3.1.1. Spatial variation of $PM_{2.5}$ Concentration

Table 3.1 shows the descriptive statistics of monthly average concentration of $PM_{2.5}$ in the three Study areas. It is evident that there are significant variations in $PM_{2.5}$ concentration across different months with respect to each of the three locations. It can be observed that the monthly average concentration for OMRF, SIIE and OLFS locations ranged from 46.33 ± 2.52 to 389.67 ± 32.33, 32.67 ± 3.0 to 196.67 ± 11.59 and 18.33 ± 2.1 to 92.87 ± 4.0 $\mu g/m^3$ respectively. The peak value was 389.67 $\mu g/m^3$ (January at OMRF) and the lowest mass concentration was 18.33 $\mu g/m^3$ observed in July at OLFS site. The annual average concentration for the OMRF, SIIF and OLFS sites were 203.43 ± 14.6, 122.5 ± 5.7 and 60.42 ± 3.5 $\mu g/m^3$ respectively. These values exceeded the Nigerian Annual National Ambient Air Quality standard (NAAQS) of 35$\mu g/m^3$ and World Health Organization (WHO) guideline of 25$\mu g/m^3$ for $PM_{2.5}$. The highest concentration observed in the three sampling locations were 389.6 ± 33 $\mu g/m^3$ (ranging from 355 to 419 $\mu g/m^3$), in January,

196.67 ± 11.6 μg/m^3 (ranging from 186 to 209 μg/m^3 in January) and 92.67 (ranging from 89 to 97 μg/m^3 in December) while the lowest monthly mean concentrations observed in locations OMRF, SIIE and OLFS were 46.33 ± 2.52 μg/m^3 (ranging from 44 to 49μg/m^3 in July) 32.67 ± 3.0 μg/m^3 (ranging from 30 to 36μg/m^3 in July) and 18.33 ± 2.2 (ranging from 16 to 20 μg/m^3 in July) respectively.

Also, the lowest concentrations of $PM_{2.5}$ observed were 46.33 ± 2.52 (at OMRF in July), 32.67 ± 3.0 (at SIIE in July) and 18.33 ± 2.2 μg/m^3 (at OLFS in July) respectively. The Annual mean concentrations of the three study areas were 203.43 ± 14.65 (at OMRF site), 122.5 ± 5.75 (at SIIE site) and 61.42 ± 3.25μg/m^3 (at OLFS site).

The Annual mean concentrations of OMRF, SIIE and OLFS were 8:5:2.5 times higher than WHO standard of 25μg/m^3. This may pose serious health challenges on the young children and adults, within the vicinity of the industrial areas leading to short term health effects, such as coughing, asthma, difficulty in breathing, and worsening the cases of those with underlying health problems leading to eventual death, if the $PM_{2.5}$ concentration is not reduced and precaution not taken by persons living in that environment for 8–24 h (Zalakeviciute *et al*. 2018). This indicate that $PM_{2.5}$ pollution in Sagamu, Ogun State, Nigeria is of great health concern.

Table 3.1. Descriptive Statistics of Monthly Average Mass Concentration of $PM_{2.5}$ (ug/m^3) at different sites from January to December, 2022

	JANUARY		FEBRUARY		MARCH		APRIL	
Location of Sampling	**Range**	**Mean + S.D**	**Range**	**Mean + S.D**	**Range**	**Mean + S.D**	**Range**	**Mean + S.D**
OMRF	355 – 419	389.7 ± 32.3	297 – 340	320.3 ± 16.5	224 – 268	245.3 ± 22.0	142 - 190	164.7 ± 24.1
SIIE	186 – 209	196.7 ± 11.6	170 – 178	174.3 ± 4.0	154 – 166	160.8 ± 6.1	133 - 139	135.7 ± 3.1
OLFS	82 – 95	88.3 ± 6.5	67 – 77	70.7 ± 5.5	62 – 68	64.7 ± 3.1	53 - 60	56.3 ± 3.5

	MAY		JUNE		JULY		AUGUST	
Location of Sampling	**Range**	**Mean + S.D**	**Range**	**Mean + S.D**	**Range**	**Mean + S.D**	**Range**	**Mean + S.D**
OMRF	74 – 80	78.3 ± 3.1	56 – 59	57.5 ± 1.7	44 – 49	46.3 ± 2.5	58 - 73	65.7 ± 7.5
SIIE	51 – 76	64.3 ± 12.6	39 – 47	42.7 ± 3.0	30 – 36	32.7 ± 3.1	46 - 52	48.7 ± 3.1
OLFS	26 – 30	28.3 ± 2.1	20 – 26	22.7 ± 3.1	16 – 20	18.3 ± 2.1	34 - 39	36.3 ± 2.5

	SEPTEMBER		OCTOBER		NOVEMBER		DECEMBER	
Location of Sampling	**Range**	**Mean + S.D**	**Range**	**Mean + S.D**	**Range**	**Mean + S.D**	**Range**	**Mean + S.D**
OMRF	87 – 98	92.3 ± 4.2	104 – 117	109.7 ± 6.7	297 – 324	3103 ± 13.5	304 - 357	329.7 ± 26.5
SIIE	61 – 65	62.7 ± 2.1	75 – 95	84.7 ± 10.0	172 – 180	176.3 ± 4.0	175 - 183	180.3 ± 4.6
OLFS	62 – 67	64.3 ± 2.5	75 – 81	77.7 ± 3.1	78 – 83	80.7 ± 2.5	89 - 97	92.7 ± 4.0

3.1.2 Temporal Variation of $PM_{2.5}$ Concentration

Table 3.2 shows the mass concentrations of $PM_{2.5}$ in dry and wet seasons .It is evident that there is a significant variation in the levels of $PM_{2.5}$ with respect to each sampling locations.as shown in Table 3.2. for both within and across the seasons. The calculated average seasonal $PM_{2.5}$ concentrations for OMRF, SIIE and OLFS locations during dry season were 319.07 $\mu g/m^3$ (ranging from 245.33 to 389.67), 177.67 $\mu g/m^3$ (ranging from 160.67 to 196.67) and 79.40 $\mu g/m^3$ (ranging from 64.67 to 92 .67) respectively.

Also, the measured seasonal mean $PM_{2.5}$ mass concentration observed in wet season at locations OMRF, SIIE and OLFS were 87.79 $\mu g/m^3$ (ranging from 46.33 to 164.67) , 67.33 $\mu g/m^3$ (ranging from 32.67 to 135.67) and 43.43 $\mu g/m^3$ (ranging from 18.33 to 77.67) respectively.

The $PM_{2.5}$ values obtained for the dry season at locations OMRF, SIIE and OLFS exceed by 13:7:3 times greater than stipulated limits of values 25$\mu g/m^3$ and 9:5:2 times greater than the value of 35$\mu g/m^3$ stipulated by National Ambient Air Quality Standard (NAAQS). Thus, a clear seasonal pattern in the concentration of $PM_{2,5}$ was observed in the order dry > wet

The implication of these results includes high and variable pollution health risk. This include; cardiovascular disease, respiratory disorder, degradation of air and water quality, impacting biodiversity and soil health, increased health care expenses, reduction and lowering property values which may be tagged economic consequences of high pollution.

The observed high value of $PM_{2.5}$ during the dry season (November to March) may be attributed to various anthropogenic activities and meteorological condition such as increase in temperature, low precipitation from rainfall, low wind speed and low relative humidity recorded in the sampling environment. These elevated peaks of $PM_{2.5}$ concentration were observed in all the three locations

with the peak period from (November – February) due to strong dry wind (Harmattan) that aid long- range transport, Other Man-made contributing factors to increased $PM_{2.5}$ obtained in this study during the dry season include road dust re –suspension from the unpaved roads with metal scraps loaded heavy trucks plying the road leading to the industrial sites, vehicular emission road construction activities, biomass/ solid waste burning, smoke from industrial power generating plant and smelting activities. All these activities listed above are anthropogenic, so we can say that the variations in anthropogenic activities with respect to land use patterns in various sampling sites could be a major contributing factors to the observed differences in particulate matter level ..

The levels of $PM_{2.5}$ experienced a gradual decrease from the months of April – October. These months are characterized with increased rainfall, high relative humidity, high wind speed, low temperature and less anthropogenic activities resulting to decrease in mass concentration of fine particulate during wet season.

Table 3.2: Mass Concentration in dry and wet season for $PM_{2.5}$ (ug/m^3)

Months	OMRF	SIIE	OLFS
PM 2.5 (µg/m³) Dry season			
JAN	389.67±32.33	196.67±11.59	88.33±6.51
FEB	320.33±16.50	174.33±4.04	70.67±5.51
MAR	245.33±22.03	160.67±6.11	64.67±3.06
NOV	310.33±13.50	176.33±4.04	80.67±2.52
DEC	329.67±26.54	180.33±4.62	92.67±4.04
Seasonal average per location	**319.07±22.18**	**177.67±6.08**	**79.40±4.33**
PM 2.5 (µg/m³) Wet season			
APR	164.67±24.11	135.67±3.06	56.33±3.51
MAY	78.33±3.06	64.33±12.58	28.33±2.08
JUNE	57.50±1.73	42.67±4.04	22.67±3.06
JULY	46.33±2.52	32.67±3.06	18.33±2.08
AUG	65.67±7.51	48.67±3.06	36.33±2.52
SEPT	92.33±4.24	62.67±2.08	64.33±2.52
OCT	109.67±6.66	84.67±10.02	77.67±3.06
Seasonal average per location	**87.79±7.12**	**67.33±5.41**	**43.43±2.69**
Annual average per location	**203.43±14.65**	**122.5±5.75**	**61.42±3.51**
WHO Limit	25	25	25
NAAQS limit	35	35	35

3.1.3 Comparison of $PM_{2.5}$ levels with other Studies

Table:3.3 shows the comparison between this present study and previous studies on $PM_{2.5}$ air pollution. The data provided reveals significant variation in $PM_{2.5}$ concentrations across different Nigeria cities.

Table;3.3 Comparison of $PM_{2.5}$ results ($\mu g/m^3$) of this study with others from different Nigerian cities

S/N	Location	$PM_{2.5}(\mu g/m^3)$	References
1	Sagamu	61.42 – 203.43	The study
2	Lagos	15.63 – 65.61	Suriano *et al* 2024
3	Kaduna	37.2 – 135.7	Orogade *et al* 2016
4	Abuja	30.79 – 105.43	Lala *et al* 2023
5	Ile-Ife	9.1 – 236.6	Abulude *et al* 2021
6	Kano	22 – 110	Meseke *et al* 2022
7	Ilorin	44.36 – 60.70	Salami *et al* 2020
8	Owerri & Ezibe village	99.30 – 124.70	Nicholas and Ukoha 2023
9	Nsuka	57 – 106	Osimobi *et al* 2019
10	Port-Harcourt	7200	Akinfolarin *et al* 2017
11	Lagos	Dry (18.67 – 34.67) Wet (14.0032.67)	Okuo *et al* 2017

The results reported by Suriano *et al* in 2024 in eight (8) different locations for $PM_{2.5}$ concentration ranged (15.63 – 65.61 $\mu g/m^3$) in Lagos and Lala *et al* (2023) in Abuja ranged (30.79 – 105.43$\mu g/m^3$) were lower than (61.42 – 203.43$\mu g/m^3$) obtained in this study.

However, the results published by Abulude in 2021 and his research group for $PM_{2.5}$ in Ile-Ife were higher when compared to this study. Likewise, the results reported in Kano, (Meseke *et al* 2019), Nsuka (Osimobi *et al* 2019), Ilorin (Salami *et al* 2020) and Yenegoa (Abulude *et al,* 2022) were also lowered than the level of $PM_{2.5}$ obtained in this study. In addition, Okuo *et al* 2017 conducted a field study on $PM_{2.5}$ in an industrial area of Lagos State and obtained $PM_{2.5}$ level ranged from

14.00 to 32.67μg/m^3 during wet 18.67 to 34.67 μg/m^3 during dry season and found to be lowered in value when compared to this study.

It is evident that the level of $PM_{2.5}$ reported in all these studies were found to be above the stipulated guidelines set by WHO and associated with significant health risks. However, variation in anthropogenic activities, data collection methodologies and sampling period across different studies could have contributed to the differences

3.2 Spatial Variation of $PM_{2.5}$-Bound Metals in the Study Areas

The spatial variability of the fine particle bound trace metals in the study areas are discussed by comparing their atmosphere coverage concentrations with respect to meteorological factors and land use patterns.

The annual average trace metal concentrations in $PM_{2.5}$ for OMRF, SIIE and OLFS study areas are presented in Table 3.4. The monthly mean concentrations for the three study areas are depicted in appendixes i, ii and iii. It can be observed that Sixteen (16) metals were detected and quantified by the ICP-OES instrument as follow; Cr, Mn, Fe, Ni, V, Ti, Cu, Zn, As, Cd, Pb, Na, Mg, Al, K and Ca respectively.

The Crustal elements (Al, Ca, Fe, Mg Na and K) identified and quantified in this study were the predominant and most abundant species detected in all the three study areas. It can be observed that sodium had the highest concentration. The highest and lowest peak values of Na were 261.64 ± 24.66μg/m^3 and 24.99 ± 15.64μg/m^3 observed at OLFS and OMRF sites respectively. The least abundant crustal specie was Iron (6.07 ± 2.77μg/m^3) which was observed at SIIE site. In general, the concentration of elements is in the order of Na > K > Zn > Ca > Al > Mg > Fe. These crustal elements must have polluted the three sampling locations through various natural and anthropogenic activities. Paved and unpaved roads dust are the major sources of Ca, Al, Fe, Mg,

Zn, Na and K from the individual area. The rate of dust re-suspension from the loaded heavy trucks is high during the peak of dry season (November to March) and low in the rainy season. K is associated with biomass burning, road construction and demolition (Wang *et al.,* 2016; Jiang *et al*.,2018a)

The trace metals that were identified include Cr, Ni, Cu and V. It was observed that only V and Ni were below detection limit (BDL) at OLFS (control site). It was observed that Cr is identified at the three sampling sites. The highest mean value was $0.42 \pm 0.28 \mu g/m^3$ (at OMRF) and the lowest was $0.25 \pm 0.01 \mu g/m^3$ (at OLFS). Ni was identified at two sampling sites with site SIIE indicating below detection limit (BDL) of the instrument. The highest and the lowest concentration values were 0.62 ± 0.19 (at OMRF site) and 0.16 ± 0.07 (at SIIE site). Cu was also identified in all the three sampling sites. The highest and the lowest concentration values were 0.92 ± 0.29 observed at SIIE site and $0.10 \pm 0.13 \mu g/m^3$ at OLFS site

Table 3.4 : Annual average concentrations of $PM_{2.5}$- bound metals across the study Locations ($\mu g/m^3$)

	SITES		
Element	**OMRF**	**OLFS**	**SIIE**
Na	24.99±15.64	261.64±24.66	111.83±14.81
Mg	6.60±5.42	6.30±1.22	11.59±3.32
Al	24.76±18.70	47.97±11.70	47.64±27.56
Ca	0.76±0.15	57.34±16.94	51.33±4.27
K	11.35±0.54	88.68±7.10	51.72±21.18
Cr	0.42±0.28	0.01±0.01	0.25±0.01
Mn	0.47±0.43	0.02±0.01	0.18±0.01
Ti	0.23±0.28	2.55±0.37	1.06±1.21
V	0.03±0.01	ND	0.04±0.03
Fe	10.14±5.98	7.65±1.85	6.07±2.77
Ni	0.62±0.19	ND	0.16±0.07
Zn	82.27±25.27	50.30 ±9.11	66.97±14.81
As	0.27±0.17	0.07±0.07	0.08±0.04
Cd	0.05±0.04	0.016± 0.013	0.02±0.01
Pb	2.96±0.93	0.12±0.01	1.64±0.93
Cu	0.15±0.04	0.10±0.13	0.92±0.29

The maximum and minimum concentration of V were 0.04 ± 0.03µg/m^3 (SIIE sites) and 0.03 ± 0.01µg/m^3 (OMRF site) while site OLFS recorded below detection limit.

Since trace metals are typically associated with anthropogenic emission such as (V and Ni) combustion of fossil fuel (Tian *et al* 2012; Cercasov *et al* 1998) , (Cu) diesel combustion and brake lining wear (Gao, 2011) and smelting furnace burning (Yang *et al* 2003). However, heavy metals (Pb, Cd, As, Mn, Fe and Zn) are significant component of $PM_{2.5}$ with their concentrations higher in OMRF site than the other sites due to more anthropogenic activities observed during the sampling

Trace elements especially heavy metals are significant components of $PM_{2.5}$ in industrial environments. These elements are of particular concern due to their persistence in the environmental media and their toxicity in particles, non-biodegradability of these heavy metals leads to their accumulation in the environment.

It is observed that Zn is identified in all sampling sites with the highest concentration (82.27 ± 25.27µg/m^3) at OMRF than all the other metals in this study . The lowest concentration of all the heavy metals quantified was Cd (0.02 ± 0.01µg/m^3) at SIIE site. Fe was identified at the three sampling sites. The highest mean value was observed at OMRF (10.14 ± 5.98µg/m^3 and the lowest value was obtained SIIE site (6.07 ± 2.77µg/m^3). However, Zn and Fe have been reported as a major dominant component of galvanized steel (Owoade *et al* 2015; Ogundele *et al*, 2017) in Iron and steel factory environment. Apart from smelting, Fe is an abundant element in the Earth crust (Maryam *et al.,*2012). Its concentration in the ambient air might also be from the wind-blown soil dust from the unpaved surface of the factory environment. Among the anthropogenically derived toxic heavy metals, (Pb, Cd, As, Cr, Mn and Ni) detected and quantified in this study, Cd and Pb are known to be emitted from high temperature coal and combustion processes as well as

steel production (Li *et al* 2012; Tian *et al* 2010; Zhang *et al* 2009), Cd was identified in all the sampling sites. The highest and the lowest peak values were ($0.05 \pm 0.04 \mu g/m^3$) observed at OMRF site and $0.016 \pm 0.013 \mu g/m^3$ at OLFS site. Similarly, the maximum and minimum concentration of Pb was $2.96 \pm 0.93 \mu g/m^3$ (OMRF site) and $0.12 \pm 0.01 \mu g/m^3$ (OLFS site) respectively.

Other anthropogenic sources influencing the concentration of Cd in control site (OLFS) is the application of Cd based fertilizer and pesticides during soil and crop cultivation. The highest and lowest peak values of Arsenic were $0.27 \pm 0.17 \mu g/m^3$ observed at OMRF site and $0.07 \pm 0.02 \mu g/m^3$ at OLFS site. Man-made sources of Arsenic can be attributed to smelting of Iron and steel as exemplified by OMRF location (Yang *et al* 2003). According to Tian *et al* 2010, Arsenic could have been emitted from the combustion of coal in an individual area atmosphere. The likely reason for arsenic in OLFS (control site) may be ascribed to application of arsenic-containing pesticides to the farm (Lenntech 2016; WHO 2000).

Table3.5 Comparison of the mean concentration of heavy metal with other studies

		Mean ($\mu g/m^3$)						
References	**Location**	**Cr**	**V**	**Mn**	**Ni**	**As**	**Pb**	**Cd**
This study (Sagamu)	OMRF	0.42	0.03	0.47	0.62	0.27	2.96	0.05
	SIIE	0.25	0.04	0.18	0.16	0.08	1.64	0.02
Ezeh *et al* (2014)	Ikoyi	0.003	0.002	0.001	0.013	-	0.0066	-
Ezeh *et al* (2012)		0.028	0.004	0.003	0.006	-	0.001	-
Orogade *et al* (2016)	Kaduna	-	0.002	0.017	0.011	-	0.008	-
Uzoekwe and Ajayi (2018)	Yenegua	0.0008	-	0.0044	0.0126	-	0.0053	-

The high significant levels of As, Cd, Pb, Zn, Ni, and Fe obtained in the samples from OMRF site is a signature of greater anthropogenic activities than the other sampling sites and therefore calls for urgent attention for environmental pollution control due to public health concern among factory workers and residence population in the vicinity of the factories. However, OLFS is a control environmental area with little anthropogenic activities from agricultural practices.

Table 3.5 shows the comparison of results obtained from Sagamu city with others studies. The elemental concentration values obtained in this research compared well with other similar research works that have been carried out in some part of Nigerian cities (Ezeh *et al* 2014; Orogade *et al* 2016; Uzoekwe and Ajayi 2018) and also they compared with those obtained from some advanced countries such as the Uk, China, India, Pakistan, Iran, as evident in Table 3.5

The variations in the level of elemental concentration in this study with other studies can be attributed to the peculiarity of anthropogenic activities, sampling period, prevailing meteorological conditions and choice of analytical methods and instrumentations employed.

Table 3.6 depicts the comparison of levels of some heavy metal species concentrations with United State Environmental Agency (USEPA), EU and WHO guidelines (µg/m^3) for $PM_{2.5}$

Table 3.6: Trace metal standard in ambient air (µg/m^3)

Trace Metals	WHO	EU	USEPA	Values obtained in this study
Lead (Pb)	0.5	0.5	0.15	
Arsenic (As)	0.00066	0.006		
Cadmium (Cd)	0.005	0.005		
Nickel (Ni)	0.0025	0.02		
Chromium (Cr)	0.00002 5			
Manganese (Mn)	0.15			

Source: EC, 2015; USEPA, 2015c; WHO, 2000

The highest and lowest peak values of As were 0.047 ± 0.017 at OMRF site and $0.072 \pm 0.04 \mu g/m^3$ at OLFS site. This indicates that the concentration of As in Sagamu exceeds the WHO permissible limit of 0.00066 and EU of 0.006. The results of Pb and Cr concentrations observed from the three receptor sites also indicate that they are both above the stipulated guidelines with the exception of Pb which falls below the WHO guideline at OLFS. Also, the results of the concentration values of Ni and Mn are above stipulated guideline with the exception of Mn at OLFS site which falls below the threshold limit.

3.3 Temporal Variation of Metals in $PM_{2.5}$- in the Study Areas

The seasonal mean concentration of $PM_{2.5}$ – bound metals is depicted in Table 3.7

It was observed that the concentration of Na in the three sampling locations was more than the other crustal elements (Ca, Al, Mg, K, Fe, Ti and Mn) for both dry and wet seasons. This could be attributed to both crustal dust or re-suspended dust from unpaved road and sea spray. It is a signature of both natural and anthropogenic sources. Possible other anthropogenic sources include: vehicle emission, biomass burning, agricultural activities and industrial processes. However, the background site (OLFS) had the highest concentration of Ca. The high level of Ca measured in this site can be linked to agricultural practices ranging from application of calcium-based fertilizer, wind-blown dust from unpaved road, construction activities and tilling of soil as observed at the time of sampling.

The high concentration of light elements, a representative of marine aerosol (Na and K) and soil represented (Ca and Mg), may be as a result of their easy transportation along with particulate matter through a long distance due to their smaller molecular weight when compared to the heavy

metals. Therefore, concentrations of these light/ crustal elements were observed to be higher in dry season than wet season. The seasonal variation of metals in aerosols could be affected by the sources, transportation, and meteorological conditions. This seasonal variations in elemental concentration can be associated with differences in atmospheric conditions, emission sources and deposition processes. In dry season, higher temperature, lower humidity, enhanced solar radiation and minimal rainfall were observed to be responsible for the increase in virtually all the light/ crustal elemental concentration as observed across the three sampling locations.

Conversely, in wet season, lower temperature, higher humidity, reduced solar radiation and frequent precipitation were observed to be responsible for the decrease in the concentration of most metals observed in locations OMRF, SIIE and OLFS respectively.

However, elements of anthropogenic origin (Pb, Cd, Ni, Cu, and As) exhibited relatively higher concentration. These increase in metal concentrations can be ascribed to man-made activities emanating from vehicular emission, industrial emission, coal and oil combustion, agricultural practices and road dust re-suspension as observed more at OMRF and SIIE study areas than the background OLFS location. This has become a serious problem and it is more severe during dry season period. These heavy metals (Pb, Cd, Ni, Cu, and As) are non - biodegradable pollutants. They are not readily detoxified and removed by metabolic activities once they are available in the environment. This may subsequently lead to their buildup to toxic levels or bioaccumulation in the ecosystem (Lawal *et al.,* 2011). Heavy metals are dangerous because they tend to bio-accumulate

Table 3.7: Average concentrations of $PM_{2.5}$ bound metals across the seasons ($\mu g/m^3$)

	Dry Season			Wet Season		
	SITES					
Element	**OMRF**	**OLFS**	**SIIE**	**OMRF**	**OLFS**	**SIIE**
Na	15.10±4.68	192.18±30.84	69.42±14.30	9.89±1.62	68.82±15.28	42.41±10.50
Mg	4.40±1.47	4.12±0.30	7.24±1.81	2.20±0.22	2.18±0.73	4.35±1.79
Al	14.36±3.54	31.22±6.72	28.96±2.03	8.65±2.50	16.75±6.54	18.68±8.99
Ca	0.55±0.05	34.88±10.75	22.22±2.32	0.21±0.67	29.46±10.11	23.11±4.64
K	7.20±0.07	59.26±12.50	31.59±9.60	4.15±1.23	29.12±9.34	20.13±9.39
Cr	0.03±0.01	0.01±0.01	0.10±0.05	0.41±0.20	ND	0.15±0.08
Mn	0.31±0.11	0.02±0.01	0.10±0.02	0.16±0.08	0.01±0.00	0.08±0.04
Ti	0.19±0.10	1.35±0.38	0.83±0.22	1.20±0.03	0.01±0.02	0.23±0.10
V	0.03±0.01	ND	0.06±0.02	0.00±0.00	ND	0.02±0.01
Fe	6.22±1.11	4.75±0.81	4.24±0.55	3.92±1.09	2.90±0.66	1.83±1.10
Ni	0.44±0.12	ND	0.10±0.03	0.18±0.10	ND	0.06±0.02
Zn	61.55±10.5	31.55±8.90	41.25±9.05	20.72±7.62	18.75±8.80	25.72±10.44
As	0.19±0.09	0.05±0.02	0.05±0.02	0.08±0.02	0.02±0.00	0.00±0.00
Cd	0.04± 0.02	ND	0.02±0.01	0.01±0.01	ND	0.01±0.00
Pb	2.18±1.04	0.08±0.02	1.49±0.34	0.78±0.34	0.04±0.02	0.15±0.01
Cu	0.04±0.02	0.07±0.02	0.34±0.03	0.19±0.05	0.03±0.01	0.58±0.80

Bawuro *et al.,* 2018) after penetrating into the human body and pose a great threat to human (Aeolian *et al.,* 2008; Lu *et al.,* 2010). This calls for serious health concern

3.4 Pollution indices

Pollution Indices (PI) are useful tools in risk communication. Pollution indices are used to inform the public of the local levels of the ambient air pollution; and the potential health risk. The PIs can also be used to forecast the future pollution level of an area (Wang, 2012).

The PI values are typically grouped into ranges. Each range is assigned a value which gives the public health advisory of the expected population (USEPA, 2012)

A variety of methods have been developed and employed for the assessment of contamination status of the heavy metals concentrations and their toxic response, In this study, Contamination Factor (CF), Degree of Contamination, (DC) and Pollution Load Index (PLI) were determined in OMRF and SIIE industrial sites in order to assess their level of pollution. .

3.4.1 Contamination Factor

Table 3.9 shows the results of the contamination factors (CF), of heavy metals in location OMRF and SIIE industrial factory**.** The contamination factor was calculated using equation 2.6.

The CF is indicated on a contamination factor scale of 1-6 viz;

CF less than 1, low level of contamination,

1 ≤ CF 3 moderate low level of contamination

3<Cf <6 – considerable level of contamination

CF >6 very level of contamination (Du *et al*.,2013; Nasr *et al* 2006).

The contaminator factor CF was adopted to measure contamination level of each heavy metals (Cr, Mn, As and Pb) in location OMRF and SIIE. The contaminator factor shows a very high contamination level of heavy metals across the sampling sites. Mn and Cr had the highest contamination factors of 42 and 23.50 which were far higher than other heavy metals in both sites. Similarly, high CF was also reported for Pb (CF; 9.27) indicating very high level of contamination. The presence of high concentration of Cr, Mn and Pb in OMRF from their respective CF values, can be attributed to scrap metal shredding and recycling operations (Querol *et al* 2006; Li *et al* 2013; Chen *et al.*, 2016)). Therefore, the CF values of Cr, Mn, As and Pb revealed that anthropogenic emissions from smelting/ industrial emission, fossil fuel combustion and traffic emission are attributable to the high levels of heavy metals concentrations in both OMRF and SIIE study areas.

3.4.2 Degree of Contamination and Pollution Load Indices (PLI)

The results of the Degree of contamination (DC) and Pollution Load Index (PLI) are presented in Table 3. 10. The degree of contamination (CD) and pollution load index (PLI) both of which relate to the extent of contamination can be obtained from the values of CF thus: CD = ΣCF and PLI = $\sqrt[n]{\pi CF}$, where n denotes the number of metals Contaminants in the test soil and or site. According to Faiz *et al.* (2009), (CD value) is described in Table 3.8 as shown below:

Table 3.8 Degree of contamination Index

Contamination Index	Degree of Contamination (CD)
$8 \leq CD < 16$	Low contamination (CD)
$16 \leq CD < 32$	Medium degree of contamination (CD)
$CD > 32$	High degree of contamination (CD)

PLI provides a rather simple means of assessing the site air quality. A PLI value of zero indicates a perfect situation, a value of 1.0 indicate baseline level and site quality (Tomlinson *et al* 1980). In this study, the calculated values of CD were 79.02 and 18.99 for $PM_{2.5}$ at OMRF and SIIE sites. These values implied that a very high degree of contamination (DC>32) at OMRF could be related to frequent pollutants emission from smelting activities, traffic emission and re-suspended road dust.. The value of CD (18.99) at SIIE site implies a considerable degree of contamination for $16 \leq CD \leq 32$.. This can be attributed to industrial emission with a lesser degree of pollution compared to OMRF site.

Also the PLI values were 14.40 and 4.0 for the OMRF and SIIE sites respectively. The PLI values were greater than 1 (PLI > 1) at both sites, showing a significant worsening of the ambient air quality within the industrial environment.

.

Table 3.9 Contamination factor of Heavy metals emitted from OMRF and SIIE industrial Areas

	CF Values	
Metals	**OMRF**	**SIIE**
Cr	42.00	2.50
Mn	23.50	9.00
As	4.27	2.36
Pb	9.25	5.13

Table 3.10 Degree of contamination factors (C_{deg}) and pollution load index (PLI) of the heavy metals.

	OMRF	SIIE
C_{deg}	79.02	18.99
PLI	14.02	4.0

3.5 Enrichment Factor analysis

Enrichment factor (EF) was calculated and the results presented in Table 3.11. The EF distinguishes the crustal source from the anthropogenic sources of atmosphere heavy and light metals. In site OMRF, the average values for Al, Mg, Mn and Na are 1.5, 1.55, 2.42, and 4.35. This show that they are less enriched (EF < 10). While the values for Cr, Cu, Ni (EF between 10 and 100) are moderately enriched, Cd, As, Pb, and Zn (EF > 100) show that they are highly enriched. However, K and Ca having EF approach unity (EF < 1)., crustal is the predominant source. Therefore, highly enriched Cd, As, Pb and Zn from the samples collected at OMRF site can be attributed to smelting activities associated with industrial emission, coal combustion and vehicular emission . This is because large amount of Zn and Cd plated steel scrap are recycled in the production process (Querol *et al* 2006; Tian *et al* 2010). Road traffic involves the emission of wide range of trace elements that includes Pb, Cu, Zn and Cd (Gunawardena *et al* 2012). Cr, Cu and Ni are also associated with industrial emission. At SIIE site, Mg, Al, and Mn are less enriched (Ef < 10) while K, Na, Ca, Cr, Ni are moderately enriched (Ef between 10 and 100). However, Zn, As, Pb, Cu, Cd are highly enriched, This can be attributed to industrial emission and coal combustion (AEA,2011; Zhang *et al*.,2009)

In site OLFS, Mg and Al are less enriched while Ca, K, Zn, Cu and Na are moderately enriched. As and Pb are highly enriched. This implies that moderate enrichment of Ca, K, Zn, Cu, and Na. can be attributed to dust. Therefore, the EF calculated in this study tends to suggest strongly that Anthropogenic sources such as vehicular emission, industrial emission, dust, fossils fuel combustion influenced trace metal pollution of ambient air of Sagamu and its environment.

Table 3.11 Enrichment factor analysis of the sampling sites

Element	OMRF	SIIE	OLFS
Na	4.353	32.549	60.425
Mg	1.555	4.566	1.968
Al	1.501	4.826	3.856
K	0.256	16.447	22.378
Ca	0.101	11.647	10.323
Cr	12	34.5	0.5
Mn	2.421	1.526	0.105
Fe	1	1	1
Zn	3542.85	7880	11.4071
Ni	40.66	17.33	-
As	866.66	436.66	300
Pb	11192.30	8230.76	1192.30
Cu	12.727	137.27	11.818
Cd	1000	750	-

3.6 Inter- Metallic Correlation Matrix

In this study, Pearson Correlation Coefficient Matrix was used to indicate probable relationship that could exist between Heavy metals, light metal and crustal elements for the locations OMRF, SIIE and OLFS aa depicted in Table 3.12 to 3.14.

More so, moderate to strong positive and negative correlations were observed across the three study areas. The negative correlation observed suggests different sources or opposite environmental behavior while positive correlation suggests possible common sources.

A Correlation co-efficient analysis shown in Table 3.12 revealed that Na, Mg, Al ,K, Fe, Ni, Zn, As, Cd and Pb showed very high positive correlations among each other. The correlation ranged from 0.712 to 0.978 at 0.01 statistical significance level.

Also, there are moderate positive correlations between Mn, T,V with several other metals like Na, Mg, Al and K with correlation coefficient ranged from 0.020 to 0.840. These positive correlation co-efficient suggest common atmospheric sources associated with industrial emission, re-suspended dust, vehicular \ traffic emission and fossil fuel combustion This corroborates the information on the activities at Metal recycling factory activities at OMRF study area.

In site SIIE, the result of inter- elemental correlation as depicted in Table 3.13 showed that there are strong positive correlation between Pb and Zn (r = 0.749) As (r = 0.737) ,Cd (r= 0.767), V(r = 0.839), Fe(r = 0.902), Ti (r = 0.899). Also between As and Zn (r=0.730), Fe (r=0.666), V(r=0.607) between Cu and Cr (r=0.798) between Zn and Fe (r=0.713), Ti (r=0.692) and V (r=0.617). Most of these association are certainly attributed to anthropogenic sources. Correlation results in SIIE site show relationship between Pb, Zn, As, Cd, Fe, Ti, V, Cu, Cr, K, Mg and Al indicating a common source pointing more to industrial emitted trace metals with a tendency of re-suspended dust due to unpaved roads and fossil fuel combustion from industrial power generating plants.

At the background site OLFS, the result of correlation analysis performed on the variables is depicted in Table 3.14. Correlation results in OLFS show that there are strong positive correlation between Fe and Ca (r = 0.905), Zn and Fe (r = 0.926) and Zn and Ca (r = 0.875) suggesting common sources from both natural and anthropogenic sources such as crustal dust, demolition and construction activities. Also, Cu shows strong correlation with Ca, Mg, Fe, Zn and As with a correlation co-efficient raged from 0.741 to 0.856 suggesting common sources from anthropogenic activities such agricultural practices, Biomass burning and road re- suspended dust.

Table 3.12: Correlation Matrix for Metals in $PM_{2.5}$ at OMRF Study Area

	Na	Mg	Al	Ca	K	Cr	Mn	Ti	V	Fe	Ni	Zn	As	Cd	Pb	Cu
Na	1.000															
Mg	0.953	1.000														
Al	0.969	0.978	1.000													
Ca	-0.323	-0.292	-0.313	1.000												
K	0.939	0.950	0.962	-0.432	1.000											
Cr	-0.812	-0.839	-0.864	0.238	-0.888	1.000										
Mn	0.804	0.808	0.784	-0.172	0.740	-0.622	1.000									
Ti	0.812	0.837	0.840	-0.197	0.803	-0.696	0.775	1.000								
V	0.704	0.696	0.661	-0.186	0.620	-0.491	0.877	0.748	1.000							
Fe	0.960	0.973	0.980	-0.342	0.966	-0.850	0.781	0.850	0.662	1.000						
Ni	0.712	0.682	0.690	-0.404	0.738	-0.561	0.654	0.676	0.587	0.716	1.000					
Zn	0.824	0.775	0.795	-0.554	0.821	-0.652	0.718	0.624	0.608	0.792	0.688	1.000				
As	0.880	0.842	0.864	-0.422	0.866	-0.774	0.732	0.723	0.658	0.853	0.771	0.837	1.000			
Cd	0.866	0.880	0.863	-0.223	0.813	-0.682	0.839	0.778	0.732	0.869	0.702	0.774	0.757	1.000		
Pb	0.805	0.741	0.748	-0.248	0.692	-0.574	0.838	0.633	0.762	0.735	0.649	0.768	0.763	0.767	1.000	
Cu	-0.309	-0.374	-0.414	-0.130	-0353	0.494	-0.193	-0.295	-0.006	-0.373	-0.139	-0.004	-0.234	-0.198	-0.057	1.000

Table 3.13: Correlation Matrix of Metals in $PM_{2.5}$ at SIIE Study Area

	Na	Mg	Al	Ca	K	Cr	Mn	Ti	V	Fe	Ni	Zn	As	Cd	Pb	Cu
Na	1.000															
Mg	0.532	1.000														
Al	0.531	0.891	1.000													
Ca	-0.192	-0.317	-0.426	1.000												
K	0.545	0.890	0.964	-0.345	1.000											
Cr	-0.270	-0.504	-0.687	0.726	-0.637	1.000										
Mn	-0.016	0.098	0.112	0.263	0.103	0.105	1.000									
Ti	0.446	0.792	0.865	-0.288	0.891	-0.570	0.132	1.000								
V	0.484	0.703	0.744	-0.211	0.745	-0.482	0.391	0.724	1.000							
Fe	0.476	0.894	0.946	-0.367	0.951	-0.617	0.215	0.863	0.757	1.000						
Ni	0.351	0.404	0.515	-0.185	0.536	-0.371	0.313	0.579	0.541	0.533	1.000					
Zn	0.294	0.662	0.662	-0.071	0.691	-0.343	0.306	0.692	0.617	0.713	0.384	1.000				
As	0.313	0.660	0.555	-0.057	0.599	-0.270	0.196	0.635	0.607	0.666	0.297	0.730	1.000			
Cd	0.534	0.708	0.800	-0.289	0.826	-0.535	0.168	0.697	0.715	0.782	0.586	0.608	0.452	1.000		
Pb	0.514	0.830	0.843	-0.222	0.871	-0.494	0.345	0.899	0.839	0.902	0.564	0.749	0.737	0.767	1.000	
Cu	-0.423	-0.781	-0.866	0.668	-0.821	0.798	0.135	-0.732	-0.597	-0.801	-0.397	-0.480	-0.405	-0.625	-0.658	1.000

Table 3 .14 Correlation Matrix of Metals in PM $_{2.5}$ at OLFS Study Area

	Na	Mg	Al	Ca	K	Mn	Ti	Fe	Zn	As	Cd	Cu
Na	1.000											
Mg	0.449	1.000										
Al	0.499	0.603	1.000									
Ca	0.588	0.749	0.691	1.000								
K	0.375	0.544	0.427	0.448	1.000							
Mn	0.016	0.232	0.313	0.274	0.409	1.000						
Ti	0.173	0.490	0.329	0.465	0.340	0.255	1.000					
Fe	0.575	0.736	0.629	0.915	0.538	0.263	0.477	1.000				
Zn	0.504	0.810	0.605	0.875	0.474	0.220	0.458	0.926	1.000			
As	0.513	0.641	0.633	0.808	0.492	0.391	0.551	0.782	0.744	1.000		
Cd	-0.121	0.047	0.145	0.012	0.203	0.148	-0.079	0.131	0.144	-0.006	1.000	
Cu	0.494	0.700	0.692	0.834	0.417	0.439	0.494	0.762	0.741	0.856	-0.180	1.000

3.7 Source Apportionment of $PM_{2.5}$-Bound Trace Metals

Source identification analysis of particulate matter was performed based on the principal component analysis method which is widely used to factorize the input concentration data of different species having a linear relationship between total mass concentration and the individual concentration (Atkinson *et al*.,2010; Stanek *et al* 2011).

Principal Component Analysis (PCA) with varimax rotation was used in order to identify the possible sources contributing to heavy and light metals in ambient air particles in the study areas. Factors with eigen values greater than 1.0 were used to identify major elements associated with different sources.

PCA was applied to determine the correlation between pollutants and to identify the source profile of trace metals in $PM_{2.5}$.in ambient air of sites OMRF, SIIE and OLFS respectively.

Table 3.15 describes the significant principal component (PC) or factor loadings for the trace metals in ambient $PM_{2.5}$ samples in site OMRF with corresponding eigen values and variances.

Table 3.15 shows the Principal Component Analysis (PCA) results for the OMRF location, which involves the relationships and underlying patterns of heavy metals as they load onto each principal component or factor.

Two major factors were observed contributing to elemental load/ pollution in this sampling site.

Table 3.15: **Principal Component Analysis of $PM_{2.5}$-Bound metals in OMRF Location**

Metals	Factor 1	Factor 2	Factor 3
Na	**0.998**	-0.029	-0.021
Mg	**0.995**	-0.074	-0.025
Al	**0.995**	-0.074	-0.045
Ca	**-0.748**	**-0.614**	0.227
K	**0.996**	-0.012	-0.078
Cr	**-0.984**	0.132	0.065
Mn	**0.980**	-0.031	0.186
Ti	**0.984**	-0.100	0.044
V	**0.948**	0.055	0.295
Fe	**0.996**	-0.054	-0.049
Ni	**0.970**	0.123	-0.049
Zn	**0.970**	0.220	-0.032
As	**0.993**	0.061	-0.042
Cd	**0.993**	-0.026	0.059
Pb	**0.974**	0.087	0.159
Cu	**-0.756**	**0.613**	0.194
Eigen values	14.692	0.874	0.262
% of Variance	91.827	5.465	1.64
Cumulative %	91.827	97.292	98.932
Possible sources	Industrial emission/ Road dust re-suspension	Vehicular emission / Wear and tear of tire and brake pads	

Factor 1 has high positive loading in Na, Mg, Al, K, Mn, Ti, V, Fe, Ni, Zn, As, Cd, and Pb. and high negative loadings in Ca, Cr and Cu. This implies that Factor 1 accounts for 91.83% of the total variance with an eigen value of 14.692 indicating a dominant component. These elements likely represent a major source attributed to industrial pollution associated with iron and steel smelting activities (Taiwo *et al.*, 2014;AEA,2011); and road dust re-suspension (Jiang *et al.*, 2018a) due to unpaved road leading to OMRF site. The crustal/soil dust factors are dominated by high concentrations of Mg, Al, Si, K, Ca, Ti Mn, and Fe that are the major constituents of soil (Begum *et al.,*2010; Gu et al.,2011; Jang *et al.,*2018a).

The strong negative loadings of Ca, Cu and Cr suggest they have an inverse relationship with these elements, possibly indicate different sources or opposing industrial activities in the study area.

Factor 2 has high positive loadings in Cu (0.613) and high negative loadings in Ca (-0.614). This implies that Factor 2 accounts for 5.47% of the total variance. This component is distinguished by high positive loadings of Cu, indicating a secondary source or an indirect emitter of pollutants or environmental behaviours influencing these metals. This may be attributed to vehicular emission (Pan *et al.*, 2013) and wear and tear of vehicle brake pads (Bozlaker *et al.*, 2013; Manoli *et al*., 2002; Xia and Gao, 2011)) . The high negative loading of Ca suggests it is associated with road dust re-suspension (Jiang *et al.*, 2018a) and sea salt aerosols.

Factor 3 has no high positive loadings greater than 0.5. It accounts for only 1.64% of the variance. The addition of third component increases the explained variance to 98.9%, by providing a comprehensive view of the data structure.

Metals that form a 90 degrees angle are uncorrelated. Metals pointing in opposite directions (180 degrees apart) are negatively correlated while metals that are close to each other and form

small angles between their vectors are highly correlated. On the right side, Ni, Zn, Pb, V, K, Mg, Na, and As are clustered, indicating that these metals have similar profiles and may be correlated with each other in this location. On the left side, Cr, Ca, and Cu form another group, indicating that these metals have similar profiles but different from those on the right side. The biplot in Fig. 3.5 is in good agreement with the result of the PCA.

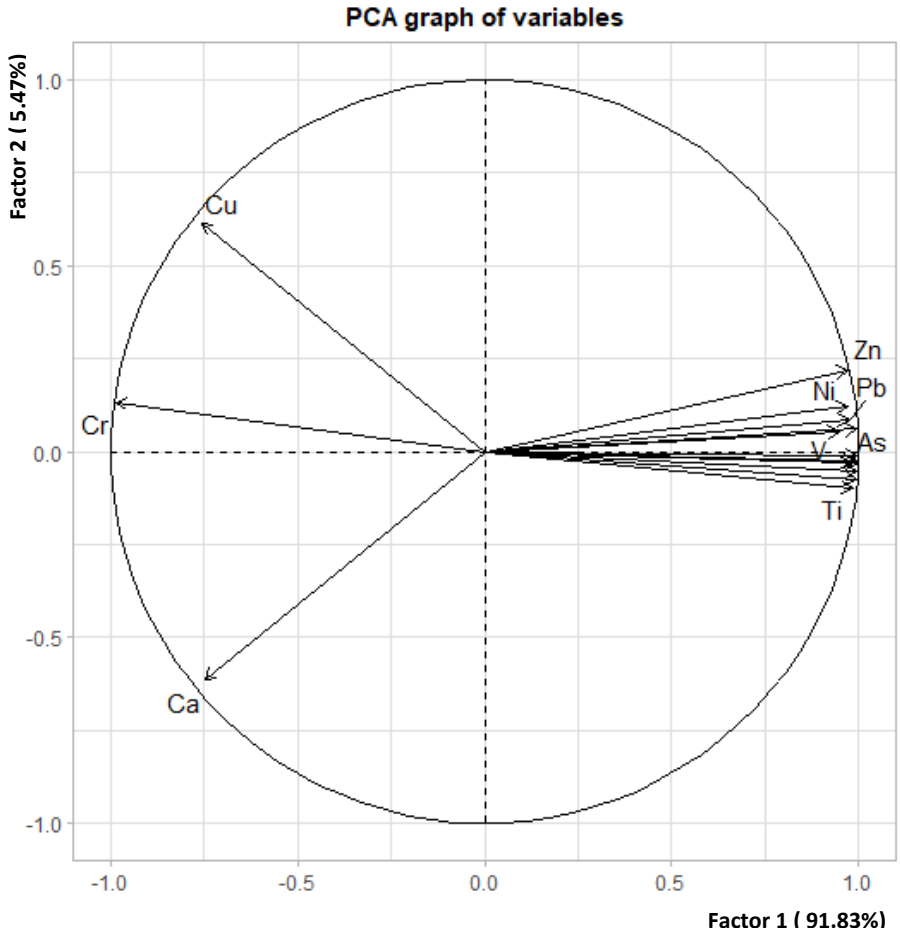

Figure 3.1 PCA Biplot of Metals in $PM_{2.5}$ at OMRF Location

Table 3.16: **PCA of $PM_{2.5}$-bound Metals in SIIE Location**

Metals	Factor 1	Factor 2	Factor 3
Na	**0.876**	-0.273	-0.220
Mg	**0.990**	-0.052	0.082
Al	**0.997**	-0.024	-0.001
Ca	**-0.955**	0.109	0.156
K	**0.997**	-0.034	0.015
Cr	**-0.989**	0.013	0.079
Mn	-0.071	**0.986**	-0.084
Ti	**0.993**	0.007	0.043
V	**0.978**	0.147	-0.015
Fe	**0.997**	0.024	0.041
Ni	**0.885**	0.179	-0.328
Zn	**0.944**	0.141	0.257
As	**0.912**	0.073	0.362
Cd	**0.985**	-0.009	-0.074
Pb	**0.993**	0.085	0.058
Cu	**-0.994**	0.073	0.017
Eigen values	14.013	1.156	0.411
% of Variance	87.582	7.225	2.567
Cumulative %	87.582	94.808	97.374
Possible sources	Industrial emission/Crustal/ Soil dust	Coal or fossil fuel combustion	

Table 3.16 shows the PCA of heavy metals in the SIIE location,

Similarly, 3 factors were observed in this location

Factor1 shows strong loadings in Na, Mg , Al, K , Ti, V, Fe, Ni, Zn , As, Cd and Pb . These metals have high positive loadings in Factor 1. It also has high negative loadings for, Ca, Cu and Cr. implying that they have an inverse relationship with these elements, possibly indicating different sources or opposing industrial pollution in the study area. Factor 1 accounts for 87.58% of the total variance with an eigen value of 14.013 indicating a dominant component This component is primarily characterized by high positive loadings of Na, Mg, Al, K, , Ti, V, Fe, Zn, Ni, As, Cd and Pb. These elements likely represent a major source attributed to industrial emission (Tian *et al*., 2010; Taiwo *et al* 2014) and crustal/ soil dust (Begum *et al.,*2010; Gu *et al.,*2011). The crustal/soil

dust factors are dominated by high concentrations of Mg, Al, Si, K, Ca, Ti Mn, and Fe that are the major constituents of soil

For Factor 2, this component shows strong loadings for Mn. Only Manganese has high positive loadings on Factor 2. It accounts for 7.225% of the total variance with an Eigen value of 1.156. indicating Manganese being the only element with a strong positive loading in factor 2. This can be attributed to coal or fossil fuel combustion (Deng *et al*., 2014; Bhangare *et al.*, 2011).

For. Factor 3, component shows both very low positive and negative loadings for all metals.

It accounts for 2.567% of the total variance with an eigen value (0.411) which is less than 1.

Figure 3.6 is a Principal Component Analysis (PCA) biplot, which shows the relationships among metals in the SIIE location. The plot shows two principal components (Factor 1 and Factor 2). Factor 1 (horizontal axis) explains 87.58% of the variance. Factor 2 (vertical axis) explains 7.23% of the variance. On the right side, clustered closely together are ; Ni, Zn, Pb, V, K, Mg, Na, and As , indicating that these metals have similar profiles and may be correlated with each other

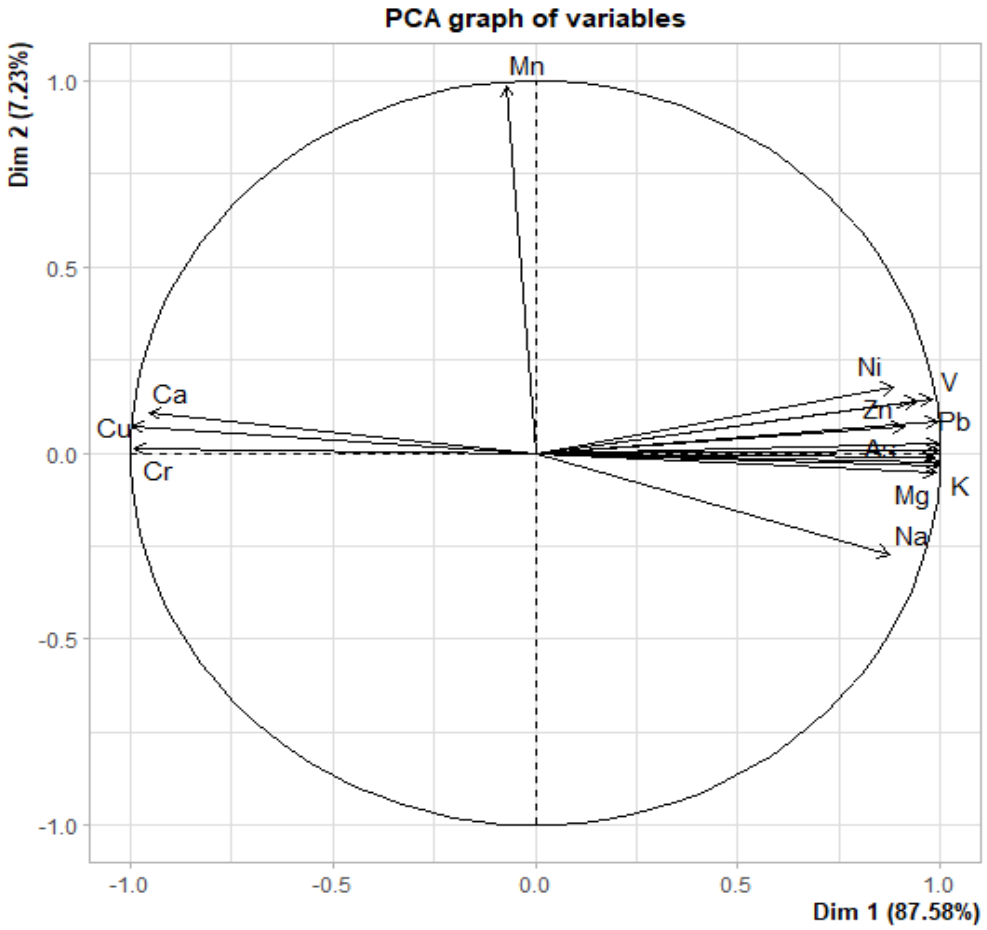

Figure 3.2 PCA Biplot of Metals in $PM_{2.5}$ at SIIE Location

in this study location. The metals on the left side, Cr, Ca, and Cu form another group, indicating that these metals have similar profiles but different from those on the right side. Mn stands out at the top, indicating that it behaves distinctly from the other metals in the data set.

Table 3.17: PCA of PM $_{2.5}$-bound Metals in OLFS Location using Varimax rotation

Elements	Factor 1	Factor 2	Factor 3
Na	**0.737**	-0.407	0.096
Mg	**0.910**	-0.043	0.108
Al	**0.789**	-0.125	0.069
Ca	**0.977**	-0.090	-0.025
K	0.298	0.259	**0.848**
Mn	-0.183	**0.866**	0.156
Ti	**0.553**	0.465	-0.418
Fe	**0.947**	-0.156	0.061
Zn	**0.926**	-0.183	0.029
As	**0.942**	0.185	-0.069
Cd	**-0.768**	-0.355	0.181
Cu	**0.946**	0.232	-0.076
Eigen values	7.503	1.496	0.993
% of Variance	62.521	12.464	8.272
Cumulative %	62.521	74.985	83.258
Possible sources	**Fugitive/Soil dust Coal combustion**	**Agricultural emission**	**Sea salt/Biomass burning**

Table 3.17 shows the PCA of heavy metals in the OLFS location (Background site)

Factor 1 shows strong positive loadings in Na, Mg, Al, Ca, Ti, Fe, Zn, As and Cu and shows.

strong negative loading in Cd. Factor 1 which has the highest eigen value (7.503) and variance of 62.521%, is dominant component.. The crustal/soil dust factors are dominated by high concentrations of Mg, Al, Ca, Ti and Fe that are the major constituents of soil (Begum *et al*.,2010; Gu *et al*.,2011). This soil dust may possible be originated from unpaved road, agricultural operations from plowing of soil, bush clearing and harvesting. Possible source of As and Cu in factor 1 can be attributed to coal combustion (Tian *et al*., 2010; Thurston and Spengler, 1985).

Factor 2 shows strong positive loadings for Mn. This factor varies in a pattern distinct from factor 1. Possible sources in Factor 2 can be ascribed to emissions from agricultural activities such as

application of Manganese -based fertilizer and pesticides, decomposing manure and organic matter and fossil fuel combustion from farm equipment and machinery.

Factor 3 The principal component of the element shows strong positive loadings for K and this also has a distinct variation pattern from both Factors 1 and 2. Possible sources of K in factor 3 can be attributed to natural sources such as soil / dust and sea salt and anthropogenic sources from agricultural activities such as biomass burning, fertilizer application and decomposition of manure from livestock.

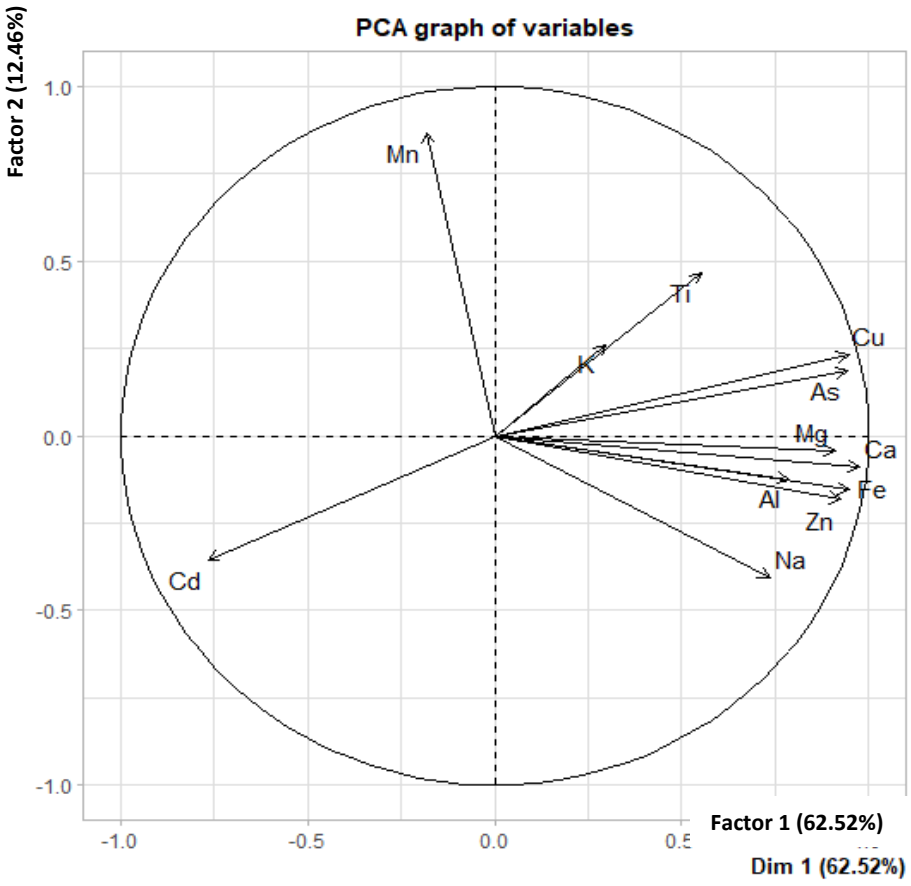

Figure 3.3: PCA Biplot of Metals in $PM_{2.5}$ at OLFS Location

Figure 3.7 shows PCA biplot of metals in OLFS background location. The plot shows that Factor 1(horizontal axis) explains 62.52% of the variance while Factor 2 (vertical axis) explains 12.46% of the variance. On the right side, clustered closely together Ti, Cu, As, Mg, Ca, Fe, Al, Zn, and Na are clustered, indicating that these metals have similar profiles and may be correlated with each other

In OLFS location, the metals on the left side Mn and Cd form another group, indicating that these metals have similar profiles but different from those on the right side. Mn stands out at the top while Cd is down indicating that they behave differently from the other metals in the data set.

Therefore, the Biplot in Figure 3.7 is in agreement with Table 3.17

3.8 Cluster Analysis of Trace Metals in PM $_{2.5}$

In this study, hierarchical agglomerative clustering analysis (HACA). HACA was used to group the trace metals into clusters so that those within a cluster are similar to one another while metals located in other clusters are different from one another.

Table 3.18 Cluster labelling of $PM_{2.5}$ Bound Metals in the study areas

Metal	Na	Mg	Al	Ca	K	Cr	Mn	Ti	V	Fe	Ni	Zn	As	Cd	Pb	Cu
Cluster number	1	2	3	4	5	6	7	8	9	10	11	12	13	14	15	16

Table 3.18 shows that there are 16 heavy metals detected and quantified in this study. The 16 heavy metals are labelled from 1 to 16, where Na is labelled 1 and Cu is labelled 16. These numbers were used as labels in the cluster mapping plot. Both dendrogram and cluster mapping are used to explain the hierarchical cluster analysis in all the three study areas in terms of metal distribution.

3.8.1. Cluster Analysis of Location OMRF

Table 3.15 shows that there are 16 metals observed in this study with their respective cluster numbers labelled from 1 to 16, where Na is labelled 1 and Cu 16. These numbers were used to generate the mapping plots along with the dendrograms in order to explain the identification patterns and relationship among the metals with respect to locations OMRF, SIIE and OLFS respectively. The cluster mapping and dendrogram produced by HACA on metals clustering pattern for OMRF location are shown in Figures 3.5 and 3.6.

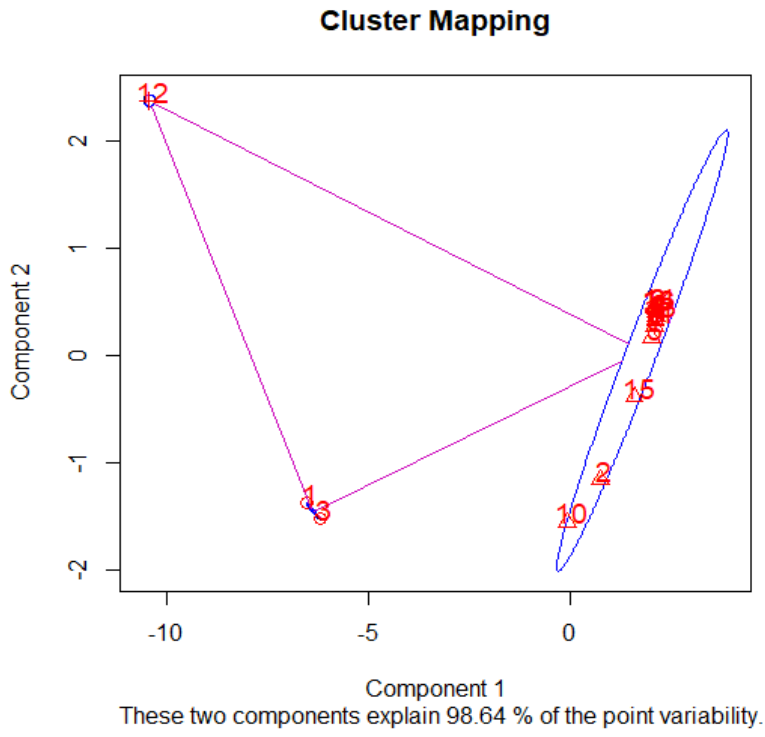

Figure 3.4: Cluster Mapping for OMRF Location showing 3 Clusters

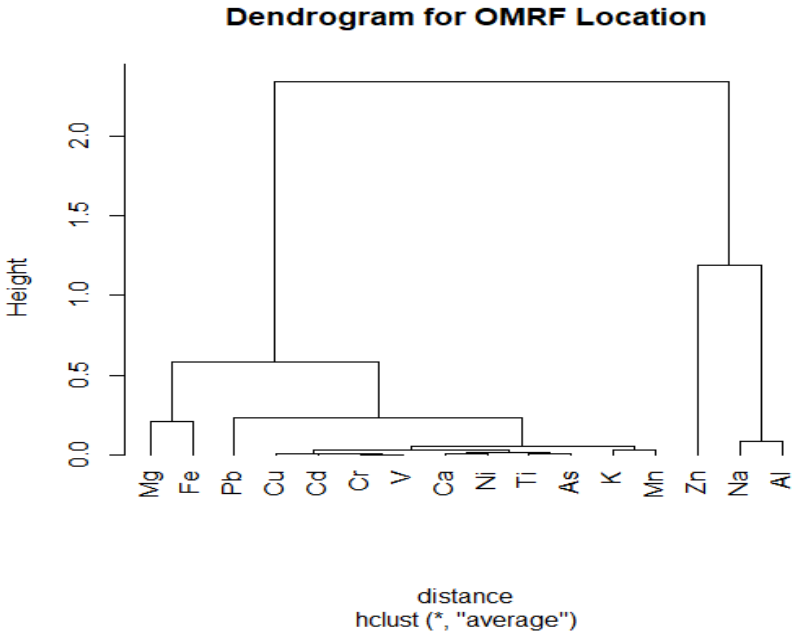

Figure 3.5: Dendrogram for OMRF Location

Sixteen metals have been grouped into three clusters. The strongest metals cluster in $PM_{2.5}$ was cluster 3 with isolated Zn metal only followed by cluster 1 with both Na and Al. However, all the remaining 13 trace metals in the dendrogram (Mg, Fe, Pb, Cu, Cd, Cr, V, Cu, Ni, Ti, As, K and Mn) made up cluster 2. This is supported by the cluster mapping shown in Figure 3.5. However, pollution sources from cluster 1 (Zn) could have emanated from smelting activities (Querol *et al* 2006) and vehicular emission (Fang *et al* 2006).

In cluster 2 which consists of (Mg, Fe, Pb, Cu, Cd, Cr, V, Ni, Ti, As, K and Mn), it may be attributed to complexity of metal pollution from industrial emission (Taiwo *et al* 2014; AEA,2011) and road dust and soil re-suspension (Begum *et al.,*2010; Gu et al.,2011; Jang *et al.,*2018a).

. Cluster 3 comprises of two metals (Na, and Al). Na pollution sources may have been originated from sea salt aerosol or wind -blown dust (natural sources) and vehicles fossil fuel combustion (anthropogenic sources) while Al may be attributed to wind- blow or crustal dust and steel/Aluminum smelting. This is in good agreement with the result of PCA obtained for location OMRF.

3.8.2 Cluster Analysis of location SIIE

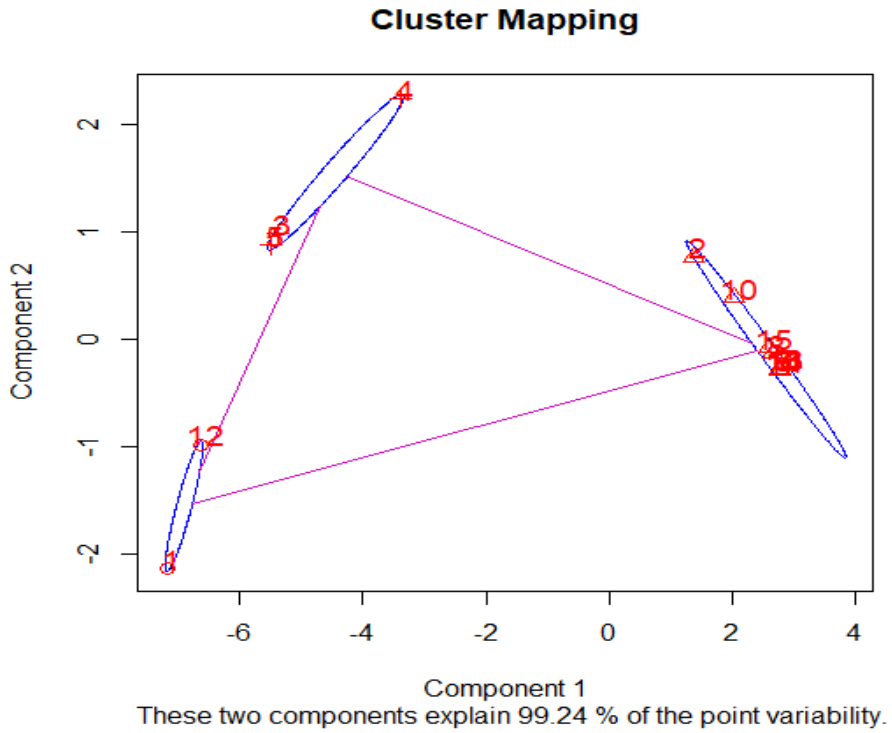

Figure 3.6: **Cluster Mapping for SIIE Location showing 3 Clusters**

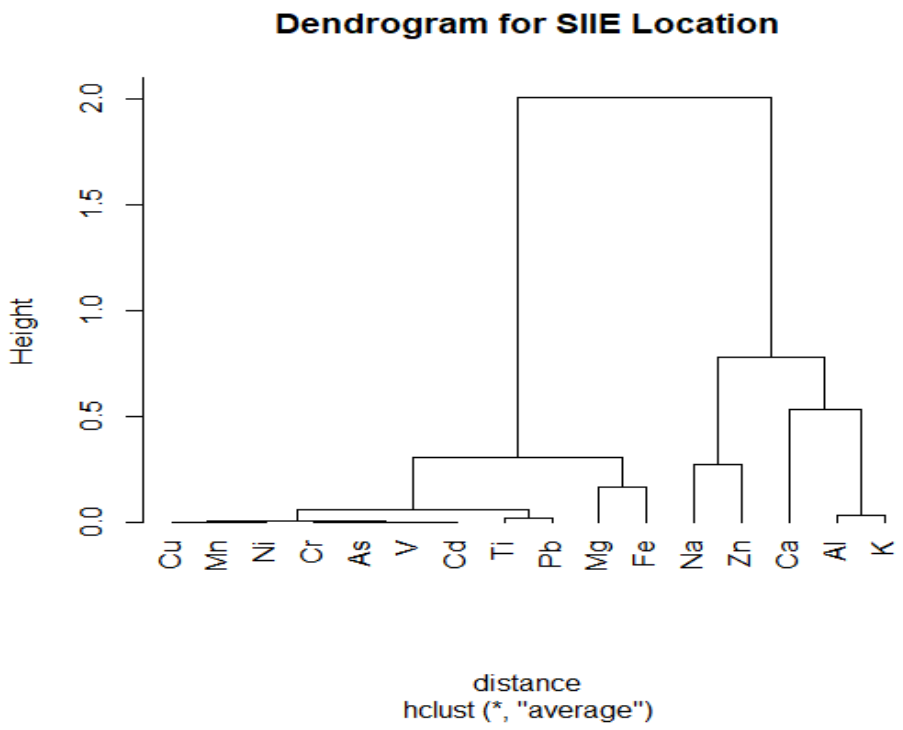

Figure 3.7: **Dendrogram for SIIE location**

The SIIE location cluster mapping and dendrogram produced by HACA on metals clustering pattern as presented in figure 3.7 and 3.8 also grouped into three clusters from the analyzed sixteen (16) metals. Clusters 1 is a cluster of Na and Zn. Na may be attributed to sea salt aerosol or wind -blow dust while Zn may be associated with the pollution sources from industrial emission and fossil fuel combustion.

Cluster 2 consists of 11 metals (Cu, Mn, Ni, Cr, As, V, Cd, Ti, Pb, Mg and Fe). This cluster includes a wide variety of metals, many of which are toxic heavy metals and environmental pollutants and health concerns. This cluster indicates possible common sources attributed to industrial emission, fossil fuel combustion and vehicular emission.

Cluster 3 which is a cluster of 3 metals (Ca, Al, and K). These are crustal elements that are abundant in soil and rock formation. Their clustering suggests that they might have originated

predominantly from wind- blown dust, unpaired road or road construction (Trapp *et al*.,2010) and biomass burning.

3.8.3 Cluster Analysis of location OLFS

Furthermore, three categories of $PM_{2.5}$ bound trace metals cluster mapping and dendogram were observed in the background site (OLFS) as shown in Figures 3.9 and 3.10 respectively. In OLFS, cluster, cluster 1 has 1 metal (Na), cluster 2 has 11 metals (Cu, Mn, N, Cr, As, V, Cd, Ti, Pb, Mg and Fe) and cluster 3 has 4 metals (Al, Ca, K and Zn). The three clustering patterns from the dendrogram is in agreement with cluster mapping

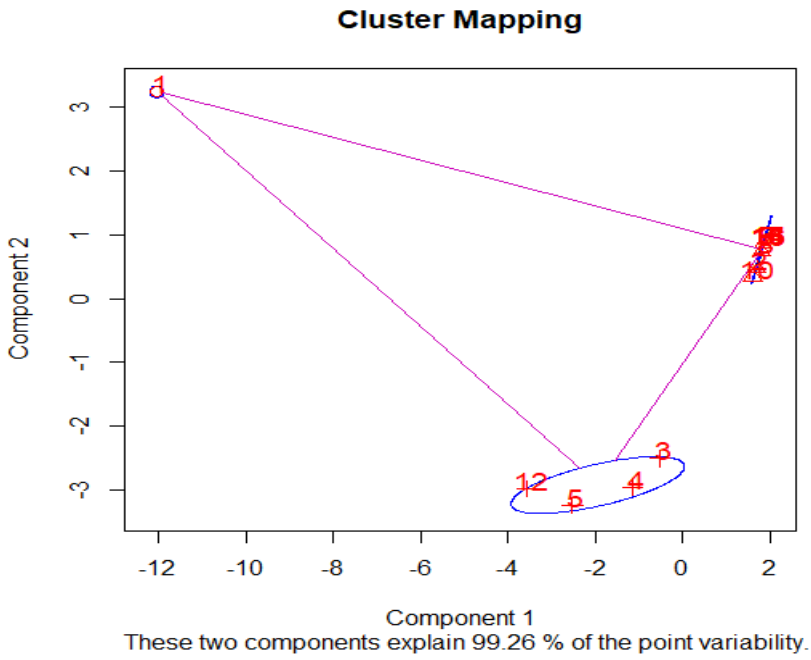

Figure 3.8 Cluster Mapping for OLFS Location showing 3 clusters

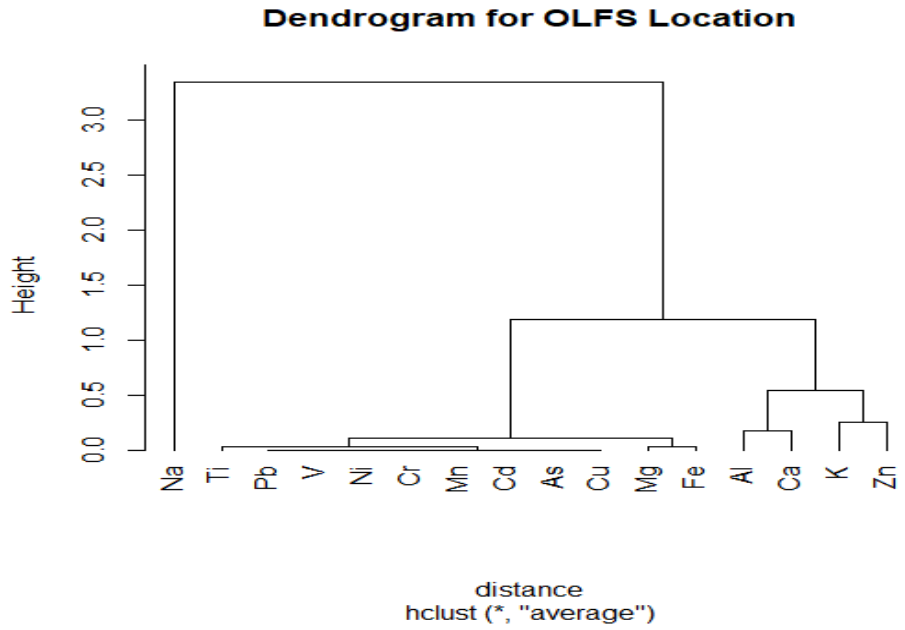

Figure 3.9: **Dendrogram for OLFS location**

Cluster 1 (Na), a cluster that suggests that the isolated Na metals may be attributed to sea salt aerosol or a wind- blown dust and anthropogenic activities from sodium – based fertilizers during crop cultivation or tillage of soil.

Cluster 2 (Ti, Pb, V, Ni, Cr, Mn, Cd, As, Cu, Mg and Fe) includes a wide variety of metals many of which are toxic heavy metals (Ni, Pb, Mn, Cr, Cd, As) known as carcinogens indicating common sources from Agricultural activities such as applications of variety of fertilizers, manures, pesticides and herbicides and fossil fuel combustion from farm machinery and Mg, Fe, Ti and Mn attributed to soil dust re-suspension (Trapp *et al.,*2010;Jiang *et al* 2018a).

Cluster 3 (Al, Ca, K, and Zn). The inclusion of these four metals in this cluster may reflect their geochemical association or shared sources. This grouping could indicate crustal dust and biomass burning or mixed input from both natural and anthropogenic activities.

3.9 Model Prediction of Toxic Metals in Location SIIE

Table 3.19. Average Monthly Concentration of Selected Heavy Metals and $PM_{2.5}$ at SIIE Location

Months	Cr	As	Cd	Pb	$PM_{2.5}$ (ug/m^3)
January	0.13	0.12	0.04	2.537	196.67
February	0.09	0.09	0.03	2.3	174.33
March	0.08	0.06	0.01	1.647	160.67
April	0.08	0.06	0.02	1.173	135.67
May	0.82	0.02	0.01	0.88	64.33
June	0.55	0.07	0.002	0.803	42.67
July	0.47	0.03	0.002	0.699	32.67
August	0.78	0.06	0.005	0.922	48.67
September	0.81	0.07	0.005	1.096	62.67
October	0.86	0.05	0.007	1.261	84.67
November	0.4	0.09	0.03	2.41	176.33
December	0.39	0.11	0.03	2.587	180.33
Mean	0.45500	0.06917	0.01592	1.52625	113.307
Std. Dev.	0.311229	0.029683	0.013372	0.733084	62.765

A year data collected in SIIE location are presented in Table 3.19 and Table 3.20. Using the generated or experimented data, four different models were obtained using R software version 4.3.1 program.

Table 3.20. Average Monthly of Meteorological Parameter values at SIIE Location

Months	Temperature (°C)	Relative Humidity (%)	Pressure (hPa)	Wind Speed (m/s)	Wind direction	Solar radiation	Rainfall
January	33.2	68.4	920.4	2.54	96	760	1.8
February	32.4	71.2	902.6	2.94	164	740	2
March	30.6	72.4	918.3	3.1	172	680	2.2
April	31.2	73.1	919.4	3.42	184	810	2.6
May	28.5	82	920.5	2.8	254	98	360
June	27.4	83	921.2	2.7	262	84	484
July	26.7	85	923.3	2.7	268	86	540
August	28	84	925.6	2.9	246	140	284
September	27.8	78.4	924.2	3.2	210	260	210
October	28.4	78.8	924.7	3.5	168	280	148
November	29.6	69.3	925.2	2.15	84	810	1.4
December	30.3	67.5	925.4	1.84	88	780	0.6
Mean	29.508	76.092	920.9	2.816	183.000	460.667	169.717
Std. Dev.	2.055	6.486	6.298	0.484	67.627	323.516	203.714

The developed models are presented in equations 3.1 - 3.4 for the Gaussian regression model and equations 3.5 – 3.8 for GRM.

The experimented Gaussian or linear regression models are stated as follows:

$$Cr = \beta_0 + \beta_1 PM_{2.5} + \beta_2 Tem + \beta_3 ReH + \beta_4 Pre + \beta_5 WiS + \beta_6 WiD + \beta_7 SoR + \beta_8 RaF + e \quad (3.1)$$

$$As = \beta_0 + \beta_1 PM_{2.5} + \beta_2 Tem + \beta_3 ReH + \beta_4 Pre + \beta_5 WiS + \beta_6 WiD + \beta_7 SoR + \beta_8 RaF + e \quad (3..2)$$

$$Cd = \beta_0 + \beta_1 PM_{2.5} + \beta_2 Tem + \beta_3 ReH + \beta_4 Pre + \beta_5 WiS + \beta_6 WiD + \beta_7 SoR + \beta_8 RaF + e \quad (3.3)$$

$$Pb = \beta_0 + \beta_1 PM_{2.5} + \beta_2 Tem + \beta_3 ReH + \beta_4 Pre + \beta_5 WiS + \beta_6 WiD + \beta_7 SoR + \beta_8 RaF + e \quad (3.4)$$

The experimented Gamma regression models are stated as follows:

$$Cr = 1/(\beta_0 + \beta_1 PM_{2.5} + \beta_2 Tem + \beta_3 ReH + \beta_4 Pre + \beta_5 WiS + \beta_6 WiD + \beta_7 SoR + \beta_8 RaF + e) \quad (3.5)$$

$$As = 1/(\beta_0 + \beta_1 PM_{2.5} + \beta_2 Tem + \beta_3 ReH + \beta_4 Pre + \beta_5 WiS + \beta_6 WiD + \beta_7 SoR + \beta_8 RaF + e) \quad (3.6)$$

$$Cd = 1/(\beta_0 + \beta_1 PM_{2.5} + \beta_2 Tem + \beta_3 ReH + \beta_4 Pre + \beta_5 WiS + \beta_6 WiD + \beta_7 SoR + \beta_8 RaF + e) \quad (3.7)$$

$$Pb = 1/(\beta_0 + \beta_1 PM_{2.5} + \beta_2 Tem + \beta_3 ReH + \beta_4 Pre + \beta_5 WiS + \beta_6 WiD + \beta_7 SoR + \beta_8 RaF + e) \quad (3.8)$$

Where Cr is Chromium, Tem is temperature, ReH is relative humidity, Pre is pressure, WiS is wind speed, SoR is solar radiation, RaF is rainfall, As is Arsenic, Cd is Cadmium, Pb is Lead,

e is the error term, and the β are the unknown parameters to be estimated.

Table 3.21. Parameter Estimation for Linear Regression Model at SIIE location

	Chromium		Arsenic		Cadmium		Lead	
	Parameter estimates	p-value	Parameter estimates	p-value	Parameter estimates	p-value	Parameter estimates	p-value
(Constant)	8.888	0.451	1.195	0.607	0.198	0.585	33.612	0.040*
PM2.5	-0.008	0.232	-0.001	0.320	0.000	0.196	0.000	0.950
Temp	-0.002	0.975	0.015	0.303	0.007	0.037*	0.041	0.526
Rel.Hum	-0.010	0.819	-0.005	0.600	0.001	0.649	0.006	0.889
Pressure	-0.005	0.662	-0.001	0.669	0.000	0.329	-0.033	**0.041***
Wind.speed	-0.199	0.295	-0.031	0.404	-0.011	0.109	-0.477	**0.048***
Wind.direction	-0.003	0.260	0.000	0.441	0.000	0.082	-0.009	**0.034***
Solar.radiation	-0.001	0.073	0.000	0.956	0.000	0.311	-0.001	0.275
Rainfall	-0.002	0.082	0.000	0.919	0.000	0.775	-0.001	0.375

*Significant at 5%

Tables 3.21 is the parameter estimate result for the linear regression model (LRM). It shows that Cr has an inverse relationship with all the meteorological parameters in SIIE Location with different levels of relationship. The most important meteorological parameters that have relationship with chromium are solar radiation and rainfall based on their p-value. As also has an inverse relationship with all the meteorological parameters in SIIE Location except for solar radiation that has direct relationship with it, and wind direction does not have any relationship with it. Cd has a direct relationship with all the meteorological parameters in SIIE Location except for wind speed which has an inverse relationship with it, and $PM_{2.5}$, pressure and wind direction do not have any relationship with it. Temperature is the most significant meteorological parameters that have a relationship with Cd ($p < 0.05$). Pb also has an inverse relationship with all the meteorological parameters in SIIE Location except for temperature and relative humidity which have direct relationship with it, and $PM_{2.5}$ does not have any relationship with it. Pressure, wind speed and wind direction are the most significant meteorological parameters that have a

relationship with lead ($p < 0.05$). However, wind speed has more negative impact on all the four heavy metals than all other meteorological parameters in the model.

The predicted linear regression models for SIIE location are presented in equations 3.9 - 3.12.

$$\widehat{Cr} = 8.888 - 0.008PM_{2.5} - 0.002Tem - 0.01ReH - 0.005Pre - 0.199WiS - 0.003WiD - 0.001SoR - 0.002RaF \quad (3.9)$$

$$\widehat{As} = 1.195 - 0.001PM_{2.5} + 0.015Tem - 0.005ReH - 0.001Pre - 0.031WiS \quad (3.10)$$

$$\widehat{Cd} = 0.198 + 0.007Tem + 0.001ReH - 0.011WiS \quad (3.11)$$

$$\widehat{Pb} = 33.612 + 0.041Tem + 0.006ReH - 0.033Pre - 0.477WiS - 0.009WiD - 0.001SoR - 0.001RaF \quad (3.12)$$

Table 3.22. **Parameter Estimation of Gamma Regression Model at SIIE Location**

	Chromium		Arsenic		Cadmium		Lead	
	Parameter estimates	p-value	Parameter estimates	p-value	Parameter estimates	p-value	Parameter estimates	p-value
(Constant)	-122.200	0.626	-330.831	0.626	600.105	0.912	-11.740	0.016*
$PM_{2.5}$	-0.006	0.924	0.284	0.525	0.909	0.772	-0.002	0.216
Temp	1.432	0.237	-2.662	0.566	-22.959	0.505	0.017	0.346
Rel. Hum	0.158	0.488	0.964	0.762	-15.099	0.658	0.007	0.624
Pressure	0.047	0.856	0.312	0.641	0.934	0.821	0.011	0.011*
Windspeed	3.518	0.120	4.843	0.711	80.146	0.556	0.067	0.276
Wind direction	0.039	0.315	0.107	0.623	0.515	0.743	0.003	0.027*
Solar radiation	0.024	0.019*	-0.005	0.914	-0.097	0.781	0.001	0.025*
Rainfall	0.015	0.119	0.010	0.881	0.694	0.497	0.001	0.034*
Scale	0.088		0.271		0.647		0.002	

*Significant at 5%

Tables 3.22 is the parameter estimates result for the gamma regression model (GRM). It shows that Cr has a direct relationship with all the meteorological parameters in SIIE location, but it is

inversely related to $PM_{2.5}$. The most significant meteorological parameters that have relationship with Cr is solar radiation ($p < 0.05$). As also has a direct relationship with all the meteorological parameters in SIIE location except for temperature and solar radiation that have inverse relationship with it. Cd has a direct relationship with all the meteorological parameters in SIIE Location except for temperature, relative humidity and solar radiation that have inverse relationship with it. Pb also has a direct relationship with all the meteorological parameters in SIIE Location except for $PM_{2.5}$, which has inverse relationship with it. Pressure, wind direction, solar radiation and rainfall are significant meteorological parameters that have a significant relationship with lead ($p < 0.05$). However, wind speed has more direct impact on all the four heavy metals than all other meteorological parameters in the SIIE location model.

From equation 3.9, the expected value of chromium when it is not affected by these other variables is 8.888 µg/m^3 .Also 96% of the variation of Cr can be explained by the variation of these variables provided other factors remain constant. However, only pressure, wind speed and wind direction have significant inverse effect on Cr at 5% level of significant (Table 3.21).

The predicted Gamma regression models for SIIE location are stated from equation 3.13 to equation 3.16 as follows:

$$\widehat{Cr} = 1/(-122.200 - 0.006PM_{2.5} + 1.432Tem + 0.158ReH + 0.047Pre + 3.518WiS + 0.039WiD + 0.024SoR + 0.015RaF) \quad (3.13)$$

$$\widehat{As} = 1/(-330.831 + 0.284PM_{2.5} - 2.662Tem + 0.964ReH + 0.312Pre + 4.843WiS + 0.1076WiD - 0.005\text{SoR} + 0.010RaF) \quad (3.14)$$

$$\widehat{Cd} = 1/(600.105 + 0.909PM_{2.5} - 22.959Tem - 15.099ReH + 0.934Pre + 80.146WiS + 0.515WiD - 0.097\text{SoR} + 0.694RaF) \quad (3.15)$$

$$\widehat{Pb} = 1/(-11.740 - 0.002PM_{2.5} + 0.017Tem + 0.007ReH + 0.011Pre + 0.067WiS + 0.003WiD + 0.001SoR + 0.001RaF) \quad (3.16)$$

Table 3.23. **Experimental and Predicted Values of Selected Heavy Metals at SIIE Location**

	Chromium			Arsenic			Cadmium			Lead		
	Expt	LRM	GRM	*Expt*	LRM	GRM	*Expt*	LRM	GRM	*Expt*	LRM	GRM
Jan	*0.13*	0.159	0.118	*0.12*	0.114	0.113	*0.040*	0.040	0.041	*2.537*	2.495	2.512
Feb	*0.09*	0.101	0.094	*0.09*	0.089	0.090	*0.030*	0.030	0.030	*2.300*	2.287	2.300
Mar	*0.08*	0.144	0.118	*0.06*	0.049	0.050	*0.010*	0.012	0.012	*1.647*	1.592	1.630
Apr	*0.08*	0.027	0.070	*0.06*	0.069	0.069	*0.020*	0.019	0.018	*1.173*	1.233	1.197
May	*0.82*	0.668	0.721	*0.02*	0.048	0.046	*0.010*	0.006	0.005	*0.880*	1.001	0.920
Jun	*0.55*	0.587	0.625	*0.07*	0.050	0.046	*0.002*	0.004	0.003	*0.803*	0.826	0.781
Jul	*0.47*	0.499	0.458	*0.03*	0.036	0.041	*0.002*	0.002	0.003	*0.699*	0.641	0.709
Aug	*0.78*	0.841	0.813	*0.06*	0.047	0.048	*0.005*	0.007	0.007	*0.922*	0.870	0.900
Sep	*0.81*	0.839	0.763	*0.07*	0.065	0.063	*0.005*	0.004	0.005	*1.096*	1.028	1.057
Oct	*0.86*	0.846	0.900	*0.05*	0.055	0.058	*0.007*	0.008	0.007	*1.261*	1.302	1.296
Nov	*0.40*	0.336	0.320	*0.09*	0.093	0.086	*0.030*	0.027	0.027	*2.410*	2.447	2.382
Dec	*0.39*	0.414	0.460	*0.11*	0.114	0.120	*0.030*	0.032	0.032	*2.587*	2.593	2.631

Tables 3.23 shows the experimental values and the predicted values for both models, LRM and GRM and for the four heavy metals that are used as dependent (outcome) variables. The experimental values and the predicted values for both models, LRM and GRM are depicted on Figures 3.14a and 3.14b for Cr , Figures 3.15a and 3.15b for As , Figures 3.16a and 3.16b for Cd and Figures 3.17a and 3.17b for Pb in that order.

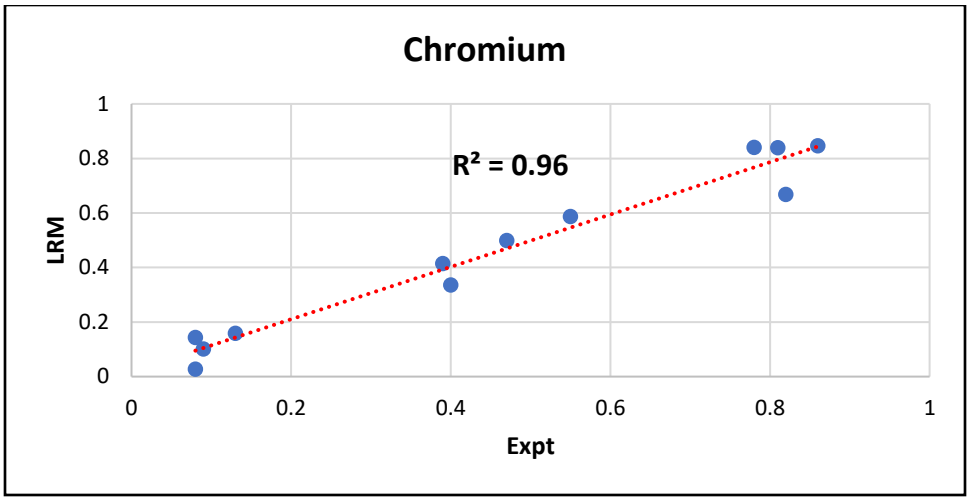

Figure 3.10a. Experimental vs Predicted (LRM) for chromium in SIIE Location

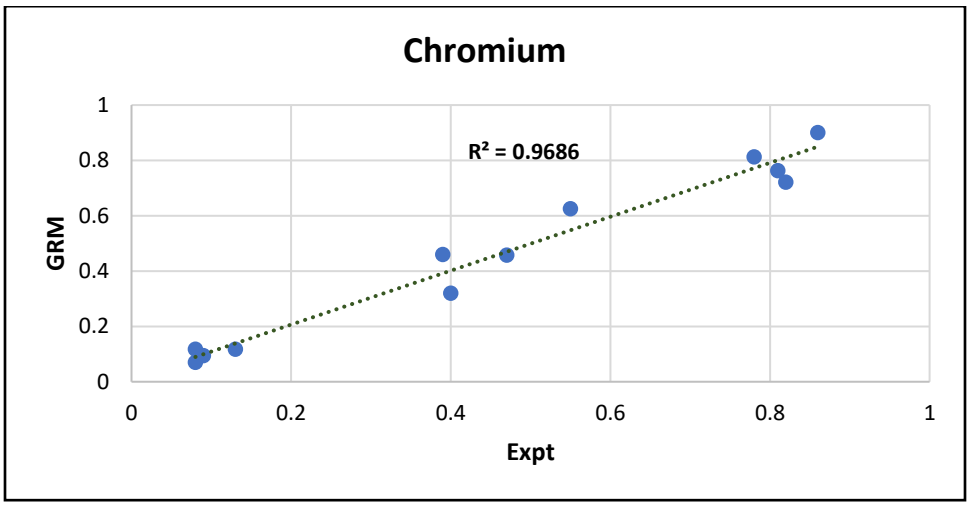

Figure 3.10b. Experimental vs Predicted (GRM) for chromium in SIIE Location

The predicted and experimental values of chromium for LRM and GRM are depicted in Figures 3.14a and 3.14b. However, Figure 3.14a suggests that LRM is highly accurate in predicting Cr levels based on experimental values, as evidenced by the R^2 value of 0.96. Most data points are close to the regression line, indicating minimal prediction errors. Figure 3.14b shows that the GRM model is more accurate than LRM with an R^2 value of 0.97.

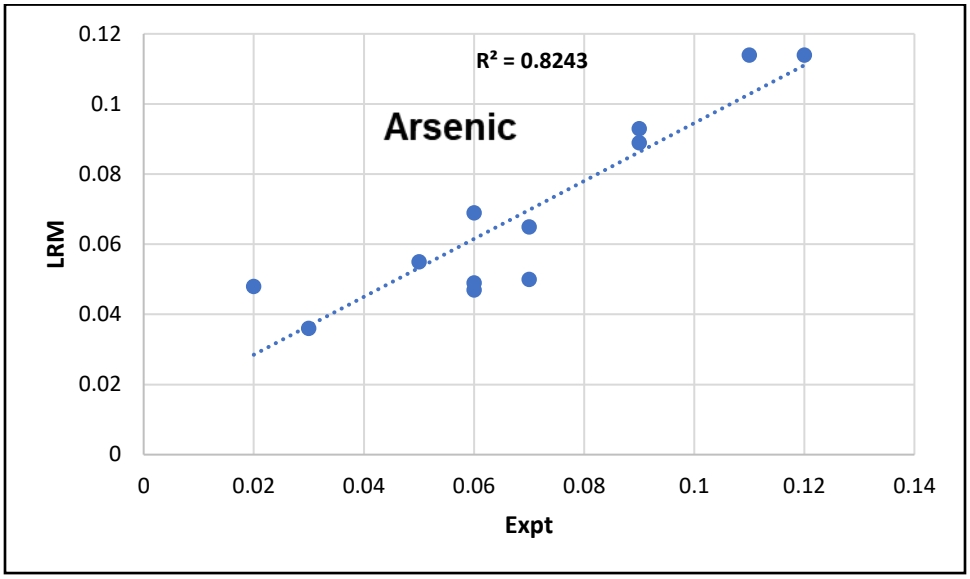

Figure 3.11a. Experimental vs Predicted (LRM for arsenic in SIIE Location

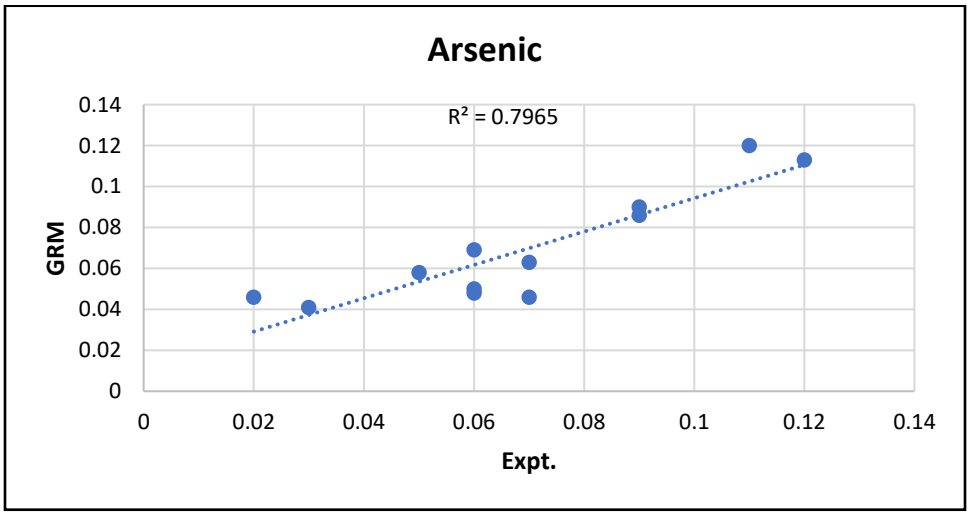

Figure 3.11b. Experimental vs Predicted (GRM) for arsenic in SIIE Location

The predicted and experimental values of As for both LRM and GRM models are depicted in Figures 3.15a and 3.15b. However ,Figure 3.16a suggests that LRM model accurately predicts As levels based on experimental values, as evidenced by the R^2 value of 0.82. Most data points are close to the regression line, indicating minimal prediction errors. Figure 3.15b shows that the GRM is less accurate than LRM with an R^2 value of 0.80.

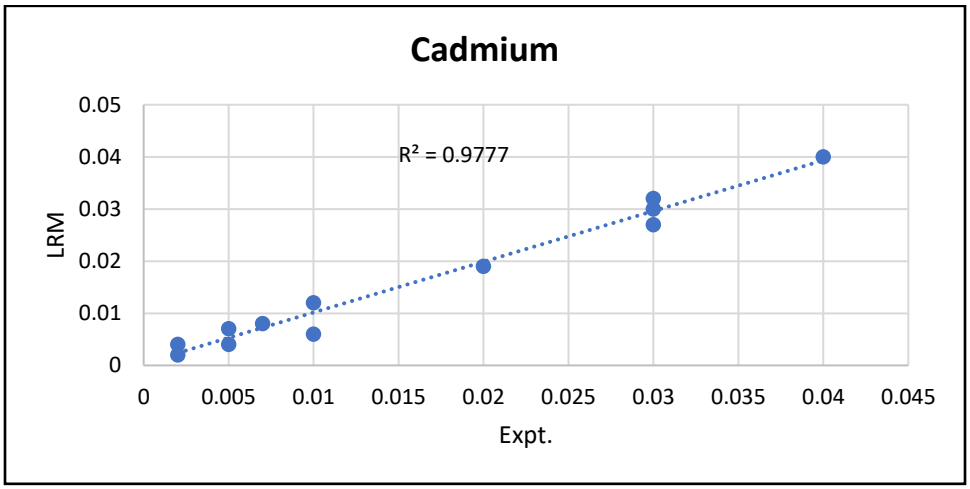

Figure 3.12a. Experimental vs Predicted (LRM) for Cadmium in SIIE Location

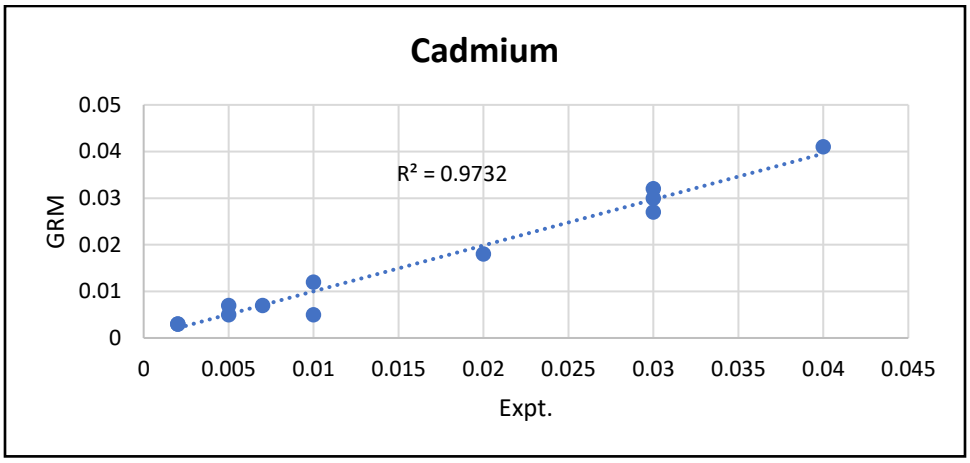

Figure 3.12b. Experimental vs Predicted (GRM) for cadmium in SIIE Location

The predicted and experimental values of Cd for both LRM and GRM are depicted in Figures 3.16a and 3.16b. However, Figure 3.17a suggests that LRM accurately predicts Cd levels based on experimental values, as evidenced by the R^2 value of 0.98. Most data points are near the regression line, indicating minimal prediction errors. Figure 3.16b shows that GRM is less accurate than LRM with an R^2 value of 0.97.

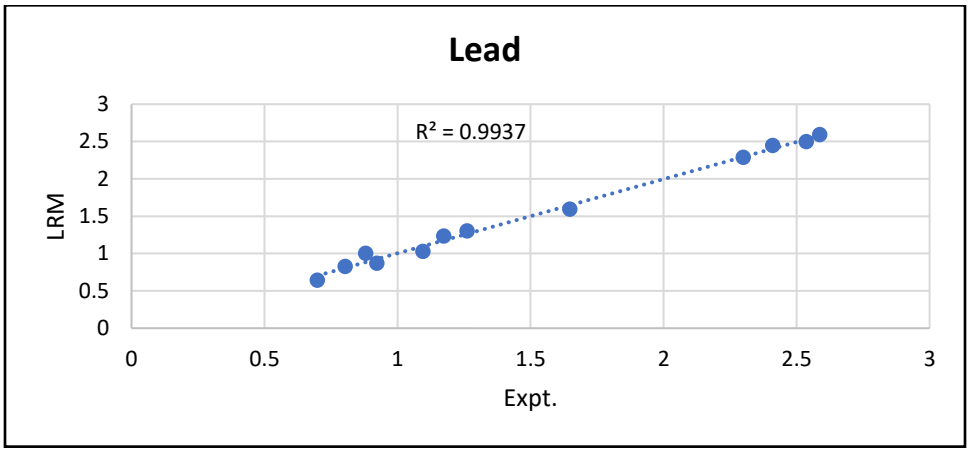

Figure 3.13a. Experimental vs Predicted (LRM) for Lead in SIIE Location

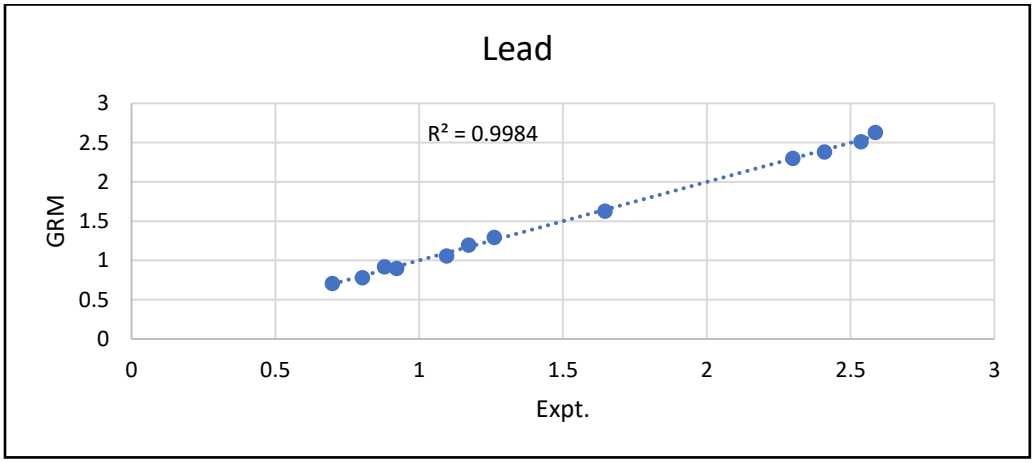

Figure 3.13b. Experimental vs Predicted (GRM) for Lead in SIIE Location

The predicted and experimental values of lead for LRM and GRM are depicted in Figures 3.17a and 3.17b. Figure 3.18a suggests that LRM accurately predicts lead levels based on experimental values, as evidenced by the R^2 value of 0.994. Most data points are near the regression line,

indicating minimal prediction errors. Figure 3.17b shows that GRM is more accurate than LRM with an R^2 value of 0.998.

Table 3.24. Error Evaluation Functions Values of the Developed Models for SIIE Location

	Chromium		Arsenic		Cadmium		Lead	
Error function	LRM	GRM	LRM	GRM	LRM	GRM	LRM	GRM
ARE	0.0924	0.0501	0.1257	0.1191	0.1119	0.0972	0.0164	0.0068
ERRSQ	0.0035	0.0028	0.0001	0.0002	0	0	0.0031	0.0008
MPSD	0.3697	0.2003	0.5029	0.4765	0.4475	0.389	0.0658	0.027
HYBRID	0.4101	0.1204	0.7589	0.6811	0.6007	0.4539	0.013	0.0022
RMSE	0.06522	0.057799	0.0132	0.014	0.0021	0.0024	0.0612	0.0308
EABS	0	0	0	0	0	0	0	0
SEE	0.0206	0.0183	0.0042	0.0044	0.0007	0.0008	0.0193	0.0097
MRPE	-0.0350	-0.0249	-0.0951	-0.0954	-0.095	-0.1131	-0.0008	-0.0005
MSE	0.0043	0.0033	0.0002	0.0002	0	0	0.0037	0.0009

Table 3.24 shows the goodness of fit between the predicted and experimental data was assessed using Average Error Estimate (ARE), Sum of Error Square (ERRSQ), Marquardt's Percent Standard Deviation (MPSD), Hybrid Fractional Error Function (HYBRID), Root Means Square Error (RMSE), Sum of Absolute Errors (EABS), Standard Error of Estimate (SEE), Mean Relative Percentage Error (MRPE) and Mean Square Error (MSE). A model with a smaller value of ARE, ERRSQ, MPSD, HYBRID, RMSE, EABS, SEE, MRPE and MSE predicts the data better than the one with a higher one. Average relative error (ARE) reduces the fractional error distribution over the whole inclusive range of data (Salami, 2022; Rahman *et al.,* 2008). A tool called sum of error square (ERRSQ) is used in regression analysis to determine the distribution of data and the degree to which a given set of data will fit a model. It is one of the frequently utilized error evaluation

functions. The model's ability to predict the experimental data increases with decreasing ERRSQ value (Serafin and Dziejarski, 2023). The MPSD and HYBRID are measures of error in statistics. MPSD is a statistical measure commonly used to assess the goodness -of- fit in regression analysis. It evaluates the standard deviation of the residuals as a percentage of the standard deviation of the observed data (Serafin and Dziejarski, 2023)

The HYBRID is used in nonlinear regression and curve fitting tasks. It combines characteristics of both the absolute and squared error functions, offering a balance between sensitivity to outliers and overall goodness-of-fit. The RMSE offers data regarding a model's performance. The disadvantage of RMSE is that a small number of significant errors in the sum are probably going to cause the RMSE to rise noticeably. Large RMSE values denote large errors, thus it is best to stay away from models with high RMSE values (Conn et al., 2023). The EABS is a measure used to quantify the overall error between observed and predicted values in statistics. EABS provides a simple and intuitive way to evaluate the accuracy of a predictive model. It gives equal weight to all errors regardless of their direction (overestimation or underestimation), making it particularly useful when the sign of errors is not of primary concern. The SEE calculates the difference between data from experiments and predictions. It is crucial for verifying the prediction's accuracy (Deng *et al.*, 2023).

The MRPE and MSE are common measures used to assess the accuracy of predictions or models in statistics. MRPE provides a measure of the average percentage error relative to the observed values, offering insight into the overall accuracy of predictions. It is particularly useful when you want to understand the proportional error in relation to the actual values. MSE measures the average of the squares of the errors between predicted and observed values. MSE is used in regression analysis to quantify the average squared deviation between predictions and

observations, providing a measure of the overall model fit or prediction accuracy (Hewamalage *et al*., 2023).

3.9.1. Chromium result in SIIE location

Table 3.24 shows that ARE values for GRM and LRM are 0.0501 and 0.0924, respectively. GRM was found to have a better ability to predict the experimental data because of a lower ARE value than the LRM. For LRM and GRM, the corresponding ERRSQ values in this work are 0.0035 and 0.0028. Given that GRM has a lower value of ERRSQ, this indicates that it predicted the experimental data very well. The HYBRID values for LRM and GRM are 0.4101 and 0.1204, respectively, while the MPSD values were 0.3697 and 0.2003 for LRM and GRM, respectively. GRM has a better goodness of fit between the developed models because the lower the MPSD and HYBRID values, the better the goodness of fit. GRM has a lower RMSE value in this work, indicating a lower error in predicting the experimental data for chromium. The SEE values for LRM and GRM were 0.0206 and 0.0183 respectively, indicating that the GRM predicted the experimental data more accurately than the developed models. The GRM also predicts the experimental data than LRM using the absolute values of MRPE and MSE.

3.9.2. Arsenic result in SIIE location

Table 3.24 shows that for predicting the experimental values of arsenic, GRM performs better LRM when ARE, MPSD, and HYBRID criteria are used, while LRM performs better than GRM when ERRSQ, RMSE, SEE and MRPE criteria are used. However, when SEE and MSE criteria are used both GRM and LRM performed equally well in predicting Arsenic in SIIE location.

3.9.3. Cadmium result in SIIE location

Table 3.24 shows that for predicting the experimental values of cadmium, GRM performs better LRM when ARE, MPSD, HYBRID criteria are used, while LRM performs better than GRM when RMSE, SEE and MRPE criteria are used. However, when ERRSQ, EABS and MSE criteria are used both GRM and LRM performed equally well in predicting cadmium in SIIE location.

3.9.4. Lead result in SIIE location

Table 3.24 shows that for predicting the experimental values of cadmium, GRM performs better LRM when ARE, ERRSQ, MPSD, RMSE, SEE, MRPE and MSE criteria are used, while LRM performs better than GRM when HYBRID criterion is used. However, when EABS criterion is used both GRM and LRM performed equally well in predicting lead in SIIE location.

Table 3.25. **Statistical Evaluation Values of the Developed Models for SIIE Location**

	Chromium		Arsenic		Cadmium		Lead	
Statistic	LRM	GRM	LRM	GRM	LRM	GRM	LRM	GRM
R	0.9798	0.9842	0.9054	0.8933	0.9892	0.9849	0.9968	0.9992
R^2	0.9601	0.9686	0.8197	0.798	0.9785	0.97	0.9937	0.9984
Adj. R^2	0.8902	0.9138	0.5042	0.4445	0.9408	0.9176	0.9826	0.9956
K^2	0.0399	0.0314	0.1803	0.202	0.0215	0.03	0.0063	0.0016
t-test	0	0	0	0	0	0	0	0
F-test	1.0416	1.0197	1.2199	1.1991	1.022	1.0179	1.0064	1.0023
χ^2	0.1993	0.0745	0.0346	0.0391	0.0058	0.0094	0.0355	0.0073

The strength of the linear relationship between two variables, in this case the experimental and predicted data, is indicated by the r values. The degree of linearity is indicated by the values, which range from -1 to +1. Strong negative and positive relationships between the experimental and predicted data are indicated by values of r that are close to -1 and +1. R^2 is the percentage that can be accounted for by $PM_{2.5}$ and meteorological parameters in the experimental data when predicting

the heavy metals data. In the evaluation of regression analysis, R^2 yielded more information than ERRSQ, MPSD, RMSE, and SEE because it can be expressed as a percentage, whereas the latter measures have arbitrary ranges. A high R^2 number suggests that the data and the model fit each other well. Between experimental and predicted data, K^2 accounts for the amount of unexplained and unaccounted for data. The model is better the lower the K^2 value.

An F-test is a statistical tool where the test statistics, under the null hypothesis, have an F-distribution. In order to determine which statistical model best fits the experimental data, it is frequently and widely used for analyzing and comparing models that have been fitted to a set of data. The χ^2 test evaluates the relationship between developed models and experimental data. It contrasts how much the experimental and predicted data differ from one another. The χ^2 test can be used to assess the goodness of fit between the experimental and predicted data in addition to determining whether the two sets of data are related or not. The t-test from Table 3.25 showed that both models performed well in predicting all the four heavy metals equally.

3.9.5. Chromium result in SIIE location

The r values for LRM and GRM in Table 3.25 were, respectively, 0.9798 and 0.9842. The GRM in this study has a higher r value of 0.9842, indicating that it is the superior model to LRM. The R^2 values for the LRM and GRM are 0.9601 and 0.9686, respectively. With an R^2 value of 0.9686, the GRM model is the superior model among the developed models, accounting for 96.66% of the variation in the predicted chromium. GRM has the lower K^2 value of 0.0314 as compared with LRM with a value of 0.0399, meaning that less than 5% of the experimental data could not be explained by GRM. This suggested that, in comparison to LRM, GRM is more accurately represented the experimental data. The F-test results for LRM and GRM are 1.0416 and 1.0197, respectively ($p \geq 0.05$). The null hypothesis, which stated that the means of the experimental and

predicted data were statistically significant equal at the 5% significant level, could not be rejected because the F-test p-values were greater than the significance level ($\alpha = 0.05$). Since every developed model passed the F-test, the experimental data will be represented by the model with the lowest F-test value. As a result, GRM was chosen as the ideal model, and LRM and NPRM were dropped.

In this study, the χ^2 test values for LRM and GRM were 0.1993 and 0.0745, respectively ($p < 0.05$). The developed models have p-value of less than 0.05. This suggested that there is no sufficient data to reject the null hypothesis, which stated that there was no significant difference between the experimental and predicted data. This indicates that there is no significant difference between the data from the developed models and the experimental data. Given that the developed models scaled through the χ^2 test, the model that best represented the experimental data at a p-value of 0.05 was determined to be GRM, which has the lower χ^2 test value. It is evident that GRM has the least deviation from the experimental data when compared to LRM based on the analysis of error evaluation functions performed in this work to assess the error deviation of the developed models. As a result, GRM was chosen as the statistical model to forecast the concentration of chromium in SIIE location. The GRM model was chosen for the prediction of chromium concentrations in SIIE location because it clearly represented the experimental data better than LRM, as demonstrated by the statistical evaluation tools used to examine the applicability of the developed models. This study has demonstrated that GRM predicts chromium more accurately than LRM.

3.9.6. Arsenic result in SIIE location

Table 3.25 shows that LRM has a higher coefficient of correlation (r), coefficient of determination (R^2), and adjusted coefficient of determination (Adj R^2) than GRM in predicting Arsenic. With an R^2 value of 0.8197, the LRM model is the superior model between the developed models, accounting for 81.97% of the variation in the predicted arsenic. LRM has the lower K^2 value of 0.1803 as compared with GRM with a value of 0.202, meaning that less than 19% of the experimental data could not be explained by LRM. Although, the F-test statistic shows that GRM is better than LRM, but the Chi-square test statistic shows that LRM performed better than GRM in predicting arsenic in SIIE location. Thus, this study has demonstrated that LRM predicts Arsenic more accurately than GRM is SIIE.

3.9.7. Cadmium results in SIIE location

Table 3.25 shows that LRM has a higher r, R^2 and Adj R^2 than GRM in predicting cadmium. With an R^2 value of 0.9785, the LRM model is the superior model between the developed models, accounting for 97.85% of the variation in the predicted cadmium. LRM has a lower K^2 value of 0.0215 as compared with GRM with a value of 0.03, meaning that less than 3% of the experimental data could not be explained by LRM. Although, the F-test statistic shows that GRM is better than LRM, the Chi-square test statistic shows that LRM performed better than GRM in predicting cadmium in SIIE location. Thus, this study has demonstrated that LRM predicts Cadmium (Cd) more accurately than GRM is SIIE.

3.9.8. Lead result in SIIE location

Table 3.25 shows that GRM has a higher r, R^2 and Adj R^2 than LRM in predicting lead. With an R^2 value of 0.9984, the GRM model is the superior model between the developed models, accounting for 99.84% of the variation in the predicted lead. GRM has the lower K^2 value of

0.0016 as compared with LRM with a value of 0.0063, meaning that less than 0.5% of the experimental data could not be explained by GRM. The F-test results for LRM and GRM are 1.0064 and 1.0023, respectively ($p \geq 0.05$). Since every developed model passed the F-test, the experimental data will be represented by the model with the lowest F-test value. As a result, GRM was chosen as the ideal model, and LRM and NPRM were dropped. The χ^2 test values for LRM and GRM are 0.0355 and 0.0073, respectively ($p < 0.05$). This shows that GRM is better than LRM. As a result, GRM is chosen as the statistical model to forecast the amounts of lead in SIIE location.

Table 3.26. Model Selection Criteria of the Developed Models for SIIE Location

	Chromium		Arsenic		Cadmium		Lead	
Criteria	LRM	GRM	LRM	GRM	LRM	GRM	LRM	GRM
Log Lik.	16.8266	18.9515	35.9806	31.3215	58.29649	50.44489	17.5925	24.2979
AIC	-13.653	-17.903	-51.961	-42.643	-96.593	-80.890	-15.185	-28.596
AICC	76.3468	72.097	38.039	47.357	-6.593	9.110217	74.81508	61.40414
BIC	-8.8041	-13.054	-47.11	-37.794	-91.744	-76.041	-10.3359	-23.7468
CAIC	-17.804	-22.054	-56.112	-46.794	-100.743	-85.041	-19.3358	-32.7468
KS-Stat (D)	0.1667	0.1667	0.25	0.8382	0.1667	0.1667	0.0833	0.0833
KS p-value	0.9977	0.9977	0.25	0.8382	0.9923	0.9949	1	1

Table 3.26 shows the selection criteria, which are Log Likelihood (Log Lik), Akaike's Information Criterion (AIC), Finite Sample Corrected AIC (AICC), Bayesian Information Criterion (BIC), Consistent AIC (CAIC), Kolmogorov Smirnov statistic (KS stat) and p-value (KS p-value). The higher the Log Likelihood the better the model, but the lower the AIC, AICC, BIC, CAIC, KS-Stat, the better the model. The higher the KS p-value the better the model.

3.9.9. Chromium result in SIIE location

Table 3.26 shows that GRM is better than LRM using log likelihood (LRM = 16.8266, GRM = 18.9515), AIC (LRM = -13.653, GRM = -17.903), AICC (LRM = 76.3468, GRM = 72.097), BIC

(LRM = -8.8041, GRM = -13.054), CAIC (LRM = -17.804, GRM = -22.054) criteria. Using all the criteria, the GRM is better than LRM. However, both models are good fit for the data using KS-Stat and its p-value.

3.9.10. Arsenic result in SIIE location

Table 3.26 shows that LRM (35.9806) is better than GRM (31.3215) using log likelihood criterion. More so, LRM is better than GRM using the AIC (LRM = -51.961, GRM = -42.643), AICC (LRM = 38.039, GRM = 47.357), BIC (LRM = -47.11, GRM = -37.794), CAIC (LRM = -56.112, GRM = -46.794) criteria. However, both models are good fit for the data using KS-Stat and its p-value.

3.9.11. Cadmium result in SIIE location

Table 3.26 shows that LRM (58.29649) is better than GRM (50.44489) using log likelihood criterion. More so, LRM is better than GRM using the AIC (LRM = -96.593, GRM = -80.890), AICC (LRM = -6.593, GRM = 9.1102), BIC (LRM = -91.744, GRM = -76.041), CAIC (LRM = -100.743, GRM = -85.041) criteria. However, both models are equally good fit for the data using KS-Stat and its p-value.

3.9.12. Lead result in SIIE location

Table 3.26 shows that GRM (24.2979) is better than LRM (17.5925) using log likelihood criterion. More so, GRM is better than LRM using the AIC (LRM = -15.185, GRM = -28.596), AICC (LRM = 74.8151, GRM = 61.40414), BIC (LRM = -10.3359, GRM = -23.7468), CAIC (LRM = -19.3358, GRM = -32.7468) criteria.

However, both models are equally good fit for the data using KS-Stat and its p-value. Therefore, having gone through all the tests and using all the criteria, the GRM is the better model for

predicting chromium and Lead while the LRM is the better model for predicting arsenic and cadmium in SIIE location

3.9.1. Model Prediction of Toxic Metals in Location OMRF

Table 3.27. Average Monthly Concentration of Selected Heavy Metals at OMRF Location

Months	Cr	As	Cd	Pb	$PM_{2.5}$ (ug/m^3)
January	0.018	0.517	0.084	5.093	389.67
February	0.017	0.387	0.051	3.113	320.33
March	0.025	0.294	0.041	2.393	245.33
April	0.014	0.317	0.018	2.513	164.67
May	0.551	0.170	0.022	2.100	78.33
June	0.579	0.035	0.010	1.910	57.50
July	0.537	0.022	0.005	1.930	46.33
August	0.558	0.114	0.017	2.407	65.67
September	0.577	0.123	0.034	2.397	92.33
October	0.520	0.290	0.013	2.830	109.67
November	0.032	0.334	0.081	3.333	310.33
December	0.020	0.422	0.089	4.180	329.67
Mean	0.287	0.252	0.039	2.850	184.15
Std. Dev.	0.279	0.158	0.031	0.959	126.58

A year data collected in OMRF location are presented in Table 3.27.

The developed models are presented in equations 3.17 – 3.20 for the linear regression model (LRM) and equations 3.21 – 3.24 for the GRM.

.

Table 3.28. Parameter Estimation of Linear Regression Model of OMRF Location

	Chromium		Arsenic		Cadmium		Lead	
	Parameter estimates	p-value	Parameter estimates	p-value	Parameter estimates	p-value	Parameter estimates	p-value
(Constant)	4.8150	0.4589	0.748	0.8605	-0.250	0.776	-40.459	0.344
$PM_{2.5}$	-0.0012	0.3546	-0.001	0.3627	0.000	0.339	0.000	0.955
Temp	0.0062	0.8695	0.073	0.0544	-0.002	0.772	0.514	0.101
Rel. Hum	-0.0099	0.6420	0.000	0.9861	-0.003	0.320	0.018	0.890
Pressure	-0.0032	0.6264	-0.002	0.6467	0.001	0.472	0.034	0.431
Windspeed	0.0052	0.9588	-0.040	0.5768	-0.020	0.218	-0.238	0.711
Wind direction	-0.0019	0.3118	-0.002	0.1118	0.000	0.660	-0.016	0.210
Solar radiation	-0.0010	0.0231*	0.000	0.3501	0.000	0.164	-0.002	0.277
Rainfall	-0.0001	0.8380	0.000	0.7543	0.000	0.353	0.002	0.534

*Significant at 5%

Tables 3.28 is the parameter estimate result for the linear regression model (LRM). It shows that chromium has an inverse relationship with all the meteorological parameters in OMRF location with different levels of relationship, except for temperature and wind speed that have direct relationship with it. The most important meteorological parameters that has significant relationship with Chromium is solar radiation based on the p-value ($p < 0.05$). Arsenic also has an inverse relationship with all the meteorological parameters in OMRF Location except for temperature that has direct relationship with it, and relative humidity, solar radiation and rainfall do not have any relationship with it. Cadmium also has an inverse relationship with all the meteorological parameters in OMRF Location except for pressure that has direct relationship with it, and $PM_{2.5}$, wind direction, solar radiation and rainfall do not have any relationship with it. Wind speed is the most important meteorological parameters that has a relationship with Cd. Pb has a direct relationship with temperature, relative humidity, pressure and rainfall, but inverse relationship with speed, wind direction and solar radiation in OMRF Location, while $PM_{2.5}$ does not have any

relationship with it. The most important meteorological parameters that have a relationship with lead is temperature.

The predicted linear regression models for OMRF location are derived by equation 3.17 to 3.20 as follows:

$$\widehat{Cr} = 4.8150 - (-0.0012)PM_{2.5} - 0.0062Tem - (-0.0099)ReH - (-0.0032)Pre - 0.0052WiS - (-0.0019)WiD - (-0.0010)SoR - (-0.0001RaF \quad (3.17)$$

$$\widehat{As} = 0.748 - (-0.001)PM_{2.5} + 0.073Tem - 0.000ReH - (-0.002)Pre - (-0.040)WiS + (-0.002)WiD - 0.000SoR - 0.000RaF \quad (3.18)$$

$$\widehat{Cd} = -0.250 + 0.000\mathrm{PM}_{2.5} + (-0.002)Tem + (-0.003)ReH - 0.001Pre + (-0.020)WiS + 0.000WiD + 0.000SoR + 0.000RaF \quad (3.19)$$

$$\widehat{Pb} = -40.459 + 0.000PM_{2.5} + 0.514Tem + 0.018ReH - 0.034Pre - (-0.238)WiS - (-0.016)WiD - (-0.002)SoR - 0.002RaF \quad (3.20)$$

Table 3.29. Parameter Estimation for Gamma Regression Model of OMRF Location

	Chromium		Arsenic		Cadmium		Lead	
	Parameter estimates	p-value	Parameter estimates	p-value	Parameter estimates	p-value	Parameter estimates	p-value
(Constant)	-321.700	0.730	-37.773	0.875	-59.7494	0.972	0.302	0.928
$PM_{2.5}$	-0.156	0.238	0.048	0.415	-0.30689	0.518	0.001	0.463
Temp	8.680	0.115	-2.032	0.349	7.59712	0.604	-0.049	0.109
Rel. Hum	0.665	0.420	-0.404	0.785	0.7323	0.936	-0.005	0.713
Pressure	0.015	0.988	0.090	0.683	-0.1779	0.906	0.001	0.749
Windspeed	-4.845	0.465	5.259	0.423	1.12435	0.976	0.075	0.268
Wind direction	0.010	0.875	0.048	0.509	-0.17849	0.725	0.002	0.115
Solar radiation	0.128	0.019*	0.020	0.317	0.08843	0.463	0.000	0.196
Rainfall	0.053	0.159	0.069	0.214	0.19844	0.454	0.000	0.455
Scale	0.0541		0.4184		0.3762			

*Significant at 5%

Tables 3.29 is the parameter estimates result for the gamma regression model (GRM). It shows that chromium has a direct relationship with all the meteorological parameters in OMRF Location with different levels of relationship except the windspeed, $PM_{2.5}$ and solar radiation having a significant relationship based on the p value ($p < 0.05$) The most important meteorological parameters that have relationship with chromium are $PM_{2.5}$, wind speed, wind direction solar radiation and rainfall based on their p-value. As also has a direct relationship with all the meteorological parameters in OMRF Location except for temperature and relative humidity that has indirect relationship with it. that has direct relationship with it. Cd has a direct relationship with all the meteorological parameters in OMRF Location except for pressure, $PM_{2.5}$ and wind direction that have indirect relationship with it. Pb also has a direct relationship with all the meteorological parameters in OMRF Location except for temperature and relative humidity have indirect relationship with it, while solar radiation and rainfall that do not have any relationship with it.

The predicted Gamma regression models for OMRF location are stated by equation 3.21 to 3.24 as follows:

$$\widehat{Cr} = -321.700 - (-0.156)PM_{2.5} - 8.680Tem - 0.665ReH - 0.015Pre - (-4.845)WiS - 0.010WiD - 0.128SoR - 0.053RaF) \quad (3.21)$$

$$\widehat{As} = -37.773 - 0.048PM_{2.5} + (-2.032)Tem - (-0.404)ReH - 0.090Pre - 5.259WiS - 0.048WiD - 0.020SoR - 0.069RaF) \quad (3.22)$$

$$\widehat{Cd} = -59.7494 - (-0.30689)PM_{2.5} + 7.59712Tem + 0.7323ReH - (-0.1779)Pre - 1.12435WiS - (-0.17849)WiD + 0.08843SoF - 0.19844RaF) \quad (3.23)$$

$$\widehat{Pb} = 0.302 + 0.001PM_{2.5} - (-0.049)Tem - (0.005)ReH - 0.001Pre - 0.075WiS3. - 0.002WiD - 0.000SoR - 0.000RaF) \quad (3.24)$$

Table 3.30. **Experimental and predicted values of selected heavy metals at OMRF location**

	Chromium (Cr)			Arsenum (As)			Cadmium (Cd)			Lead (Pb)		
	Expt	LRM	GRM	*Expt*	LRM	GRM	*Expt*	LRM	GRM	*Expt*	LRM	GRM
Jan	0.018	0.001	0.020	0.517	0.528	0.513	0.084	0.082	0.080	5.093	5.042	5.069
Feb	0.017	0.003	0.019	0.387	0.390	0.403	0.051	0.050	0.051	3.113	2.997	3.041
Mar	0.025	0.071	0.024	0.294	0.275	0.286	0.041	0.047	0.049	2.393	2.615	2.518
Apr	0.014	0.008	0.013	0.317	0.318	0.318	0.018	0.017	0.017	2.513	2.481	2.495
May	0.551	0.582	0.519	0.170	0.150	0.090	0.022	0.022	0.015	2.100	2.415	2.305
Jun	0.579	0.578	0.614	0.035	0.063	0.050	0.010	0.013	0.011	1.910	2.030	1.986
Jul	0.537	0.543	0.519	0.022	0.003	0.041	0.005	0.005	0.010	1.930	1.776	1.823
Aug	0.558	0.537	0.572	0.114	0.128	0.143	0.017	0.016	0.017	2.407	2.264	2.318
Sep	0.577	0.513	0.577	0.123	0.151	0.125	0.034	0.025	0.021	2.397	2.126	2.248
Oct	0.520	0.555	0.520	0.290	0.269	0.309	0.013	0.018	0.023	2.830	2.894	2.852
Nov	0.032	0.019	0.025	0.334	0.355	0.257	0.081	0.077	0.065	3.333	3.583	3.516
Dec	0.020	0.039	0.025	0.422	0.398	0.490	0.089	0.094	0.105	4.180	3.979	4.028

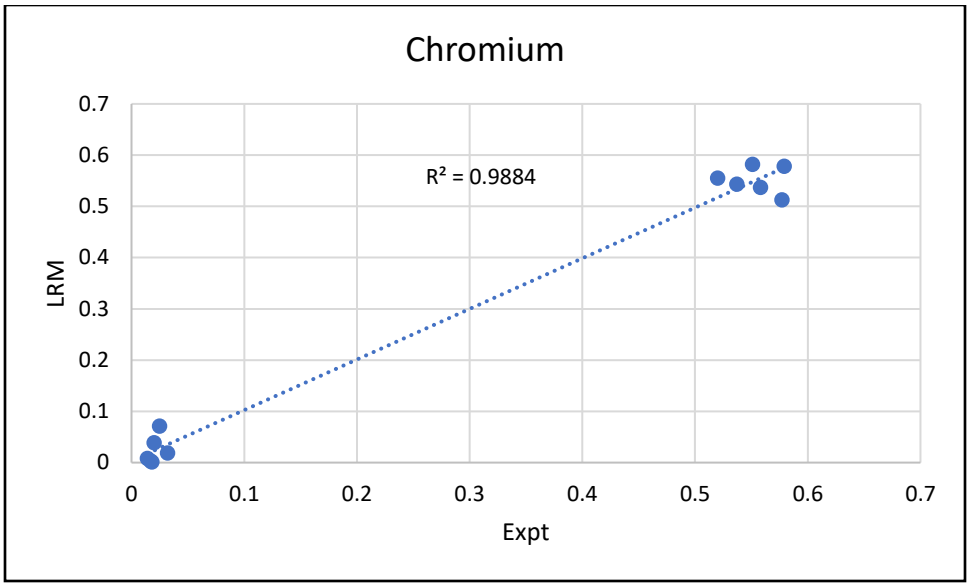

Figure 3.14a. Experimental vs Predicted (LRM) for Chromium (Cr) in OMRF Location

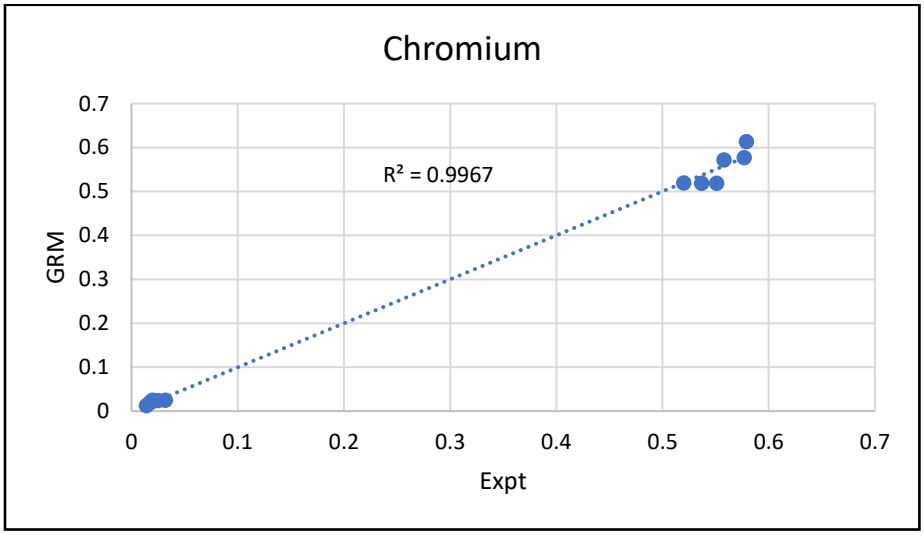

Figure 3.14b. Experimental vs Predicted (GRM) for Chromium (Cr) in OMRF Location

The predicted and experimental values in OMRF location of Cr for both models, linear regression model (LRM) and Gamma regression model (GRM) respectively are depicted on Figures 3.18a and 3.18b. Figure 3.18a suggests that the linear regression model (LRM) is highly accurate in predicting Cr levels based on experimental values, as evidenced by the R^2 value of 0.9884. Most data points are close to the regression line, indicating minimal prediction errors. Figure 3.18b

shows that the Gamma regression model (GRM) is more accurate than LRM with an R^2 value of 0.9967.

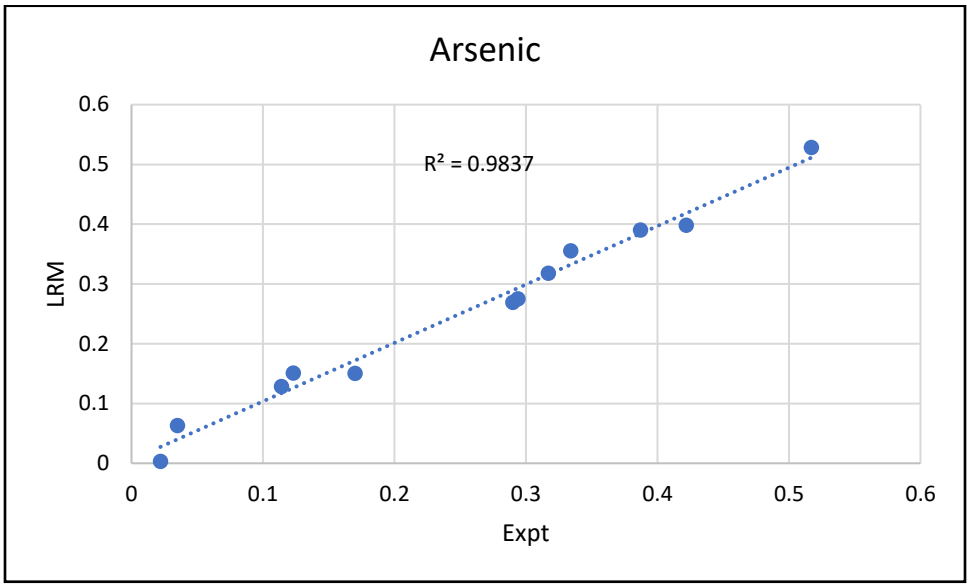

Figure 3.15a Experimental vs Predicted (LRM) for Arsenic in OMRF Location

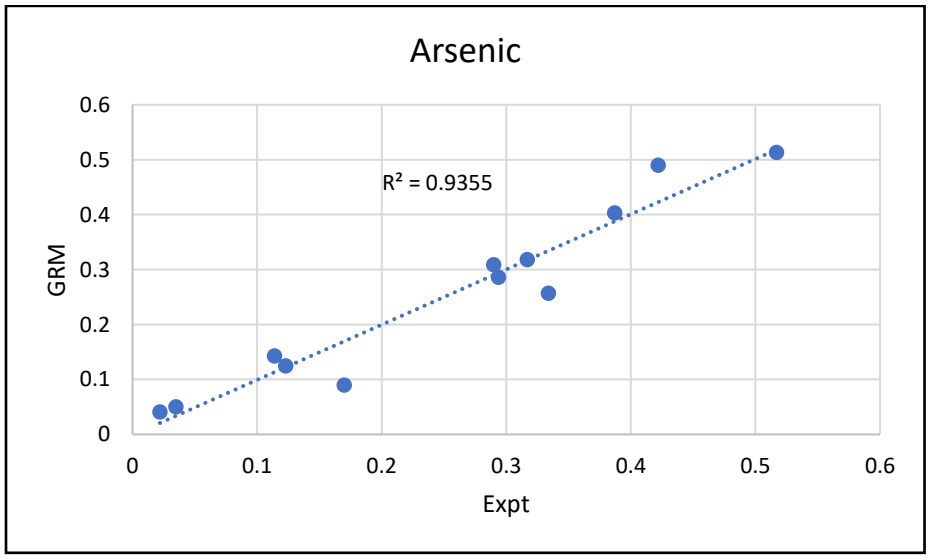

Figure 3.15b. Experimental vs Predicted (GRM) for Arsenic in OMRF Location

The predicted and experimental values for As in OMRF location for both LRM and GRM models are depicted on Figures 3.19a and 3.19b. However, Figure 3.19a suggests that the linear regression model (LRM) accurately predicts Arsenic levels based on experimental values, as evidenced by the R^2 value of 0.9837. Most data points are close to the regression line, indicating minimal

prediction errors. Figure 3.19b shows that the Gamma regression model (GRM) is less accurate than LRM with an R^2 value of 0.9355.

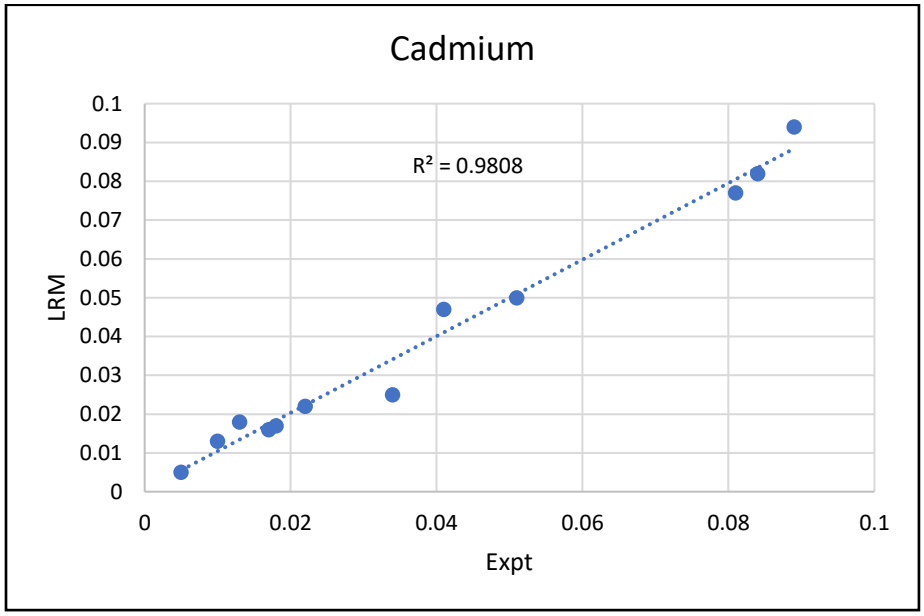

Figure 3.16a. Experimental vs Predicted (LRM) for Cadmium in OMRF Location

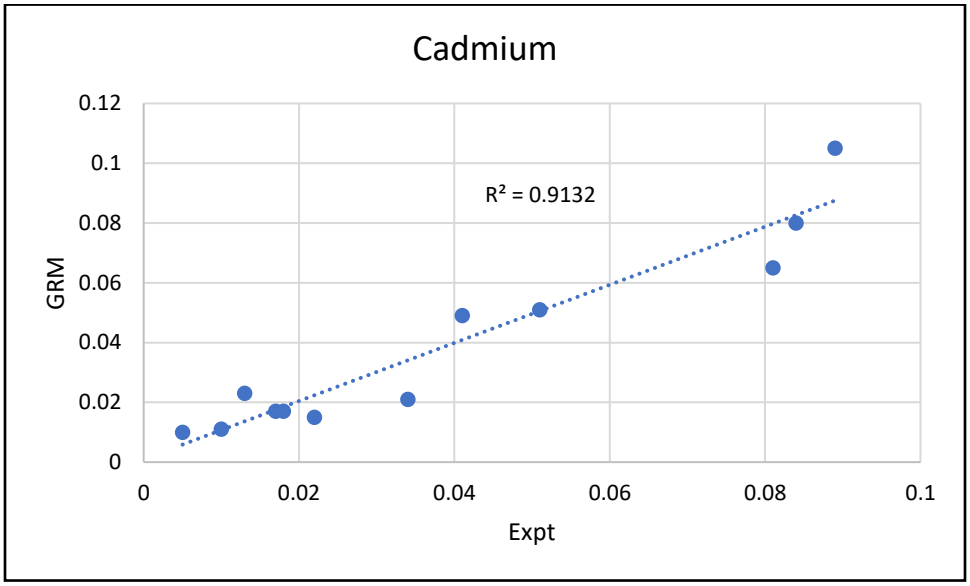

Figure 3.16b. Experimental vs Predicted (GRM) for Cadmium in OMRF Location

The predicted and experimental values in OMRF location of Cd for LRM and GRM models are depicted on Figures 3.20a and 3.20b. Figure 3.20a suggests that LRM accurately predicts Cd

levels based on experimental values, as evidenced by the R^2 value of 0.9808. Most data points are near the regression line, indicating minimal prediction errors. Figure 3.20b shows that GRM is less accurate than LRM with an R^2 value of 0.9132.

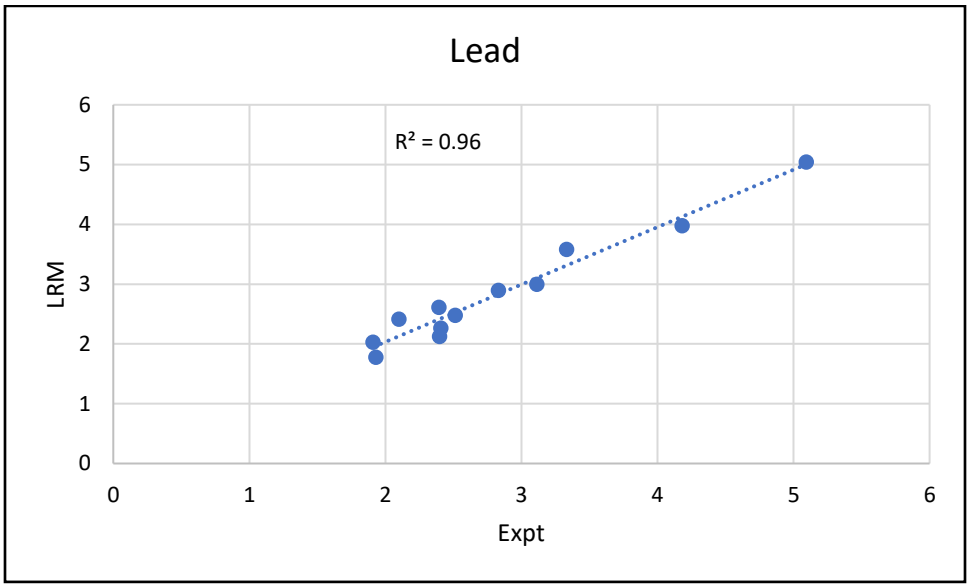

Figure 3.17a. Experimental vs Predicted (LRM) for Lead in OMRF Location

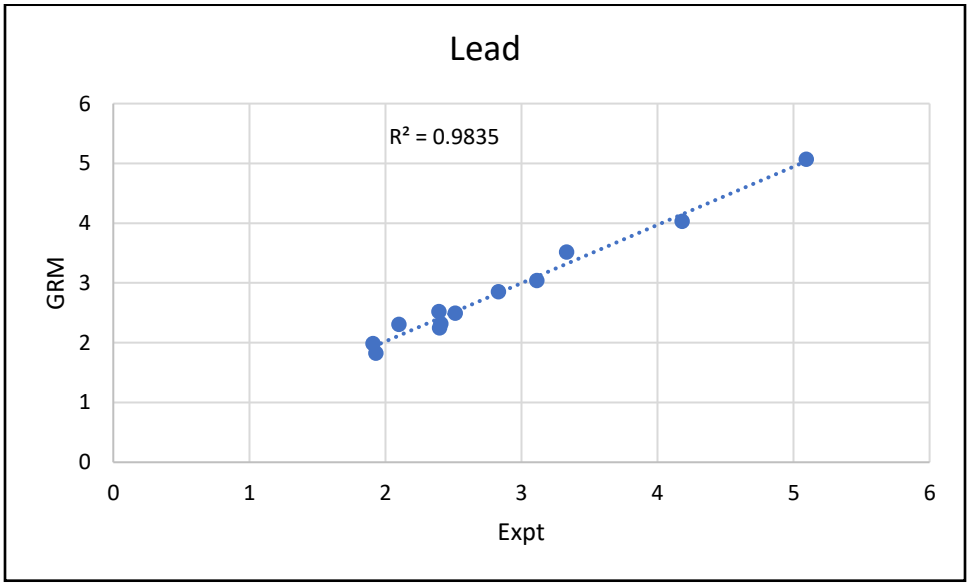

Figure 3.17b Experimental vs Predicted (GRM) for Lead in OMRF Location

The predicted and experimental values in OMRF location of Pb for LRM and GRM are depicted on Figures 3.21a and 3.21b. Figure 3.21a suggests that LRM accurately predicts Pb levels based on experimental values, as evidenced by the R^2 value of 0.96. Most data points are near the

regression line, indicating minimal prediction errors. Figure 3.21b shows that the GRM model is more accurate than LRM with an R^2 value of 0.9835.

In summary, the GRM performed better than LRM in OMRF location for Cr and Pb, while for As and Cd predictions, the LRM outperformed the GRM based on R^2 value.

Thus, when predicting Cr and Pb, GRM should be used as the appropriate model but when predicting As and Cd, LRM should be used as the appropriate model.

Table 3.31. Error Evaluation Function Values of the Developed Models at OMRF Location

	Chromium		Arsenic		Cadmium		Lead	
Error function	LRM	GRM	LRM	GRM	LRM	GRM	LRM	GRM
ARE	0.2107	0.0317	0.1180	0.0947	0.0507	0.1221	0.0217	0.0137
ERRSQ	0.0008	0.0002	0.0004	0.0016	0	0.0001	0.0337	0.014
MPSD	0.8427	0.1268	0.4720	0.3787	0.2027	0.4882	0.0867	0.0548
HYBRID	2.1302	0.0482	0.6683	0.4302	0.1232	0.7151	0.0226	0.009
RMSE	0.0316	0.0170	0.0218	0.0436	0.0045	0.0096	0.2010	0.1294
EABS	0	0	0	0	0	0	0	0
SEE	0.0100	0.0054	0.0069	0.0138	0.0014	0.003	0.0636	0.0409
MRPE	-0.0068	-0.0125	0.0141	-0.0912	-0.033	-0.1155	-0.0035	-0.0022
MSE	0.0010	0.0003	0.0005	0.0019	0	0.0001	0.0404	0.0168

3.9.1.1. Chromium result in OMRF location

Table 3.31 shows that ARE values for GRM and LRM are 0.0317 and 0.2107, respectively. GRM was found to have a better ability to predict the experimental data because of a lower ARE value than the LRM. For LRM and GRM, the corresponding ERRSQ values in this work are 0.0008 and 0.0002. Given that GRM has a lower value of ERRSQ, this indicates that it predicted the experimental data very well. The HYBRID values for LRM and GRM are 2.1302 and 0.0482 respectively, while the MPSD values were 0.8427 and 0.0482 for LRM and GRM, respectively. GRM has a better goodness of fit between the developed models because the lower the MPSD and

HYBRID values, the better the goodness of fit. GRM has a lower RMSE value in this work, indicating a lower error in predicting the experimental data for Cr. The SEE values for LRM and GRM were 0.010 and 0.0054 respectively, indicating that the GRM predicted the experimental data more accurately than the developed models. The GRM also predicts the experimental data than LRM using the absolute values of MRPE and MSE.

3.9.1.2. Arsenic result in OMRF location

Table 3.31 shows that for predicting the experimental values of arsenic, GRM performs better than LRM when ARE, MPSD, and HYBRID criteria are used, while LRM performs better than GRM when ERRSQ, RMSE, SEE and MSE criteria are used.

3.9.1.3. Cadmium result in OMRF location

Table 3.31 shows that for predicting the experimental values of cadmium, LRM performs better than GRM when ARE, ERRSQ, MPSD, HYBRID, RMSE and MSE criteria are used. while GRM performs better than LRM when RMSE, SEE and MRPE criteria are used. However, LRM performs better than GRM when the criteria were used for predicting cadmium in OMRF location.

3.9.1.4. Lead result in OMRF location

Table 3.31 shows that for predicting the experimental values of Lead, GRM performs better LRM when ARE, ERRSQ, MPSD, HYBRID, RMSE, SEE and MSE criteria are used, while LRM performs better than GRM when only MRPE criterion was used. However, GRM performs better than LRM when the criteria were used for predicting Pb in OMRF location.

Table 3.32. Statistical Evaluation Value of the Developed Models at OMRF Location

	Chromium		Arsenic		Cadmium		Lead	
Statistics	LRM	GRM	LRM	GRM	LRM	GRM	LRM	GRM
R	0.9941	0.9983	0.9913	0.9646	0.9904	0.9552	0.9798	0.9917
R^2	0.9883	0.9966	0.9826	0.9304	0.9809	0.9125	0.9601	0.9834
Adj. R^2	0.9677	0.9907	0.9522	0.8087	0.9475	0.7593	0.8903	0.9545
K^2	0.0117	0.0034	0.0174	0.0696	0.0191	0.0875	0.0399	0.0166
t-test	0	0	0	0	0	0	0	0
F-test	1.0119	0.9935	1.0177	0.9253	1.0195	0.9821	1.0416	1.0357
χ^2	0.299	0.0087	0.2018	0.125	0.0068	0.0254	0.1582	0.0641

3.9.1.5. Chromium result in OMRF location

The r values for LRM and GRM in Table 3.32 were, respectively, 0.9941 and 0.9983. The GRM in this study has a higher r value of 0.9983, indicating that it is the superior model to LRM. The study's LRM and GRM, R^2 values were 0.9883 and 0.9966, respectively. With an R^2 value of 0.9966, the GRM model is the superior model among the developed models, accounting for 99.66% of the variation in the predicted Cr. GRM has the lower K^2 value of 0.0034 as compared with LRM with a value of 0.0117, meaning that less than 5% of the experimental data could not be explained by GRM. This suggested that, in comparison to LRM, GRM more accurately represented the experimental data. The F-test results for LRM and GRM are 1.0119 and 0.9935, respectively ($p \geq 0.05$). The null hypothesis, which stated that the means of the experimental and predicted data were statistically significant equal at the 5% significant level, could not be rejected because the F-test p-values were greater than the significance level ($\alpha = 0.05$). Since every developed model passed the F-test, the experimental data will be represented by the model with the lowest F-test value. As a result, GRM was chosen as the ideal model, and LRM rejected.

In this study, the χ^2 test values for LRM and GRM were 0.299 and 0.0087, respectively ($p < 0.05$). The developed models has a p-value of less than 0.05. This suggested that there is no sufficient data to reject the null hypothesis, which stated that there was no significant difference between the

experimental and predicted data. This indicates that there is no significant difference between the data from the developed models and the experimental data. Given that the developed models scaled through the χ^2 test, the model that best represented the experimental data at a p-value of 0.05 was determined to be GRM, which has the lower χ^2 test value. It is evident that GRM has the least deviation from the experimental data when compared to LRM based on the analysis of error evaluation functions performed in this work to assess the error deviation of the developed models. As a result, GRM was chosen as the statistical model to forecast the concentration of chromium in OMRF location.

3.9.1.6. Arsenic result in OMRF location

Table 3.32 shows that LRM has a higher coefficient of correlation (r), coefficient of determination (R^2), and adjusted coefficient of determination (Adj R^2) than GRM in predicting Arsenic. With an R^2 value of 0.9826, the LRM model is the superior model between the developed models, accounting for 98.26% of the variation in the predicted arsenic. LRM has the lower K^2 value of 0.0174 as compared with GRM with a value of 0.0696, meaning that less than 18% of the experimental data could not be explained by LRM. Although, the F-test statistic shows that GRM is better than LRM and Chi-square test statistic also shows that GRM performed better than LRM in predicting arsenic in OMRF location. Thus, this study has demonstrated that GRM predicts arsenic more accurately than LRM in OMRF site.

3.9.1.7. Cadmium results in OMRF location

Table 3.32 shows that LRM has a higher r, R^2 and Adj R^2 than GRM in predicting Cd. With an R^2 value of 0.9834 the GRM model is the superior model between the developed models, accounting for 98.34% of the variation in the predicted cadmium. GRM has a lower K^2 value of 0.0166 as compared with LRM with a value of 0.0399, meaning that less than 4% of the experimental data

could not be explained by LRM. Although, the F-test statistic shows that GRM is better than LRM but the Chi-square test statistic shows that LRM performed better than GRM in predicting cadmium in OMRF location. Thus, this study has demonstrated that LRM predicts Cd more accurately than GRM is OMRF.

3.9.1.8. Lead result in OMRF location

Table 3.32 shows that GRM has a higher r, R^2 and Adj R^2 than LRM in predicting Pb. With an R^2 value of 0.9834, the GRM model is the superior model between the developed models, accounting for 98.34% of the variation in the predicted Lead. GRM has the lower K^2 value of 0.0166 as compared with LRM with a value of 0.0399, meaning that less than 0.5% of the experimental data could not be explained by GRM. The F-test results for LRM and GRM are 1.0416 and 1.0357, respectively ($p \geq 0.05$). Since every developed model passed the F-test, the experimental data will be represented by the model with the lowest F-test value. As a result, GRM was chosen as the ideal model, and LRM was dropped. The χ^2 test values for LRM and GRM are 0.1582 and 0.0641 respectively ($p < 0.05$). This shows that GRM is better than LRM. As a result, GRM is chosen as the statistical model to forecast the amount of Pb in OMRF location.

Table 3.33. **Model Selection Criteria of the Developed Models at OMRF Location**

	Chromium		Arsenic		Cadmium		Lead	
Criteria	LRM	GRM	LRM	GRM	LRM	GRM	LRM	GRM
Log Lik.	25.50337	36.08191	29.9778	17.6867	49.0061	39.6585	3.3216	7.6950
AIC	-31.0067	-52.1638	-39.956	-15.373	-39.956	-15.373	13.3568	4.6010
AICC	58.9933	37.8362	50.044	74.627	11.9878	30.6831	103.357	94.6010
BIC	-26.1577	-47.3148	-35.107	-10.524	-73.163	-54.468	18.2059	9.4590
CAIC	-35.1577	-56.3147	-44.107	-19.524	-82.163	-63.468	9.2059	0.4590268
KS-Stat (D)	0.25	0.1667	0.1667	0.1667	0.1667	0.1667	0.1667	0.1667
KS p-value	0.869	0.9985	0.9985	0.9985	0.9985	0.9985	0.9985	0.9985

3.9.1.9. Chromium result in OMRF location

Table 3.33 shows that GRM is better than LRM using log likelihood (LRM = 25.503, GRM = 36.0819), AIC (LRM = -31.0067, GRM = -52.1638), AICC (LRM = -58.993, GRM = 37.836), BIC (LRM = -26.1577, GRM = -47.3178), CAIC (LRM = -35.1577, GRM = -56.3147) criteria. Using all the criteria, the GRM is better than LRM. However, both models are good fit for the data using KS-Stat and its p-value, but the GRM fit the data best.

3.9.1.10. Arsenic result in OMRF location

Table 3.33 shows that LRM (29.9778) was better than GRM (17.6867) using log likelihood criterion. More so, LRM is better than GRM using the AIC (LRM = -39.956, GRM = -15.373), AICC (LRM = 50.044, GRM = 74.627), BIC (LRM = -35.10, GRM = -10.524), CAIC (LRM = -44.107, GRM = -19.524) criteria. However, both models are good fit for the data using KS-Stat and its p-value.

3.9.1.11. Cadmium result in OMRF location

Table 3.33 shows that LRM (49.0061) is better than GRM (39.6585) using log likelihood criterion. More so, LRM is better than GRM using the AIC (LRM = -39.956, GRM =-15.373), AICC (LRM = 11.9838, GRM = 30.6831), BIC (LRM = -73.163, GRM = -54.468 CAIC (LRM = -82.413, GRM = -63.468) criteria. However, both models are equally good fit for the data using KS-Stat and its p-value.

3.9.1.12. Lead result in SIIE location

Table 3.33 shows that GRM (24.2979) is better than LRM (17.5925) using log likelihood criterion. More so, GRM is better than LRM using the AIC (LRM = -15.185, GRM = -28.596), AICC (LRM = 74.8151, GRM = 61.40414), BIC (LRM = -10.3359, GRM = -23.7468), CAIC (LRM = -19.3358,

GRM = -32.7468) criteria. However, both models are equally good fit for the data using KS-Stat and its p-value.

In summary, the GRM performed better than LRM in OMRF location for Cr and Pb, while for As and Cd predictions, the LRM outperformed the GRM based on R^2 value and other parameters tested.

Thus, when predicting Cr and Pb, GRM should be used as the appropriate model but when predicting As and Cd, LRM should be used as the appropriate model

Having tested on the criteria on the two models, GRM is the better model for predicting Cr and Pb while the LRM is the better model for predicting As and Cr in OMRF location.

Conclusion

The pollution status of heavy metals in the particulate matter emitted from the ambient air of two industrial areas (OMRF and SIIE) in Sagamu, Ogun State have for the first time been assessed. The results obtained from spatial and temporal variations of $PM_{2.5}$ in the ambient air across the study locations follow the order: OMRF > SIIE > OLFS. The average concentration of $PM_{2.5}$ in the dry and wet season seasons were 319.07±22, 177.67±6.08 and 79.40±4.3µg/m^3 and 87.79±7.12, 67.33±5.41 and 43.43± 2.69µg/m^3 respectively for OMRF, SIIE and OLFS. Wet season accounted for only 26% of the inhalable particles while 74% was accounted for the dry season. OMRF was the most polluted of the industrial sites. The annual average $PM_{2.5}$ concentrations were 6 – 20 times and 5 – 17 times the 12hr annual standard limits established by US EPA and WHO for the three study areas.

A comparison of the 12-month average concentrations of Pb, As, Cd, Cr, Ni, Mn, V **trace** metals with the appropriate standard limit values revealed that all these trace metals have their concentration values above WHO standards except vanadium that was BDL of the instrument

used. The average trace metal concentration observed in the dry season was higher than that of the wet season. This has been attributed to difference in meteorological conditions in both seasons,

Pollution Indices (Contamination factor, Degree of contamination and Pollution load Index) were employed to assess the level of contamination of the ambient air of the industries and its immediate surrounding. The values of CF, DC and PLI obtained in this study, indicate significant deterioration of the ambient air quality in the vicinity of the investigated industries.

The results of enrichment factor analysis (EF) and principal component analysis (PCA) for source identification showed very high enrichment for the elements; Pb, Cd, As, Zn, and Cu in the fine fraction ($PM_{2.5}$) while the Principal Component Analysis explained five common contributing sources of fine particulates ($PM_{2.5}$) such as fossils fuel combustion, vehicular emission, industrial emission, biomass burning and dust. To further elucidate the relationship among pollutants in the sampling sites, the results of correlations analysis and cluster analysis also confirmed the results of the EF and PCA.

The predictive model revealed that GRM is a choice model for the prediction of Cr and Pb in both OMRF and SIIE industrial sites while LRM is a better model for the prediction of As and Cd in both OMRF and SIIE.

Findings

The findings from this study were as follows:

1. Up- to- date data and information on $PM_{2.5}$ mass concentration and meteorological data for both dry and wet seasons in the various sampling areas have been obtained.
2. Up- to- date data and information on the levels of metals in $PM_{2.5}$ bound Metals in the study areas have been obtained..

3. Up -to- date data and information on the seasonal variation of $PM_{2.5}$ and its elemental content have been provided.
4. The Pollution indices associated with heavy metals content have been assessed
5. The source of pollutants in the study areas have been identified to be mainly anthropogenic
6. Suitability of applications of developed and validated models for the prediction of Heavy metals in the study areas have been established

Contributions to Knowledge

This study has contributed to knowledge in the following ways;

(i) Baseline data on co-contamination of heavy metals and $PM_{2.5}$ within the vicinity of Industrial study areas had been generated

(i) Models for the prediction of Cr, As, Cd and Pb concentrations from $PM_{2.5}$ and meteorological parameters had been developed

Recommendation for further studies

Health risk assessment within industries surrounding the residential areas is recommended for further studies.

REFERENCES

Abdin, Z., Zafaranloo, A., Rafiee, A., Mérida, W., Lipiński, W., and Khalilpour, K. R. (2020b). Hydrogen as an energy vector. *Renewable and Sustainable Energy Reviews*, *120*, 109620. https://doi.org/10.1016/j.rser.2019.109620

Abe, J., Popoola, A., Ajenifuja, E., and Popoola, O. (2019). Hydrogen energy, economy and storage: Review and recommendation. *International Journal of Hydrogen Energy*, *44*(29), 15072–15086. https://doi.org/10.1016/j.ijhydene.2019.04.068

Abiye, O., Obioh, I. M., and Ezeh, G. (2013). Elemental characterization of urban particulates at receptor locations in Abuja, north- central Nigeria. *Atmospheric Environment*, 81, 695-701.

Abiye, O.E., Obioh, I.B., Ezeh, G.C., Alfa, A., Ojo, E.O., and Ganiyu, A.K(2014).: Receptor modeling of atmospheric aerosols in Federal Capital Territory (FCT), Nigeria. *Ife J. Sci*. 16, 107-119

Abrams, J. Y., Weber, R. J., Klein, M., Samat, S. E., Chang, H. H., Strickland, M. J., Verma, V., Fang, T., Bates, J. T., Mulholland, J. A., Russell, A. G., & Tolbert, P. E. (2017). Associations between Ambient Fine Particulate Oxidative Potential and Cardiorespiratory Emergency Department Visits. *Environmental Health Perspectives*, *125*(10). https://doi.org/10.1289/ehp1545

Abulude, F.O., Arifalo, K.M., Kenni, A.M., Akinnusotu, A., Oluwagbayide, S.D., and Sunday, A. (2022). Air Quality Index Levels of Particulate Matter ($PM_{2.5}$) In Yenogua, Nigeria. *Journal GeografiGea*, Volume 22 (2), 95-105.

Aderoju, M. A (2015). " Impact of kolanuts on socio-economic development of Sagamu, 1910-1970". *Nigerian Journal of Economics*

AEA (2011). UK emissions of air pollutants 1970 to 2009. UK Emissions Inventory Team, Department for Environment, Food and Rural Affairs. http://ukair.defra.gov.uk/reports/cat07/1401131501_NAEI_Annual_Report_2009.pdf.

Aelion, C., Davis, H., Dermett, M.C. and Lawson, A. (2008).Metal concentrations in rural top soil in South- Carolina: Potential for human health impact, *Sci. of the Total Environ.* 402, pp. 149 - 156.

Afandy, E., Azab, E., Alfi, E., & Saad, H. (2022). Throw Light on the Heavy Economic Minerals of the Northern Part of Delta, Egypt. *Middle East Journal of Applied Sciences*. https://doi.org/10.36632/mejas/2022.12.4.39

Akanni, C.O. (1992). Climate. In: Ogun State in Map. Onakomaiya, S. O., Oyesiku, K., Jegede. J.(editors). Rex Charles Publication. Ibadan, Nigeria; pp. 21 - 23.

Akinfolarin, O. M., Boisa, N., and Obunwo, C. C. (2017). Assessment of particulate matter-based air quality index in Port Harcourt, Nigeria. *Journal of Environmental Science, Toxicology and Food Technology*, 11(4), 1-6. https://doi.org/10.9790/2402-1104010106

Alsafran, M., Saleem, M. H., Jabri, H. A., Rizwan, M., & Usman, K. (2022). Principles and Applicability of Integrated Remediation Strategies for Heavy Metal Removal/Recovery from Contaminated Environments. *Journal of Plant Growth Regulation*, *42*(6), 3419–3440. https://doi.org/10.1007/s00344-022-10803-1

Alzheimer's disease facts and figures. (2023). *Alzheimer S & Dementia*, *19*(4), 1598–1695. https://doi.org/10.1002/alz.13016

American city. Atmos Pollut Res 9:66–75. https:// doi. org/ 10.1016/j. apr. 2017. 07. 00

Arshad, N., Hamzah, Z., Wood, A., Saat, A., & Alias, M. (2015). Determination of heavy metals concentrations in airborne particulates matter (APM) from Manjung district, Perak using energy dispersive X-ray fluorescence (EDXRF) spectrometer. In AIP Conference Proceedings (Vol. 1659). AIP Publishing LLC. https://doi.org/10.1063/1.4916878.

Aryal, R ., Kim, A., Lee, B., Kamruzaman, M., and Beecham, S. (2013). Characteristics of atmospheric particulate matter and metals in industrial sites in Korea Rupak. *Environment and Pollution*, 2 (4), 10-21.

Asghar. K , Alib.A,, Tabassum.A , Nadeem,S.G . Hakime, S.T, Amin.M, Raza.G, . Bashirh.S, N. Afshand .N, Usmani, N, Aurangzeba,.N, A. Naza, A and Hussain A (2024) Assessment

of particulate matter (PM) in ambient air of different settings and its associated health risk in Haripur city, Pakistan *Brazilian Journal of Biology*, ISSN 1678 -6984 (Print) ISSN 1678-4375.

Ashley K (2016) HHS Public Access. 2015:7–16

Atkinson RW, Fuller GW, Anderson HR, Harrison RM, Armstrong B. (2010); Urban ambient particles metrics and health: A time series Analysis Epidemiology 21(4):501- 511.

Awad, M., & Khanna, R. (2015). Efficient Learning Machines. *A press e Books*. https://doi.org/10.1007/978-1-4302-5990-9

Ayrault S, Senhou A, Moskura M, Gaudry A. Atmospheric trace element concentrations in total suspended particles near Paris, France. *Journal of Atmospheric Environment*. 2010;44:3700–3707.

Aziakpono, O.M, Ukpebor E.E and Ukpebor J.E (2013)Baseline, Spatial and Temporal Variation of Respirable ($PM_{2.5}$) Particulate Matter in Isoko Land , *Greener Journal of Physical Sciences* SSN: 2276-7851 Impact Factor 2012 (UJRI): 0.7799 ICV 2012: 5.88

Basha G, Prasad VK, Goudar VS. (2014) Seasonal variation of $PM_{2.5}$ and PM_{10} concentrations in urban and rural sites in India. *Atmospheric Pollution Research.* 5(4):726-735.

Bashari, A., Shirvan, A. R., & Shakeri, M. (2018). Cellulose-based hydrogels for personal care products. *Polymers for Advanced Technologies*, *29*(12), 2853–2867. https://doi.org/10.1002/pat.4290

Bawuro, A., Voegborlo, R. and Adimado, A. (2018). Bioaccumulation of heavy Metals in some tissues of fish in Lake Geriyo, Adamawa State, Nigeria. *J. of Environ. and Public Health* (1),pp. 1 - 7.

Begum, B.A., Biswas, S.K., Pandit, G.G., Saradhi, I.V., Waheed, S., Siddique, N., Seneviratne, M.C.S., Cohen, D. D., Markwitz, A., Hopke,P.K., (2010) Long–range transport of soil dust and smoke pollution in the South Asian region. *Atmospheric Pollution Research*2,151–157.

Bereiter, B., Shackleton, S., Baggenstos, D., Kawamura, K., & Severinghaus, J. (2018). Mean global ocean temperatures during the last glacial transition. *Nature*, *553*(7686), 39–44. https://doi.org/10.1038/nature25152

Bhangare, R.C., Ajmal, P.Y., Sahu, S.K., Pandit, G.G. and Puranik, V.D. (2011). Distribution of trace elements in coal and combustion residues from five thermal power plants in India. *Int. J. Coal Geol.* 86: 349‑356.

Bharati, S., & Podder, P. (2022). Machine and Deep Learning for IoT Security and Privacy: Applications, Challenges, and Future Directions. *Security and Communication Networks*, *2022*, 1–41. https://doi.org/10.1155/2022/8951961

Birth G (2003) A scheme for assessing human impacts on coastal aquatic environments using sediments. Coastal Gis. NOT COMPLETE NOTE

Bondy, M., Roth, S., & Sager, L. (2020). Crime Is in the Air: The Contemporaneous Relationship between Air Pollution and Crime. *Journal of the Association of Environmental and Resource Economists*, *7*(3), 555–585. https://doi.org/10.1086/707127

Bozlaker, A., Spada, N.J., Fraser, M.P. and Chellam, S. (2013). Elemental characterization of PM $_{2.5}$ and PM_{10} emitted from light duty vehicles in the Washburn Tunnel of Houston, Texas: Release of rhodium, palladium, and platinum. *Environ. Sci. Technol.* 48: 54‑62.

Cakmak, S., Dales, R., Kauri, L., Mahmud, M., Van Ryswyk, K., Vanos, J., Weichenthal, S. (2014). Metal composition of fine particulate air pollution and acute changes in cardiorespiratory physiology. *Environmental Pollution,* 189:208–214. https://doi.org/10.1016/j.envpol.2014.03.004

CEPA, California Environmental Protection Agency. (2002). Standard operating procedure for the determination of $PM_{2.5}$ mass in ambient air by gravimetric analysis. *Air Resources Board,* SOP MLD 005.

Changela, H. G., Chatzitheodoridis, E., Antunes, A., Beaty, D., Bouw, K., Bridges, J. C., Capova, K. A., Cockell, C. S., Conley, C. A., Dadachova, E., Dallas, T. D., De ,Dong, C.,

Ellery, A., Ferus, M., Foing, B., Fu, X., Fujita, K., Lin, Y.,Hallsworth, J. E. (2021). Mars: new insights and unresolved questions. *International Journal of Astrobiology*, *20*(6), 394–426. https://doi.org/10.1017/s1473550421000276

Chauhan, B. V. S., Corada, K., Young, C., Smallbone, K. L., & Wyche, K. P. (2024). Review on Sampling Methods and Health Impacts of Fine ($PM_{2.5}$, ≤2.5 µm) and Ultrafine (UFP, $PM_{0.1}$, ≤0.1 µm) Particles. *Atmosphere*, *15*(5), 572. https://doi.org/10.3390/atmos15050572

Chen, H., Chen, W., Chang, C., & Chuang, Y. (2013). Characterization of particles in the ambience of the high-tech industrial park of central. *Aerosol and Air Quality Research*, 13, 699-708.

Chen, W., Wang, F., Xiao, G., Wu, K., and Zhang, S. (2015). Air quality of Beijing and impacts of the new ambient air quality standard. *Atmosphere*, 6, 1243-1258.

Cheng, H., Zhou, T., Li, Q., Lu, L., & Lin, C. (2014). Anthropogenic Chromium Emissions in China from 1990 to 2009.(Research Article). PLoS ONE, 9(2). https://doi.org/10.1371/journal.pone.0087753.

Chow, J.C. (1995). "Critical Review: *Measurement Methods to Determine Compliance of Ambient Air Quality Standards for Suspended Particles*." J. Air and Waste Management Assoc., 45, 320–385

Coccia, M. (2020b). Factors determining the diffusion of COVID-19 and suggested strategy to prevent future accelerated viral infectivity similar to COVID. *The Science of the Total Environment*, *729*, 138474. https://doi.org/10.1016/j.scitotenv.2020.138474

Conn, J. G. M., Carter, J. W., Conn, J. J. A., Subramanian, V., Baxter, A., Engkvist, O., Llinas, A., Ratkova, E. L., Pickett, S. D., McDonagh, J. L., Palmer, D. S. (2023). Blinded Predictions and Post Hoc Analysis of the Second Solubility Challenge Data: Exploring Training Data and Feature Set Selection for Machine and Deep Learning Models. *J Chem Inf Model*, 63(4):1099-1113

Conti, M., and Tudino, M. (2016). Lichens as Bio-monitors of Heavy-Metal Pollution. *Comprehensive analytical chemistry* (pp. 117–145). https://doi.org/10.1016/bs.coac.2016.02.005

Croft, D. P., Zhang, W., Lin, S., Thurston, S. W., Hopke, P. K., Masiol, M., Squizzato, S., van Wijngaarden, E., Utell, M. J., and Rich, D. Q (2019).: The association between 638 respiratory infection and air pollution in the setting of air quality policy and 639 economic change. *Annals of the American Thoracic Society*, 16(3), 321–330, 640 https://doi.org/10.1513/AnnalsATS.201810-691OC

Das, R., Khezri, B., Srivastava, B., Datta, S., Sikdar, P., Webster, R., & Wang, X. (2015). Trace element composition of $PM_{2.5}$ and PM_{10} from Kolkata – a heavily polluted Indian metropolis. *Atmospheric Pollution Research*, 6(5), 742–750. https://doi.org/10.5094/APR.2015.083.

Deng, J., Yang, Z., Wang, H. (2023). A systematic study of key elements underlying molecular property prediction. *Nat Commun* 14, 6395. Doi: 10.1038/s41467-023-41948-6.

Deng, S., Shi, Y., Liu, Y., Zhang, C., Wang, X., Cao, Q.,Li, S. and Zhang, F. (2014). Emission Characteristics of Cd, Pb and Mn from Coal Combustion: Field Study at Coal-fired Power Plants in China. *Fuel Process. Technol*. 126, 469–475.

Diana, A., Bertinetti, S., Abollino, O., Giacomino, A., Buoso, S., Favilli, L., Inaudi, P., & Malandrino, M. (2022). PM_{10} Element Distribution and Environmental-Sanitary Risk Analysis in Two Italian Industrial Cities. *Atmosphere*, *14*(1), 48. https://doi.org/10.3390/atmos14010048

Ding, C., Chen, J., Zhu, F., Chai, L., Lin, Z., Zhang, K., & Shi, Y. (2022c). Biological Toxicity of Heavy Metal(loid)s in Natural Environments: From Microbes to Humans. *Frontiers in Environmental Science*, *10*. https://doi.org/10.3389/fenvs.2022.920957

Dris, R., Gasperi, J., & Tassin, B. (2017). Sources and Fate of Microplastics in Urban Areas: A Focus on Paris Megacity. *The handbook of environmental chemistry* (pp. 69–83). https://doi.org/10.1007/978-3-319-61615-5_4

Drventić, I., Šala, M., Vidović, K., & Kroflič, A. (2023). Direct quantification of PAHs and nitro-PAHs in atmospheric PM by thermal desorption gas chromatography with electron ionization mass spectroscopic detection. *Talanta*, *251*, 123761. https://doi.org/10.1016/j.talanta.2022.123761

Du, Y., Gao, B., Zhou, H., Xinxin, J., Hao, H., Yin, S., 2013. Health risk assessment of heavy metals in road dusts in 11 urban parks of Beijing, China. *Procedia Environ. Sci*. 18, 229–309. D

Duan, J., Tan, J., Wang, S., Hao, J. and Chai, F. (2012) Size distributions and sources of elements in particulate matter at curbside, urban and rural sites in Beijing. *J Environ. Sci. (China)*. 24: 87–94.

Dwivedi, Y. K., Hughes, L., Kar, A. K., Baabdullah, A. M., Grover, P., Abbas, R., Andreini, D., Abumoghli, I., Barlette, Y., Bunker, D., Kruse, L. C., Constantiou, I., Davison, R. M., De, R., Dubey, R., Fenby-Taylor, H., Gupta, B., He, W., Kodama, M., Wade, M. (2022). Climate change and COP26: Are digital technologies and information management part of the problem or the solution? An editorial reflection and call to action. *International Journal of Information Management*, *63*, 102456. https://doi.org/10.1016/j.ijinfomgt.2021.102456

EC, European Commission (2015). Air quality standards. Retrieved from http;//ec.europa.eu/air/quality/standards.htm

Eil, A., Li, J., Baral, P., & Saikawa, E. (2020). Dirty Stacks, High Stakes. In *World Bank, Washington, DC eBooks*. https://doi.org/10.1596/33727

Ezeh, G. C., Obioh, I. B., Asubiojo, O. I, and Abiye O. E. (2012). PIXE characterization of PM10 and $PM_{2.5}$ particulates sizes collected in Ikoyi Lagos, Nigeria. *Toxicological and Environmental Chemistry*, 94 (5), 884-894.

Faaique, M. (2023). Overview of Big Data Analytics in Modern Astronomy. *International Journal of Mathematics Statistics and Computer Science*, *2*, 96–113. https://doi.org/10.59543/ijmscs.v2i.8561

Faiz, Y., Tufail, M.D., Tayyeh, M.L., Chaudhry, M.M., Siddique.N.,(2009) Road dust pollution of Cd, Cu, Ni, Pb, and Zn along Islamabad Expressway, Pakistan. *Microchem*, J.92,186-192

Fang, X., Li, R., Xu, Q., Bottai, M., Fang, F., & Cao, Y. (2016). A two-stage method to estimate the contribution of road traffic to PM2.5 concentrations in Beijing, China. *International Journal of Environmental Research and Public Health*, 13(12), 2-19

Fois, G., Vega, D. L., Pereda, A., Terray, L., Chardon, P., Kolovi, S., Breton, V., and Maigne, L. (2023). Simulation of the radiation exposure of microorganisms living in submarine hydrothermal systems using GATE and Geant4-DNA Monte Carlo simulation tools. *Book of Abstracts*. https://doi.org/10.21175/rad.abstr.book.2023.39.11

Gao Y, Nelson E.D, Field M.P, Ding Q, Li H,Sherrel R.M, Gigliotti C.L, Vanry D.A, Glenn T.R, Eisenreich S.J.(2011) Characterization of Atmospheric Trace Elements on $PM_{2.5}$ Particulate Matter over the New York–New Jersey Harbor Estuary. *Journal of Atmospheric environment.* 2002;36:1077-1086.

Giordano, M. R., Malings, C., Pandis, S. N., Presto, A. A., McNeill, V., Westervelt, D. M., Beekmann, M., & Subramanian, R. (2021). From low-cost sensors to high-quality data: A summary of challenges and best practices for effectively calibrating low-cost particulate matter mass sensors. *Journal of Aerosol Science*, *158*, 105833. https://doi.org/10.1016/j.jaerosci.2021.105833

Gu, J.W., Pitz, M., Schnelle–Kreis, J., Diemer, J., Reller, A., Zimmermann, R., Soentgen,. I., Stoelzel, M., Wichmann, H.E., Peters, A., Cyrys, J.,(2011). Source apportionment of ambient particles: Comparison of positive matrix factorization analysis applied to particle size distribution and chemical composition data. *Atmospheric Environment* 45,1849–1857

Gunawardena, J; Egodawatta, P; Myoko, GA; Goonetilleke, A (2012). Role of traffic in atmospheric accumulation of heavy metals and polycyclic aromatic hydrocarbons, *Atmos. Environ*. 54:502-510.

Guo, H., Bao, A., Liu, T., Jiapaer, G., Ndayisaba, F., Jiang, L., Kurban, A., & De Maeyer, P. (2018). Spatial and temporal characteristics of droughts in Central Asia during 1966–2015. *The Science of the Total Environment*, *624*, 1523–1538. https://doi.org/10.1016/j.scitotenv.2017.12.120

Hamzehpour, N., Marcolli, C., Pashai, S., Klumpp, K., & Peter, T. (2022). Measurement report: The Urmia playa as a source of airborne dust and ice-nucleating particles – Part 1: Correlation between soils and airborne samples. *Atmospheric Chemistry and Physics*, *22*(22), 14905–14930. https://doi.org/10.5194/acp-22-14905-2022

Hewamalage, H., Ackermann, K. & Bergmeir, C. (2023). Forecast evaluation for data scientists: common pitfalls and best practices. *Data Min Knowl Disc,* 37, 788–832. Doi: 10.1007/s10618-022-00894-5.

Holland, S., Mansur, E., Muller, N., & Yates, A. (2020). *The Environmental Benefits from Transportation Electrification: Urban Buses*. https://doi.org/10.3386/w27285

Hopke, P. K., Croft, D., Zhang, W., Lin, S., Masiol, M., Squizzato, S., Thurston, S. W., van Wijngaarden, E., Utell, M. J., and Rich, D. Q (2019).: Changes in the acute response of respiratory diseases to $PM_{2.5}$ in New York State from 2005 to 2016. *Science of the Total Environment,* 677, 328-339,

Huang L, Wang K, Yuan CS, Wang G (2010) Study on the seasonal variation and source apportionment of PM_{10} in Harbin, China. *Aerosol Air Qual Res* 10: 86-93

Huang, B., Liu, M., Ren, Z., Bi, X., Zhang G., Sheng, G., and Fu, J. (2013). Chemical composition, diurnal variation and sources of $PM_{2.5}$ at two industrial sites of South China. *Atmospheric Pollution Research*, 4, 298-305.

Huang, J., Boles, S. T., & Tarascon, J. (2022). Sensing as the key to battery lifetime and sustainability. *Nature Sustainability*, *5*(3), 194–204. https://doi.org/10.1038/s41893-022-00859-y

Huang, L., Yu, C. H., Hopke, P. K., Lioy, P. J., Buckley, B. T., Shin, J. Y., & Fan, Z. T. (2014). Measurement of Soluble and Total Hexavalent Chromium in the Ambient Airborne Particles in New Jersey. *Aerosol and air quality research*, 14(7):1939–1949. https://doi:10.4209/aaqr.2013.10.0312.

Huq, S., Wu, J., Guan, Z., Ling, Y., De, A., & Roy, N. (2023). Arsenic in the Environment - Sources, Impacts and Remedies. *Intech Open eBooks*. https://doi.org/10.5772/intechopen.1001534

Irudayaraj, A. X. R., Wahab, N. I. A., Veerasamy, V., Premkumar, M., Radzi, M. M., Sulaiman, N. B., and Alhelou, H. H. (2023). Decentralized frequency control of restructured energy system using hybrid intelligent algorithm and non-linear fractional order proportional integral derivative controller. *IET Renewable Power Generation*, *17*(8), 2009–2037. https://doi.org/10.1049/rpg2.12746

Isa, Y. M. (2021). Bioremediation of acid mine drainage and crude contaminated soils. https://doi.org/10.51415/10321/3628

Islam, M. F., Majumder, S. S., Mamun, A. A., Khan, M. B., Rahman, M. A., & Salam, A. (2015). Trace Metals Concentrations at the Atmosphere Particulate Matters in the Southeast Asian Mega City (Dhaka, Bangladesh). *Open Journal of Air Pollution*, *04*(02), 86–98. https://doi.org/10.4236/ojap.2015.42009

Iyengar, S., Lelkes, Y., Levendusky, M., Malhotra, N., & Westwood, S. J. (2019). The Origins and Consequences of Affective Polarization in the United States. *Annual Review of Political Science*, *22*(1), 129–146. https://doi.org/10.1146/annurev-polisci-051117-073034

James, S. L., Abate, D., Abate, K. H., Abay, S. M., Abbafati, C., Abbasi, N., Abbastabar, H., Abd-Allah, F., Abdela, J., Abdelalim, A., Abdollahpour, I., Abdulkader, R. S., Abebe, Z., Abera, S. F., Abil, O. Z., Abraha, H. N., Abu-Raddad, L. J., Abu-Rmeileh, N. M. E.,

Accrombessi, M. M. K., Bali, A. G. (2018b). Global, regional, and national incidence, prevalence, and years lived with disability for 354 diseases and injuries for 195 countries and territories, 1990–2017: a systematic analysis for the Global Burden of Disease Study 2017. *The Lancet*, *392*(10159), 1789–1858.

Jantzi, S. C., Motto-Ros, V., Trichard, F., Markushin, Y., Melikechi, N., & De Giacomo, A. (2016). Sample treatment and preparation for laser-induced breakdown spectroscopy. *Spectrochimica Acta Part B Atomic Spectroscopy*, *115*, 52–63. https://doi.org/10.1016/j.sab.2015.11.002

Jiang, N., Dong, Z., Xu, Y.Q., Yu, F., Yin, S.S., Zhang, R.Q. and Tang, X.Y. (2018a). Characterization of PM_{10} and $PM_{2.5}$ source profiles of fugitive dust in Zhengzhou, China. *Aerosol Air Qual. Res.* 18: 314‑329.

Jiang, Y., Xing, J., Wang, S., Chang, X., Liu, S., Shi, A., Liu, B., and Sahu, S. K. (2021): Understand the local and regional contributions on air pollution from the view of human health impacts. *Frontiers of Environmental Science and Engineering,* 711 15(5),

Joseph, D., Ahuja, P., Dockrell, M., Purchase, D., Price, R., Krishna, S., García-Muñoz, J., Pérez-López, M., Soler, F., Míguez-Santiyán, M. P., Martínez-Morcillo, S., Guareschi, E., Okolo, K., Odumbe, E., Murunga, S., Ndiiri, J., Kumar, A., & Singh, R. (2023). Trace Metals in the Environment. *Intech Open eBooks*. https://doi.org/10.5772/intechopen.1001530

Karpińska, J., & Kotowska, U. (2019). Removal of Organic Pollution in Water Environment. In *MDPI eBooks*. https://doi.org/10.3390/books978-3-03921-841-7

Kendall, H., Kuznesof, S., Dean, M., Chan, M., Clark, B., Home, R., Stolz, H., Zhong, Q., Liu, C., Brereton, P., & Frewer, L. (2019). Chinese consumer's attitudes, perceptions and behavioural responses towards food fraud. *Food Control*, *95*, 339–351. https://doi.org/10.1016/j.foodcont.2018.08.006

Khalid, S., Shahid, M., Niazi, N. K., Murtaza, B., Bibi, I., & Dumat, C. (2017). A comparison of technologies for remediation of heavy metal contaminated soils. *Journal of Geochemical Exploration*, *182*, 247–268. https://doi.org/10.1016/j.gexplo.2016.11.021

Khan, M. F., Latif, M. T., Saw, W. H., Amil, N., Nadzir, M. S. M., Sahani, M., and Chung, J. X. (2016). Fine particulate matter in the tropical environment: monsoonal effects, source apportionment, and health risk assessment. *Atmospheric Chemistry and Physics*, 16, 597-617.

Khraisat, A., Gondal, I., Vamplew, P., & Kamruzzaman, J. (2019). Survey of intrusion detection systems: techniques, datasets and challenges. *Cybersecurity*, *2*(1). https://doi.org/10.1186/s42400-019-0038-7

Kim, K., Kabir, E., and Kabir S. (2015). A review on the human health impact of airborne particulate matter. *Environment International*, 74, 136-143.

Kim, K., Shon, Z., Maulida, P., and Song, S. (2014). Long-term monitoring of airborne nickel (Ni) pollution in association with some potential source processes in the urban environment. *Chemosphere,* 111:312–319. https://doi.org/10.1016/j.chemosphere.2014.03.138.

Klimont, Z., Kupiainen, K., Heyes, C., Purohit, P., Cofala, J., Rafaj, P., Borken-Kleefeld, J., & Schöpp, W. (2017). Global anthropogenic emissions of particulate matter including black carbon. *Atmospheric Chemistry and Physics*, *17*(14), 8681–8723. https://doi.org/10.5194/acp-17-8681-2017

Kumar, V., Kumar, P., & Singh, J. (2019). Contaminants in Agriculture and Environment: Health Risks and Remediation. In *Agro Environ Media - Agriculture and Environmental Science Academy, Haridwar, India eBooks* (pp. 1–301).

Kumar, V., Kumar, P., & Singh, J. (2020). Environmental Degradation: Causes and Remediation Strategies. In *Agro Environ Media - Agriculture and Ennvironmental Science Academy, Haridwar, India eBooks* (pp. 1–227). https://doi.org/10.26832/aesa-2020-edcrs

Laden, F., Neas, L.M., Dockery, D.W. and Schwartz, J. (2000). Association of Fine particulate matter from different sources with daily mortality in six U.S. cities. *Environ. Health Perspect*. 108:941–947. doi:10.1289/ehp.00108941

Lala, M.A., Onwnzo, C.S., Adesina, O.A., and Sonibare, J.A. (2023). Particulate matters pollution in selected areas of Nigeria: Spatial analysis and risk assessment. Case Studies in Chemical and Environmental Engineering. Doi: https://doi.org/10.1016/j.cscee.2022.100288

Latif, M. T., Ngah, S. A., Dominick, D., Razak, I. S., Guo, X., Srithawirat, T., & Mushrifah, I. (2015). Composition and source apportionment of dust fall around a natural lake. *Journal of Environmental Sciences*, 33, 143-155

Lawal, A.O., Batagarawa, S.M., Oyeyinka , O.D. and Lawal, M.O. (2011). Estimation of heavy metals in Neem tree leaves along Katsina - Dutsinma - Funtua Highway in Katsina State of Nigeria. *J. of Appl. Sci. Environ. Manage.,* 15(2), pp. 327- 330.

Lee, D., Fahey, D., Skowron, A., Allen, Burkhardt, U., Chen, Q., Doherty, S., Freeman, S., Forster, P., Fuglestvedt, J., Gettelman, A., De León, R., Lim, L., Lund, M., Millar, R., Owen, B., Penner, J., Pitari, G., Prather, M., Wilcox, L. (2021). The contribution of global aviation to anthropogenic climate forcing for 2000 to 2018. *Atmospheric Environment*, *244*, 117834. https://doi.org/10.1016/j.atmosenv.2020.117834

Lenntech, B.V. (2016). Heavy metals. Retrieved from http:// www.lenntech.com.html

Li, H., Aguirre-Villegas, H. A., Allen, R. D., Bai, X., Benson, C. H., Beckham, G. T., Bradshaw, S. L., Brown, J. L., Brown, R. C., Cecon, V. S., Curley, J. B., Curtzwiler, G. W., Dong, S., Gaddameedi, S., García, J. E., Hermans, I., Kim, M. S., Ma, J., Mark, L. O., Huber, G. W. (2022). Expanding plastics recycling technologies: chemical aspects, technology status and challenges. *Green Chemistry*, *24*(23), 8899–9002. https://doi.org/10.1039/d2gc02588d

Li, Q., Cheng, H., Zhou, T., Lin, C. and Guo, S. (2012). The Estimated Atmospheric Lead Emissions in China, 1990-2009. *Atmos. Environ.* 60: 1‑8.

Li, W. (2019). *Title: Employing Earth Observations and Artificial Intelligence to Address Key Global Environmental Challenges in Service of the SDGs*. https://doi.org/10.36837/chapman.000115

Li, X., Huang, L., Li, J., Shi, Z., Wang, Y., Zhang, H., Ying, Q., Yu, X., Liao, H., and Hu, J.(2019): Source contributions to poor atmospheric visibility in China. Resources, Conservation and Recycling, 143, 167-177,

Liang, L., & Gong, P. (2020). Urban and air pollution: a multi-city study of long-term effects of urban landscape patterns on air quality trends. *Scientific Reports*, *10*(1). https://doi.org/10.1038/s41598-020-74524-9

Liu X, Li C, Tu H, Wu Y, Ying C, Huang Q, Wu S, Xie Q, Yuan Z,Lu Y (2016) Analysis of the effect of meteorological factors on $PM_{2.5}$-associated PAHs during autumn-winter in urban Nanchang. *Aerosol Air Qual Res* 16:3222–3229. https:// doi. org/ 10. 4209/ aaqr.2016. 08. 0351

Liu, J., and Cui, S. (2014). Meteorological influences on seasonal variation of fine particulate matter in cities over Southern Ontario, Canada. *Advances in Meteorology*, 5, 1-15

Liu, Z., Xu, Z., Xu, L., Buyong, F., Chay, T. C., Li, Z., Cai, Y., Hu, B., Zhu, Y., & Wang, X. (2022). Modified biochar: synthesis and mechanism for removal of environmental heavy metals. *Carbon Research*, *1*(1). https://doi.org/10.1007/s44246-022-00007-3

Loomis, D., Huang, Wei., and Chen G. (2014). The international agency for research on cancer (IARC) evaluation of the carcinogenicity of outdoor air pollution: focus on China. *Chinese Journal of Cancer*, 33(4): 189-196.

Lu, X., Wang, L., Li, L. Y., Lei, K., Huang, L. and Many, D. (2010). Multivariate statistical analysis of heavy metals in street dust of Baoji, N. W. China. *J. of Hazard. Material.* 173, pp.744 -749.

Manoli, E., Voutsa, D. and Samara, C. (2002). Chemical Characterization and source Identification/Apportionment of Fine and Coarse Air Particles in Thessaloniki, Greece.

Maryam, M, (2012) Metal levels in airborne particulate matter in industrial area of Bandar, Abbas, Iran, *Eur. J. Exp. Biol*., № 2, с. 1714

Mavroulis, S., Mavrouli, M., Lekkas, E., & Tsakris, A. (2023). Managing Earthquake Debris: Environmental Issues, Health Impacts, and Risk Reduction Measures. *Environments*, *10*(11), 192. https://doi.org/10.3390/environments10110192

Megaritis, A. G., Fountoukis, C., Charalampidis, P. E., Denier van der Gon, H. A. C. , Pilinis, C., and Pandis, S. N. (2014). Linking climate and air quality over Europe: Effects of meteorology on PM2.5 concentrations. *Atmospheric Chemistry and Physics*, 14, 10283-10298

Meseke, N. O., Akpootu, D. O., Falaiye, O. A., and Targema, T. V. (2022). Comparative Assessment of Particulate Matter Using Low Cost Sensor: A Case Study of Abuja and Kano, Nigeria. *Journal of Sciences,* 6(4), 203 - 211. https://doi.org/10.33003/fjs-2022-0604-1066.

Mihai, F., Gündoğdu, S., Markley, L. A., Olivelli, A., Khan, F. R., Gwinnett, C., Gutberlet, J., Reyna-Bensusan, N., Llanquileo-Melgarejo, P., Meidiana, C., Elagroudy, S., Ishchenko, V., Penney, S., Lenkiewicz, Z., & Molinos-Senante, M. (2021). Plastic Pollution, Waste Management Issues, and Circular Economy Opportunities in Rural Communities. *Sustainability*, *14*(1), 20. https://doi.org/10.3390/su14010020

Mittal, D., Kaur, G., Singh, P., Yadav, K., & Ali, S. A. (2020c). Nanoparticle-Based Sustainable Agriculture and Food Science: Recent Advances and Future Outlook. *Frontiers in Nanotechnology*, *2*. https://doi.org/10.3389/fnano.2020.579954

Mohammad A.K., Assen O.B., Alaa R.M., Terry L.W .(2011) Multielement determination of flame atomic absorption of road dust samples in Delta, Egypt, *Microchemical journal* vol.97 issue2, 234-242

Montgomerie, R., Hemmings, N., Thompson, J. E., & Birkhead, T. R. (2021). The Shapes of Birds' Eggs: Evolutionary Constraints and Adaptations. *The American Naturalist*, *198*(6), E215–E231. https://doi.org/10.1086/716928

Moustafa, M., Mohamed, A., Ahmed, A. R., & Nazmy, H. (2015). Mass size distributions of elemental aerosols in industrial area. *Journal of Advanced Research*, 6, 827-832.

Mustaffa, N. I. H., Latif, M. T., Ali, M. M., & Khan, M. F. (2014). Source apportionment of surfactants in marine aerosols at different locations along the Malacca Straits. *Environmental Science and Pollution Research*, 21, 6590-6602.

NAAQS, 2014. United State National Ambient Air Quality (NAAQS). ⟨http://epa.gov/air/crteria.html⟩.

Nasr, S.M., Okbah, M.A., Kasem, S.M., 2006. Environmental assessment of heavy metal pollution in bottom sediment of Aden port, Yemen. *Int. J. Ocean Oceanogr*. 1 (1), 99–109.

Natarajan, R., Carr, A., Balz, F., Nauman, G., Gray, J., Parkinson, R., Levine, M., Paller, C., Foster, M., Antony, A., Peng, S., Fitzpatrick, M., Baillie, N., Castro, M., Carson, G., Mcconnell, M., Herst, P., & Prier, M. (2018). Vitamin C: Current Concepts in Human Physiology. In *MDPI eBooks*. https://doi.org/10.3390/books978-3-03897-295-2

National Cancer Institute (NCI) (2019). Nickel Compounds: Which cancers are associated with exposure to nickel and nickel compounds

NESREA. (2013). National environmental standards and regulations enforcement agency. Retrieved from http://www.nesrea.gov.ng/

Nicholas, E.S. and Ukoha, P.O. (2023). An Assessment of Atmospheric Pollutants ($PM_{2.5}$, PM_{10}, CO_2, SO_2, NO_2 and CO) concentrations on Air Quality Using Air Quality Index in Eastern Nigeria. *Journal of Chemical Society of Nigeria*, 48(4).

NPC, National and Population Commission. (2016). Population and housing census of the Federal Republic of Nigeria. Retrieved from http://www.population.gov.ng/images/Priority.

Obioh, I. B., Ezeh, G. C., Abiye, O. E, Alpha, A., Ojo, E. O., and Ganiyu, A. K . (2013). Atmospheric particulate matter in Nigerian megacities. *Toxicological and Environmental Chemistry,* 95, 3, 379-385.

Odekanle, E., Fakinle, B., Akeredolu, F., Sonibare, J., & Adesanmi, A. (2016). Personal exposures to particulate matter in various modes of transport in Lagos city, Nigeria. *Sustainable Environment*, *2*(1), 1260857. https://doi.org/10.1080/23311843.2016.1260857

Ogundele, L.T., Owoade, O.K. ,Hopke, P.K., and Olise, F.S., (2017) Heavy metals in industrially emitted particulate matter in Ile-Ife, Nigeria*, Environmental Research*,156, pp.320-325

Okuo, J. M., Chiedu, I. E., Anegbe, B., Oyibo, F. O. and Ojo, W. (2017) Elemental Characterization and Source Identification of Fine Particulate Matter (PM2.5) in an Industrial Area of Lagos State, Nigeria. *Physical Science International Journal.* 16 (2):1-1.

Okuo, J. M., Oyibo, F. O., Anegbe, B., Chiedu, I. E., Adeniyi, O. and Ojo, W. (2018). Quantification of Total Suspended Particulate (TSP) and its Elemental Content in Different Micro Environments of a Residential Area in Lagos State, Nigeria. *Science International Journal.* 19(1):1-18.

Okuo, M. O., Oyido, F. O., Anegbe, B.I., Chiedu, E.I., Ugbune, U. (2019) Chemical Composition and Source Identification of Fine Particulate Matter ($PM_{2.5}$) in Two Contrastive Areas of Lagos Megacity, Southern Nigeria. *Journal of Natural Sciences Research* Vol.9, No.24. ISSN 2224-3186 (Paper) ISSN 2225-0921 (Online)

Olafadehan O A. Fundamentals of adsorption processes, Lambert Academic Publishing, Mauritus; 2021.

Oludare, Ishola (2021-08-15). "Declare public holiday for Ifa festival like Muslims, Christians – Traditionalists tell Abiodun". Daily Post Nigeria. Retrieved 2021-12-08.

Omolaoye, T. S., Skosana, B. T., Ferguson, L. M., Ramsunder, Y., Ayad, B. M., & Du Plessis, S. S. (2024). Implications of Exposure to Air Pollution on Male Reproduction: The Role of Oxidative Stress. *Antioxidants*, *13*(1), 64. https://doi.org/10.3390/antiox13010064

Orogade A.S, Owoade K.O, Hopke P.K, Adie D.B (2016) Source Apportionment of fine and coarse particulate matter in industrial Area of Kaduna, Northern Nigeria. *Journal of Air*

Quality Resource 1179-1190 ISSN 1680-8584 print/2071- 1409 online doi;10.4209/aaqr.2015.11.0636

Osimobi, O. J., Yorkor, B. and Nwankwo, C. A. (2019). Evaluation of daily pollutant standard index and air quality index in a university campus in Nigeria using PM_{10} and $PM_{2.5}$ particulate matter. *Journal of Science, Technology and Environment Informatics*, 07(02), 517-532. https://doi.org/10.18801/jstei.070219.54

Øvrevik , J., Refsnes, M., Låg, M., Holme, J. A., & Schwarze, P. E. (2015). Review. *Biomolecules*, 5, 1399-1440.

Owoade O. K , Fawole, O. G., Olise, F. S., Ogundele, L. T., Olaniyi, H. B., Almeida, M. S., Ho M. D and Hopke, P. K. (2013). Characterization and source identification of airborne particulate loadings at receptor site, classes of Lagos mega-city, Nigeria. *Journal of the Air and Waste Management Association*, 63 (9), 1026-1035.

Owoade, O. K., Abiodun, P. O., Omokungbe, O. R., Fawole, O. G., Olise, F. S., Popoola, O. O., Jones, R. L., & Hopke, P. K. (2021). Spatial-temporal Variation and Local Source Identification of Air Pollutants in a Semi-urban Settlement in Nigeria Using Low-cost Sensors. *Aerosol and Air Quality Research*, *21*(10), 200598. https://doi.org/10.4209/aaqr.200598

Owoade, O. K., Hopke, K. P., Olise, S. F., Ogundele, L.T., Fawole, O. G., Olaniyi, H. B., and Bashiru, I. M. (2015). Chemical compositions and source identification of particulate matter ($PM_{2.5}$ and $PM_{2.5-10}$) from a scrap iron and steel industry along the Ife-Ibadan highway, Nigeria. *Atmospheric Pollution Research,* 6, 107-119.

Owoade, O.K., Abiodun, P.O., Omokungbe, O.R., Fawole, O.G., Olise, F.S., Popoola, O.O.M., Jones, R.L., and Hopke, P.K (2021).: Spatial-temporal Variation and Local Source Identification of Air Pollutants in a Semi-urban Settlement in Nigeria 793 Using Low-cost Sensors. *Aerosol Air Qual. Res.* 21, 200598, https://doi.org/10.4209/aaqr.200598,

Pan, Y., Wang, Y., Sun, Y., Tian, S. and Cheng, M. (2013).Size-resolved aerosol trace elements at a rural mountainous site in Northern China: Importance of regional transport. *Sci. Total Environ.* 461‑462: 761‑771.

Perrino, C., Canepari, S., and Catrambone, M. (2013). Comparing the performance of Teflon and quartz membrane filters collecting atmospheric pm: Influence of atmospheric water. *Aerosol and Air Quality Research,* 13: 137-147.

Petaloti, C., Triantafyllou, A., Kouimtzis, T. and Samar C. (2006). Trace Elements in Atmospheric Particulate Matter over a Coal Burning Power Production Area of Western Macedonia, Greece. *Chemosphere* 65: 2233‑2243.

Pipalatkar, P., Khaparde, V. V., Gajghate, D. G., and Ba, M. A. (2014). Source apportionment of $PM_{2.5}$ using a CMB model for a centrally located Indian City. *Aerosol and Air Quality Research,* 14, 1089-1099.

Pobi, K., Satpati, S., Dutta, S., Nayek, S., Saha, R., & Gupta, S. (2019). Sources evaluation and ecological risk assessment of heavy metals accumulated within a natural stream of Durgapur industrial zone, India, by using multivariate analysis and pollution indices. *Applied Water Science*, *9*(3):1‑16. https://doi.org/10.1007/s13201-019-0946-4.

Qasem, N. a. A., Mohammed, R. H., & Lawal, D. U. (2021). Removal of heavy metal ions from wastewater: a comprehensive and critical review. *Npj Clean Water*, *4*(1). https://doi.org/10.1038/s41545-021-00127-0

Qiao, Q., Huang, B., Zhang, C., Pipere, J. D.A., Panf, Y., and Sun, Y. (2013). Assessment of heavy metal contamination of dust fall in northern China from integrated chemical and magnetic investigation. *Atmospheric Environment*, 74, 182-193.

Querol, X., Zhuang, X., Alastuey, A., Viana, M., Liv, W., Wang, Y., Lopez, A., Zhu, Z., Wei, H. and Xu, S. (2006). Speciation and Sources of Atmospheric Aerosols in a Highly Industrialised Emerging Mega-city in Central China. *J. Environ. Monit*. 8: 1049–1059.

Rahman MM, Pal A, Uddin K, Thu K. (2008) Statistical analysis of optimized isotherm model for maxsorb 111 / ethanol and silica gel / water pairs. *Journal of Novel Carbon Resources Science and Green Asian Strategy.* 5(4):1-12.

Rani, A., Kumar, A., Lal, A. and Pant, M. (2014). Cellular mechanisms of cadmium-induced toxicity: a review. *International Journal of Environmental Health Research* 24: 378-399.

Ren, J., Li, B., Yu, D., Liu, J., and Ma, Z. (2016). Approaches to prevent the patients with chronic airway diseases from exacerbation in the haze weather. *Journal of Thoracic Disease*, 8 (1), E1-E7.

Rockström, J., Gupta, J., Qin, D., Lade, S. J., Abrams, J. F., Andersen, L. S., McKay, D. I. A., Bai, X., Bala, G., Bunn, S. E., Ciobanu, D., DeClerck, F., Ebi, K., Gifford, L., Gordon, C., Hasan, S., Kanie, N., Lenton, T. M., Loriani, S., Zhang, X. (2023). Safe and just Earth system boundaries. *Nature*, *619*(7968), 102–111. https://doi.org/10.1038/s41586-023-06083-8

Saadeh, R., and Klaunig, J. (2014). Child‟s Development and Respiratory System Toxicity. *Journal of Analytical and Environmental Toxicology*, 4(5), 1-8.

Salami, J.T., Sawyerr, H.O., Dada, A.A. (2020). Assessment of Air Quality in Major Motor Parks in Ilorin Metropolis, Kwara State, Nigeria. *International Journal of Health Sciences and Research.* 10(10), 86-95.

Salami, l. (2022). The Development of Mathematical Model for Prediction of Particulate Matter Pollutants Concentrations in Sarajevo City, Bosnial-Herzegovina. *Asian Basic and Applied Research Journal*, 5(1), 36-43.

Saleem, M. H., Afzal, J., Rizwan, M., Shah, Z., Depar, N., & Usman, K. (2022). Chromium toxicity in plants: consequences on growth, chromosomal behavior and mineral nutrient status. *Turkish Journal of agriculture and forestry*, *46*(3), 371–389. https://doi.org/10.55730/1300-011x.3010

Sause, M. G. R., & JasiūNiene, E. (2021). Structural Health Monitoring Damage Detection Systems for Aerospace. In *Springer aerospace technology*. https://doi.org/10.1007/978-3-030-72192-3

Sembhi, H., Wooster, M., Zhang, T., Sharma, S., Singh, N., Agarwal, S., Boesch, H., Gupta, S., Misra, A., Tripathi, S. N., Mor, S., & Khaiwal, R. (2020). Post-monsoon air quality degradation across Northern India: assessing the impact of policy-related shifts in timing and amount of crop residue burnt. *Environmental Research Letters*, *15*(10), 104067. https://doi.org/10.1088/1748-9326/aba714

Serafin, J., & Dziejarski, B. (2023). Application of isotherms models and error functions in activated carbon CO_2 sorption processes. *Microporous and Mesoporous Materials*, 354, 1-19. doi: 10.1016/j.micromeso.2023.112513.

Shah, M. H., Shaheen, N., and Nazir, R. (2012). Assessment of the trace elements level in urban atmospheric particulate matter and source apportionment in Islamabad, Pakistan. *Atmospheric Pollution Research*, 3, 39-45.

Shandilya, Kaushik & Khare, Mukesh. (2014). Particulate Matter: Sources, Emission Rates and Health Effects.

Shen, J., Zhao, Q., Cheng, Z., Huo, J., Zhu, W., Zhang, Y., Duan, Y., Wang, X., Antony Chen, L. W., and Fu, Q.(2020): Evolution of source contributions during heavy fine particulate matter ($PM_{2.5}$) pollution episodes in eastern China through online measurements. *Atmos. Environ.* https://doi.org/10.1016/j.atmosenv..117569,

Sillmann, J., Aunan, K., Emberson, L., Büker, P., Van Oort, B., O'Neill, C., Otero, N., Pandey, D., & Brisebois, A. (2021). Combined impacts of climate and air pollution on human health and agricultural productivity. *Environmental Research Letters*, *16*(9), 093004. https://doi.org/10.1088/1748-9326/ac1df8

Silwana, B., Van Der Horst, C., Iwuoha, E., & Somerset, V. (2017). Graphene Oxide–Antimony Nanocomposite Sensor for Analysis of Platinum Group Metals in Roadside Soil Samples. *InTech eBooks*. https://doi.org/10.5772/67699

Singh, A., Rastogi, N., Sharma, D., and Singh, D. (2015). Inter and intra-annual variability in aerosol characteristics over Northwestern Indo-Gangetic plain. *Aerosol and Air Quality Research*, 15, 376-386

Soltani, M., Kashkooli, F. M., Dehghani-Sanij, A., Kazemi, A., Bordbar, N., Farshchi, M., Elmi, M., Gharali, K., & Dusseault, M. B. (2019). A comprehensive study of geothermal heating and cooling systems. *Sustainable Cities and Society*, *44*, 793–818. https://doi.org/10.1016/j.scs.2018.09.036

Soto-Garcia, L., Andreae, M., Andreae, T., Artaxo, P., Maenhaut, W., Kirchstetter, T., Novakov, T., Chow, J., & Mayol-Bracero, O. (2011). Evaluation of the carbon content of aerosols from the burning of biomass in the Brazilian Amazon using thermal, optical and thermal-optical analysis methods. *Atmospheric Chemistry and Physics*, *11*(9), 4425–4444. https://doi.org/10.5194/acp-11-4425-2011

Sovacool, B. K., Griffiths, S., Kim, J., & Bazilian, M. (2021). Climate change and industrial F-gases: A critical and systematic review of developments, sociotechnical systems and policy options for reducing synthetic greenhouse gas emissions. *Renewable and Sustainable Energy Reviews*, *141*, 110759. https://doi.org/10.1016/j.rser.2021.110759

Stanek L, Sacks J, Dutton S, Dubois J. (2011) Attributing health effects to apportioned components and sources of particulate matter: An evaluation of collective results. *Journal of Atmospheric Environment.* ;45:5655–5663. _

Sulaymon, I. D., Zhang, Y., Hu, J., Hopke, P. K., Zhang, Y., Zhao, B., Xing, J., Li, L., and Mei, X.: (2020) Evaluation of regional transport of $PM_{2.5}$ during severe atmospheric pollution episodes in the western Yangtze River Delta, China. *Journal of Environmental Management,* 293,4270

Suriano, D., and Prato, M. (2023). An investigation on the possible application areas of low-cost PM sensors for air quality monitoring. Sensors, 23(8), 3976.

Swaffield, L., & Egan, D. (2020). *The Welsh Doughnut 2020: A framework for environmental sustainability and social justice*. https://doi.org/10.21201/2020.5983

Taira, K., Brunton, S. L., Dawson, S. T. M., Rowley, C. W., Colonius, T., McKeon, B. J., Schmidt, O. T., Gordeyev, S., Theofilis, V., & Ukeiley, L. S. (2017). Modal Analysis of Fluid Flows: An Overview. *AIAA Journal*, *55*(12), 4013–4041. https://doi.org/10.2514/1.j056060

Taiwo, A.M., Harrison, R.M. and Shi, Z. (2014). A review of receptor modeling of industrially emitted particulate matter. *Atmos. Environ.* 97: 109‑120.

Thurston, G.D. and Spengler, J.D. (1985). A Quantitative Assessment of Source Contributions to Inhalable Particulate Matter Pollution in Metropolitan Boston. *Atmos. Environ.* (1967) 19: 9–25.

Tian, H., Cheng, K., Wang, Y., Zhao, D., Lu, L., Jia, W., & Hao, J. (2012). Temporal and spatial variation characteristics of atmospheric emissions of Cd, Cr, and Pb from coal in China. *Atmospheric Environment*, 50(C):157–163. https://doi.org/10.1016/j.atmosenv.2011.12.045.

Tian, H.Z., Wang, Y., Xue, Z.G., Cheng, K., Qu, Y.P., Chai, F.H. and Hao, J.M. (2010). Trend and Characteristics of Atmospheric Emissions of Hg, As, and Se from Coal Combustion in China, 1980-2007. *Atmos. Chem. Phys. Aerosol and Air Quality Research*, 15: 875–887, 2015 88 10: 11905–11919

Tirez, K., Vanhoof, C., Peters, J., Geerts, L., Bleux, N., Adriaenssens, E., … Berghmans, P. (2015). Speciation of inorganic arsenic in particulate matter by combining HPLC/ICP-MS and XANES analyses. *Journal of Analytical Atomic Spectrometry*, 30(10):2074–2088. https://doi.org/10.1039/c5ja00105f.S

Tomlinson, D., Wilson, J., Harris, C., & Jeffrey, D. (1980). Problems in the assessment of heavy metal levels in estuaries and the formation of a pollution index. *Helgoländer Meeresunte rsuchungen*, *33*(1-4):566–575. https://doi.org/10.1007/BF02414780.

Trapp, J.M., Millero, F.J. and Prospero, J.M. (2010). Temporal variability of the elemental composition of African dust measured in trade wind aerosols at Barbados and Miami. *Mar. Chem.* 120: 71–82.

Tsai, J., Hung, T., How, V., & Chiang, H. (2023). Effect of the Method Detection Limit on the Health Risk Assessment of Ambient Hazardous Air Pollutants in an Urban Industrial Complex Area. *Atmosphere*, *14*(9), 1426. https://doi.org/10.3390/atmos14091426

Urman, R., Habre, R., Fruin, S., Gauderman, J., Lurmann, F., Gilliland, F., and Mcconnell, R. (2016). B15 Health effects of indoor/outdoor Pollution in Childhood: Exposure To Transition Metals In Particulate Matter Air Pollution And Children's Lung Function In The Southern California Children's Health Study. *American Journal of Respiratory*

US EPA, United States Environmental Protection Agency (2015c) .National ambient air quality standards (NAAQS}, Retrieved from https;//epa.gov/air/criteria.html.

US EPA, United States Environmental Protection Agency. (1999a). National air toxics program: the integrated urban strategy, United States Environmental Protection Agency's Federal Register, 64,137, Retrieved from http://www.epa.gov/ttn/uatw/urban/urbanpg.html.

US EPA, United States Environmental Protection Agency. (1999b). National air toxics program: the integrated urban strategy, United States Environmental Protection Agency's Federal Register, 64,137, Retrieved from http://www.epa.gov/ttn/uatw/urban/urbanpg.html.

US EPA, United States Environmental Protection Agency. (2012). Revised air quality standards for particle pollution and updates to the air quality index (AQI). Retrieved from www.epa.gov/airquality/particlepollution/2012/decfsstandards.pdf

US EPA, United States Environmental Protection Agency. (2012b). Waste and cleanup risk assessment. Retrieved from http://www2.epa.gov/risk/waste-and-cleanup-risk-assessment

USEPA, 2012. A Guide to Air Quality Index and Your Health. https://www3.epa.gov/airnow/aqi_brochure_02_14.pdf〉.

Uslu, B., Gao, F., García-Ferreyra, J., Sánchez-Pavón, A., Francisco, D., Gómez-Gil, F., Sanchez-Garzón, J., Orjuela-Vásquez, M., Pino-Araujo, A., Pino-Duque, M., Onuh, S., Liu, Y., Chian, R., Chen, J., Iliescu, D., Rodica, D., Nagy, G., Zorila, R., Dragusin, S., . . . Wu, B. (2023). Embryology Update. In *IntechOpen eBooks*. https://doi.org/10.5772/intechopen.101018

Van Der Pol, E., Coumans, F., Grootemaat, A., Gardiner, C., Sargent, I., Harrison, P., Sturk, A., Van Leeuwen, T., & Nieuwland, R. (2014). Particle size distribution of exosomes and microvesicles determined by transmission electron microscopy, flow cytometry, nanoparticle tracking analysis, and resistive pulse sensing. *Journal of Thrombosis and Haemostasis*, *12*(7), 1182–1192. https://doi.org/10.1111/jth.12602

Van Sebille, E., Aliani, S., Law, K. L., Maximenko, N., Alsina, J. M., Bagaev, A., Bergmann, M., Chapron, B., Chubarenko, I., Cózar, A., Delandmeter, P., Egger, M., Fox-Kemper, B., Garaba, S. P., Goddijn-Murphy, L., Hardesty, B. D., Hoffman, M. J., Isobe, A., Jongedijk, C. E., . . . Wichmann, D. (2020). The physical oceanography of the transport of floating marine debris. *Environmental Research Letters*, *15*(2), 023003. https://doi.org/10.1088/1748-9326/ab6d7d

Wang, P., Ying, Q., Zhang, H., Hu, J., Lin, Y., and Mao, H. (2018).: Source apportionment of 870 secondary organic aerosol in China using a regional source-oriented chemical 871 transport model and two emission inventories. *Environmental Pollution*, 237, 756- 766,

Wang, T. W. (2012). A Study of the Air Pollution Index Reporting System, School of Public Health and Primary Care The Chinese University of Hong Kong, Tender Ref. AP 07-085.

Wang, Y., & Chung, S. H. (2019). Soot formation in laminar counterflow flames. *Progress in Energy and Combustion Science*, *74*, 152–238. https://doi.org/10.1016/j.pecs.2019.05.003

Wang, Y., Hu, M., Wang, Y., Qin, Y., Chen, H., Zeng, L.,Lei, J., Huang, X., He, L., Zhang, R. and Wu, Z. (2016). Characterization and influence factors of PM $_{2.5}$ emitted from crop straw burning. *Acta Chim. Sinica* 74: 356‑362.

Werner, M.L., Nico, P.S., Marcus, M.A. and Anastasio, C. (2007). Use of micro-XANES to speciate chromium in airborne fine particles in the Sacramento Valley. Environmental Science and Technology, 41(14), 4919–4924. https://doi.org/10.1021/es070430q

WHO (2007). Nickel in Drinking Water. WHO/SDE/WSH/07.08/55. Geneva: World Health Organization. Available on https://www.who.int/water_sanitation_health/dwq/chemicals/Nickel110805.pdf. Date Accessed: 30 June 2019.

WHO Regional Office for Europe (2001) Air quality guidelines. Air Qual Guide 3:1–25

WHO, 2016. Guidelines for Air Quality. World Health Organization (WHO), Geneva (Retrieved April 2016) ⟨(https://www.epa.gov/risk/regional-screening-levels-rslsgeneric-tables-may-2016)

WHO, World Health Organization. (2000). Air quality guidelines, who regional office for Europe, Retrieved from http://www.euro.who.int/en/ publications/ abstracts/air–quality–guidelines–for–europe

WHO, World Health Organization. (2006). Air quality guideline: global update 2005. Copenhagen: World Health Organization regional office for Europe. Retrieved from www.who.int/phe/health_topics/outdoorair/outdoorair_aqg/en

WHO. World Health Organization (2000). Air quality guidelines for Europe. European series. 91: 2nd edition. WHO Regional Publications. http://www.euro.who.int/__data/assets/pdf_file/0005/74732/E71922.pdf. Date Accessed: 24 May 2019.

Wu, D.L., Lin, M., Chan, C.Y., Li, W.Z., Tao, J., Li, Y.P.and Bu, C.W. (2013). Influences of commuting mode, air conditioning mode and meteorological parameters on fine particle ($PM_{2.5}$) exposure levels in traffic microenvironments. *Aerosol and Air Quality Research*, 13: 709-720.

Xia, L. and Gao, Y. (2011). Characterization of Trace Elements in $PM_{2.5}$ Aerosols in the Vicinity of Highways in Northeast New Jersey in the US East Coast. *Atmos Pollut. Res. 2: 34–44.*

Yan, D., Lei, Y., Shi, Y., Zhu, Q., Li, L., and Zhang, Z (2018) Evolution of the spatiotemporal pattern of $PM_{2.5}$ concentrations in China - A case study from the Beijing-Tianjin Hebei region. *Atmos. Environ*.,183, 225–233,

Yang, F., He, K., Ma, Y., Chen, X., Cadle, S.H., Chan, T.and Mulawa, P.A. (2003). Characteristics and Sources of Trace Elements in Ambient $PM_{2.5}$ in Beijing. *Huanjing Kexue (China)* 24, 33‑37.

Yang, L., Ye, W., Jerry, M. D., and Jiming, H. (2011). Estimating the effects of meteorology on PM2.5 reduction during the 2008 summer olympic games in Beijing, China. Frontiers of *Environmental Science and Engineering in China*, 5(3), 331- 41.

Yongming H, Peixuan D, Junji C, Posmentier ES. Multivariate analysis of heavy metal contamination in Urban Dusts of Xi'an, Central China. *Science. Total Environment*. 2006;355:176–186.

Yu B., Wang Y., and Zhou Q. (2014). Human health risk assessment based on toxicity characteristic leaching procedure and simple bio-accessibility extraction test of toxic metals in urban street dust of Tianjin, China. PLoS ONE 9(3): e92459.

Yu, C. H., Huang, L., Shin, J. Y., Artigas, F., & Fan, Z. H. (2014). Characterization of concentration, particle size distribution, and contributing factors to ambient hexavalent chromium in an area with multiple emission sources. *Atmospheric environment* (Oxford, England : 1994), 94:701–708. https://doi:10.1016/j.atmosenv.2014.06.004.

Zalakeviciute R, Rybarczyk Y, Lopez-Villada J, Diaz Suarez MV (2018) Quantifying decade-long effects of fuel and traffic regulations on urban ambient $PM_{2.5}$ pollution in a mid-size South American city. *Atmos Pollut Res* 9:66–75.
https:// doi. org/ 10.1016/j. apr. 2017. 07. 001

Zhang, Q., Zheng, Y., Tong, D., Shao, M., Wang, S., Zhang, Y., Xu, X., Wang, J., He, H., Liu, W., Ding, Y., Lei, Y., Li, J., Wang, Z., Zhang, X., Wang, Y., Cheng, J., Liu, Y., Shi, Q., . . . Hao, J. (2019). Drivers of improved PM $_{2.5}$ air quality in China from 2013 to 2017.

Proceedings of the National Academy of Sciences, *116*(49), 24463–24469. https://doi.org/10.1073/pnas.1907956116

Zhang, X., Hecobian, A., Zheng, M., Frank, N. H., and Weber, R. J. (2010). Biomass burning impact on $PM_{2.5}$ over the southeastern US during 2007: integrating chemically speciated FRM filter measurements, MODIS fire counts and PMF analysis, *Atmospheric Chemistry and Physics*, 10, 6839-6853

Zhang, Y., Wang, X., Chen, H., Yang, X., Chen, J. and Allen, J.O. (2009). Source Apportionment of Lead containing Aerosol Particles in Shanghai Using Single Particle Mass Spectrometry. *Chemosphere* 74: 501‑507.

Zoran, M. A., Savastru, R. S., Savastru, D. M., & Tautan, M. N. (2020). Assessing the relationship between ground levels of ozone (O_3) and nitrogen dioxide (NO_2) with coronavirus (COVID-19) in Milan, Italy. *The Science of the Total Environment*, *740*, 140005. https://doi.org/10.1016/j.scitotenv.2020.140005

Appendix I

Monthly Average concentrations of Metals in $PM_{2.5}$ ($\mu g/m^3$) at location SIIE from January to December, 2022

	LOCATION SIIE											
Element	**January**	**February**	**March**	**April**	**May**	**June**	**July**	**Aug**	**Sept.**	**Oct.**	**Nov.**	**Dec.**
Na	76.62±71.81	61.80±8.66	57.44±5.97	51.03±4.34	45.61±5.96	42.35±4.35	38.59±6.06	48.27±16.98	55.48±16.75	58.06±14.54	62.81±4.28	70.43±26.54
Mg	7.68±2.01	6.31±2.19	5.79±1.75	4.18±2.06	3.8±0.52	3.2±0.33	2..6±0.76	3.4±0.36	3.9±0.94	4.11±0.59	6.8±1.65	7.4±2.69
Al	29.53±4.27	26.00±4.49	23.45±4.68	21.51±5.39	19.86±1.12	15.51±1.65	13.92±1.36	20.38±2.62	19.78±1.96	22.69±1.94	27.43±7.89	31.23±4.24
Ca	23.00±2.95	20.93±2.40	17.33±6.41	15.20±6.28	18.10±2.69	14.51±6.15	13.20±5.45	14.66±3.82	17.62±3.33	19.46±2.97	23.35±8.91	26.62±7.27
K	33.74±6.82	30.74±11.94	27.21±4.85	20.13±6.25	22.62±1.79	17.74±2.05	15.21±2.52	18.60±0.72	20.73±1.79	27.12±3.13	31.58±3.48	35.23±5.52
Cr	0.18±0.03	0.11±0.01	0.08±0.02	0.19±0.03	0.14±0.13	0.11±0.08	0.18±0.09	0.10±0.17	0.13±0.16	0.19±0.13	0.14±0.46	0.19±0.45
Mn	0.20±0.04	0.11±0.04	0.08±0.05	0.05±0.01	0.06±0.04	0.03±0.04	0.02±0.03	0.05±0.04	0.03±0.04	0.02±0.04	0.17±0.04	0.19±0.04
Ti	0.86±0.24	0.78±0.64	0.24±0.31	0.27±0.13	0.18±0.27	0.16±0.01	0.13±0.02	0.20±0.02	0.22±0.25	0.28±0.03	0.75±0.09	1.02±0.27
V	0.04±0.03	0.03±0.03	0.02±0.02	0.01±0.01	0.01±0.01	0.00±0.01	0.00±0.00	0.00±0.00	0.01±0.01	0.02±0.00	0.05±0.02	0.06.03
Fe	4.75±0.92	4.15±0.87	3.71±0.49	2.57±1.02	2.06±0.30	1.26±0.42	1.16±0.43	1.35±0.25	1.86±0.50	2.11±0.41	4.85±0.61	5.09±0.89
Ni	0.18±0.04	0.15±0.04	0.10±0.04	0.06±0.03	0.04±0.04	0.02±0.02	0.01±0.01	0.02±0.02	0.01±0.01	0.13±0.04	0.12±0.07	0.11±0.19
Zn	46.79±4.65	42.67±9.96	36.11±4.89	29.66±8.99	24.42±26.99	20.77±6.66	22.58±1.38	20.35±4.82	23.74±4.80	25.93±5.04	76.83±4.30	84.83±6.72
As	0.07±0.05	0.06±0.02	0.04±0.02	0.03±0.02	0.04±0.01	0.00±0.02	0.00±0.01	0.02±0.04	0.01±0.03	0.04±0.02	0.07±0.01	0.09±0.04
Cd	0.02±0.02	0.01±0.01	0.01±0.01	0.00±0.02	0.00±0.01	0.00±0.00	0.00±0.00	0.00±0.00	0.00±0.00	0.00±0.00	0.03±0.01	0.03±0.02
Pb	1.84±0.38	1.40±0.23	1.65±0.10	1.17±0.48	0.88±0.06	0.80±0.04	0.70±0.12	0.92±0.06	1.10±0.17	1.26±0.07	1.54±0.25	1.89±0.15
Cu	0.32±0.03	0.28±0.02	0.58±0.03	0.44±0.03	0.40±0.05	0.34±0.06	0.61±0.55	0.81±0.23	1.02±0.17	0.38±0.14	0.42±0.05	0.28±0.08

Appendix II

Monthly Average concentrations of Metals in $PM_{2.5}$ ($\mu g/m^3$) at location OLFS from January to December,2022

	LOCATION OLFS											
Element	**January**	**February**	**March**	**April**	**May**	**June**	**July**	**Aug**	**Sept.**	**Oct.**	**Nov.**	**Dec.**
Na	196.67±64.86	190.00±10.58	188.33±63.01	68.33±16.26	64.00±5.29	59.33±3.51	57.33±4.51	69.00±2.65	70.67±2.52	68±2.00	199.67±10.60	200.67±9.50
Mg	4.38±0.38	3.94±1.46	3.88±0.23	5.95±0.28	5.79±0.28	4.97±0.64	4.37±0.19	6.07±0.18	6.10±0.23	4.6±0.17	4.52±0.94	7.57±0.72
Al	31.87±3.22	34.43±12.53	29.24±9.42	18.85±4.71	16.86±3.13	13.59±22.72	14.29±3.05	20..87±3.72	22.45±22.20	16±3.07	34.88±6.17	37.79±2.31
Ca	34.53±1.70	36.79±4.54	32.84±3.57	22.23±4.12	20.09±4.00	18..77±2.59	16.49±3.85	22.20±2.42	20.86±2.49	24±2.28	35.51±3.02	38.91±2.74
K	58.62±9.76	55.63±8.84	54.16±10.56	29.78±2.81	24.55±1.98	22.38±2.88	26.00±3.15	24.60±2.38	26.99±1.85	28±3.20	55.72±9.13	60.39±3.55
Cr	0.02±0.02	0.01±0.00	0.01±0.01	ND	ND	ND	ND	ND	ND	ND	0.01±0.01	0.01±0.01
Mn	0.02±0.05	0.01±0.00	0.01±0.05	0.01±0.00	0.01±0.00	0.00±0.00	0.00±0.00	0.01±0.00	0.00±0.00	0±0.00	0.02±0.00	0.02±0.05
Ti	1.54±0.27	1.29±0.63	1.18±0.47	0.01±0.04	0.00±0.00	0.00±0.35	0.00±0.00	0.00±0.00	0.00±0.00	0.01±0.01	1.40±0.46	1.43±0.62
V	ND	ND	ND	ND	ND	ND	ND	ND	ND	ND	ND	ND
Fe	4..90±0.80	4.67±0.40	3.87±0.21	2.98±0.50	2.70±0.30	2.31±0.29	2.00±0.45	2.77±0.46	2.87±0.29	2.93±0.26	4.96±0.79	5.13±0.96
Ni	ND	ND	ND	ND±ND	ND±ND	ND±ND.ND	ND	ND	ND	ND	ND	ND
Zn	31.80±10.48	30.07±10.44	28.85±4.31	18.63±6.94	16.15±2.92	14.34±4.36	13.47±4.12	18.39±3.45	17.30±4.13	16.10±2.86	36.80±7.87	34.19±10.02
As	0.06±0.05	0.04±0.04	0.03±0.01	0.02±0.01	0.02±0.00	0.01±0.02	0.01±0.00	0.01±0.01	0.01±0.01	0.03±0.02	0.06±0.02	0.05±0.04
Cd	ND	ND	ND	ND	ND	ND	ND	ND	ND	ND	ND	0.393±0.21
Pb	0.08 ±0.01	0.07±0.01	0.05±0.05	0.04±0.05	0.03±0.01	0.02±0.01	0.03±0.01	0.04±0.58	0.01±0.04	0.04±0.01	0.07±0.10	0.09±0.21
Cu	0.18±0.02	0.16±0.03	0.19±0.04	0.02±0.00	0.01±0.00	0.00±0.00	0.00±0.00	0.00±0.00	0.00±0.00	0±0.01	0.17±0.04	0.20±0.03

Appendix III

Monthly Average concentrations of Metals in $PM_{2.5}$ (µg/m^3) for location OMRF from January to December, 2022

LOCATION OMRF												
Element	**January**	**February**	**March**	**April**	**May**	**June**	**July**	**Aug**	**Sept.**	**Oct.**	**Nov.**	**Dec.**
Na	16.77±2.90	13.38±1.91	12.98±2.32	10.30±3.48	8.42±1.55	6.87±1.09	6.61±0.75	4.85±0.68	5.80±0.60	7.65±0.80	18.07±3.12	19.07±1.94
Mg	4.47±0.74	3.51±0.61	2.53±0.51	1.80±1.17	1.57±0.03	1.35±0.03	1.46±0.07	1.55±0.29	2.10±0.24	2.37±0.55	4.21±0.42	5.10±0.30
Al	20.13±1.50	17.37±1.75	6.77±3.33	5.28±1.94	4.17±0.24	3.01±0.19	3.65±0.43	5.53±0.83	6.45±0.67	6.65±1. 09	18.47±1.59	20.17±1.57
Ca	0.62±0.03	0.43±0.06	0.28±0.04	0.22±0.09	0.18±1.02	0.16±0.08	0.19±0.19	0.22±0.02	0.20±0.04	0.14±0.07	0.55±0.08	0.58±0.03
K	7.75±0.04	6.11±0.04	4.64±0.02	3.37±0.14	3.01±0.03	2.72±0.06	2.14±0.06	3.99±0.15	4.06±0.07	4.47±0.11	7.73±0.05	7.83±0.08
Cr	0.02±0.00	0.02±0.00	0.43±0.02	0.31±0.00	0.35±0.12	0.48±0.17	0.34±0.18	0.46±0.13	0.48±0.16	0.44±0.14	0.03±0.03	0.02±0.00
Mn	0.33±0.39	0.28±0.16	0.14±0.08	0.16±0.05	0.15±0.00	0.12±0.17	0.14±0.00	0.16±0.04	0.17±0.01	0.14±0.06	0.32±0.10	0.27±0.36
Ti	0.19±0.08	0.15±0.21	0.28±0.11	0.10±0.02	0.02±0.01	0.00±0.00	0.00±0.00	0.04±0.05	0.02±0.00	0.04±0.01	0.18±0.06	0.17±0.16
V	0.04±0.01	0.02±0.01	0.00±0.01	0.01±0.01	0.00±0.01	0.00±0.00	0.00±0.00	0.01±0.00	0.00±0.00	0.01±0.01	0.02±0.01	0.03±0.03
Fe	7.19±0.65	6.20±0.60	3.69±0.90	3.74±1.56	3.00±0.18	2.45±0.44	2.18±0.19	3.10±0.34	3.70±0.46	3.20±0.39	6.11±0.86	6.77±1.11
Ni	0.41±0.10	0.30±0.19	0.11±0.11	0.15±0.10	0.12±0.12	0.15±0.13	0.18±0.14	0.13±0.14	0.15±0.08	0.18±0.21	0.43±0.24	0.49±0.20
Zn	63.20±2.66	58.90±3.21	22.35±4.77	24.82±2.93	20.23±4.07	14.63±4.79	14.06±4.55	17.27±4.67	20.30±3.00	22.31±2.68	61.85±4.54	64.43±0.93
As	0.52±0.04	0.39±0.07	0.29±0.01	0.32±0.06	0.17±0.06	0.03±0.01	0.02±0.01	0.11±0.05	0.12±0.04	0.29±0.04	0.33±0.02	0.42±0.03
Cd	0.04±0.01	0.03±0.02	0.01±0.01	0.00±0.00	0.00±0.00	0.00±0.00	0.00±0.00	0.01±0.01	0.00±0.00	0.00±0.00	0.04±0.01	0.03±0.02
Pb	2.19±0.69	1.21±0.38	0.79±0.22	0.51±0.60	0.60±0.22	0.41±0.19	0.73±0.27	0.41±0.28	0.40±0.62	0.83±0.17	2.23±0.53	2.28±0.75
Cu	0.06±0.02	0.02±0.02	0.03±0.01	0.16±0.03	0.15±0.04	0.15±0.05	0.19±0.03	0.17±0.03	0.20±0.07	0.18±0.05	0.04±0.04	0.06±0.03